Ice front variations and velocity changes of calving glaciers in the Southern Patagonia Icefield and northwestern Greenland

SAKAKIBARA Daiki

Ph. D. Dissertation

Division of Earth System Science
Graduate School of Environmental Science
Hokkaido University

March 2016

Abstract

This thesis studies frontal variations and changes in ice flow of calving glaciers in the Southern Patagonia Icefield (SPI) and northwestern Greenland. To quantify recent changes of calving glaciers in these regions, I measured ice front positions and flow velocities over the last 20 years at 47 calving glaciers using satellite images. The focus of the measurements and subsequent data analysis was the relationship between glacier retreat and flow acceleration. In addition to the satellite data based measurements, an intensive research was carried out at Upsala Glacier in the SPI to investigate the detailed mechanisms of rapid retreat observed at this glacier and some of the studied glaciers. In particular, recent rapid retreat of Upsala Glacier was investigated by field observations and analysis of glacier geometry using digital elevation models.

In the SPI, frontal positions and velocities of 32 termini of 28 calving glaciers were measured between 1984 and 2014 using Landsat images. During the study period, only the two termini of Pío XI Glacier advanced, 11 termini were stagnant and 17 termini retreated. The results demonstrated a large variation in the magnitude of the glacier retreat. Jorge Montt, HPS12, and Upsala Glaciers retreated by more than 200 m a^{-1} in the study period. Flow speed change was not uniform over the SPI. Flow acceleration was observed at these three rapidly retreating glaciers and the timings of the acceleration closely agree with the rapid retreats.

In northwestern Greenland, frontal positions and velocities were also measured for 19 calving glaciers along the coast of the Prudhoe Land (PL). These measurements were performed for the period between 1987 and 2014 using Landsat images. All of the studied glaciers retreated in the study period. Most of the studied termini began to retreat around 2000, which coincided with the onset of the increase in the summer temperature in northwestern Greenland. Flow speed of Heilprin, Tracy, Farquhar, Bowdoin, and Diebitsch Glaciers increased between 2000 and 2014, and the acceleration was accompanied by the rapid frontal retreat.

These results demonstrated generally retreating trends of the calving glaciers in the SPI and in northwestern Greenland. Negative mass balance due to atmospheric warming is suggested as a primary cause of the generally retreating trends. However, the rapid

frontal retreats observed at some of the studied glaciers cannot be explained by the warming alone. Flow acceleration was observed at the rapidly retreating glaciers both in the SPI and northwestern Greenland. Because ice acceleration on these glaciers was greater near the terminus, the acceleration should have enhanced stretching of ice along the glacier and induced so called dynamic thinning. Thus, results of this study suggest that thinning due to changes in flow regime played a key role in the rapid retreat of calving glaciers.

During field campaigns in 2013 and 2014, bathymetric surveys were carried out in a proglacial lake within 0.5–5 km from the front of Upsala Glacier. This is the region where the lake expanded its area after the rapid retreat began in 2008. A bedrock rise was found at the valley center 3 km from the front. While the terminus was stable on the bedrock rise in 2005–2008, it retreated by 3 km from 2008 to 2012. The main trunk of the glacier thinned at a rate more than 30 m a^{-1} in 2009–2011. Ice near the front showed twofold acceleration in 2007–2010, whereas the glacier surface steepened from 2.2 to 2.7° during the same period.

Upsala Glacier significantly thinned in 2005–2008, while the front position was stable at the location of the bedrock rise. As a result of this thinning, it is likely that the terminus got afloat and the glacier began to retreat in August 2008. As soon as the ice became thinner than that fulfills the hydrostatic equilibrium condition, active calving events occur and a large portion of ice detached from the glacier progressively. These large calving events were the driver of the rapid glacier retreat in 2008–2012. The glacier surface steepened in 2006–2011 because ice thinning rate was greater near the front. This steepening increased the glacier flow. Then, stretching flow regime along the glacier was enhanced and the dynamic thinning was induced. This positive feedback between flow acceleration and ice thinning was the most important mechanism in the frontal retreat since 2008.

Based on the study results, I propose that a calving glacier dynamically changes its geometry under a cycle of thinning, acceleration, and rapid retreat. A calving glacier gradually retreats and thins under a warming climate condition until the terminus retreats to a specific bedrock configuration such as a bedrock rise. Then the terminus

thins and reaches the hydrostatic equilibrium condition, which allows rapid retreat. The thinning near the front steepens the glacier surface and this steepening causes flow acceleration. The acceleration induces dynamics thinning, and this thinning plays a key role in rapid glacier retreat. These processes are connected by a positive feedback so that the initial thinning, retreat, and acceleration lead to further destabilization of the glacier terminus. This study revealed that changes in ice dynamics and flow acceleration play an important role in the rapid retreat of calving glaciers. Results of this study emphasized that the dynamical changes of calving glaciers should be taken into account for the future projection of the glacier mass loss.

Contents

List of figures

List of tables

Chapter 1

General introduction

1.1. Calving glaciers

Most of glaciers in the world are losing mass due to imbalance with current climatic conditions (Vaughan et al., 2013). Mass loss of the glaciers contributes significantly to the recent sea level rise (SLR). This contribution accounts for 61±19% of the total SLR between 2003 and 2008, which is equivalent to 1.51 ± 0.16 mm a^{-1} (Gardner et al., 2013). The mass loss of the glaciers is mainly driven by two processes; decrease in surface mass balance and increase in frontal ablation (iceberg discharge and subaqueous melting) from glacier fronts protruding into water (e.g. Enderlin et al., 2014; Meier et al., 2007; Pfeffer et al., 2008; Rignot and Kanagaratnam, 2006; van den Broeke et al., 2009) (Fig. 1.1). The surface mass balance becomes more negative when snow and ice melt increase and/or snow accumulation decreases. Thus, changes in the surface mass balance are largely controlled by climatic conditions such as air temperature and solid precipitation. Ice loss due to frontal ablation occurs when a glacier terminates in the ocean or lakes. This glacier is called as a calving glacier. Calving glaciers are widely distributed in Antarctica, Greenland, Alaska, Arctic, and the southern Andes. In general, calving glaciers in these regions are more rapidly retreating than glaciers terminating on land. Because the frontal ablation from a calving front is largely controlled by ice dynamics, changes in ice flow conditions are considered as a driver of rapid retreat of calving glaciers.

It is reported that approximately half of the recent mass loss of the Greenland ice sheet is due to increase in frontal ablation into the ocean from calving glaciers (e.g. Enderlin et al., 2014; Pritchard et al., 2009; Rignot and Kanagaratnam, 2006; van den Broeke et al., 2009) (Fig. 1.2). It is also assumed that the increase in frontal ablation explains nearly entire part of the mass loss from the Antarctic ice sheet (e.g. Pritchard et al., 2009; Rignot et al., 2011). In Alaska, glacier mass loss due to increase in the frontal ablation explains roughly 20% of the net mass loss between 2003 and 2010, in spite of the fact that calving glaciers cover only about 14% of the total glacier area in the region

(McNabb et al., 2015). These studies demonstrated that currently observed glacier mass loss is not entirely due to changing atmospheric conditions but the frontal ablation plays an important role in regions characterized by calving glaciers. However, our current understanding of calving glaciers is insufficient to accurately evaluate glacier mass loss all over the globe. Because observational data from rapidly changing calving glaciers are lacking, their importance in total ice loss from glaciers and ice sheets is underestimated (Church et al., 2013). To improve the future projection of SLR, dynamical response of calving glaciers is in the list of the most important unsolved uncertainties (Church et al., 2013; Nick et al., 2013).

Frontal retreat of calving glaciers is widely observed in Greenland, Arctic, Alaska, and Southern Andes (e.g. Aniya et al., 1997; Carr et al., 2014; Howat and Eddy, 2011; Masiokas et al., 2009; Moon and Joughin, 2008; McNabb and Hock, 2014). Among these retreating glaciers, several glaciers indicated extraordinary rapid frontal retreat over the last decades (e.g. Howat et al., 2005; Meier and Post, 1987). For example, Columbia Glacier in Alaska began retreat around 1980 and it has retreated by more than 20 km during the following ~30 years (e.g. Meier and Post, 1987; O'Neel et al., 2005). In coincidence with the rapid retreat, ice flow speed at the terminus of Columbia Glacier increased from 5 m d^{-1} to >27 m d^{-1} between 1980 and 2001 (O'Neel et al., 2005). Similar to these observations at Columbia Glacier, rapid retreat associated with flow acceleration was also observed at some of calving glaciers in other regions (e.g. Howat et al., 2005; Joughin et al., 2004). Jakobshavn Isbræ, one of the largest glaciers in Greenland, doubled its speed from 1998 to 2003 (Fig. 1.3), and lost its floating ice tongue (Joughin et al., 2004). It is reported that rapid changes of calving glaciers significantly contributed to the glacier mass loss in the region (e.g. McNabb et al., 2015; Enderlin et al., 2014). However, it is unknown how common are such rapid changes as observed at Columbia Glacier and Jakobshavn Isbræ occur in other calving glaciers. This is primarily due to the lack of observational data on calving glaciers, and thus it is crucial to increase temporal and spatial coverage of the observational data to solve the problem.

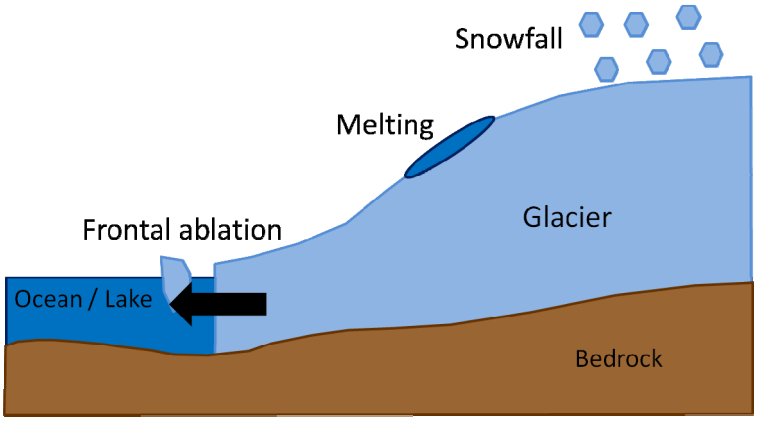

Figure 1.1. Schematic diagram of a calving glacier, showing processes controlling change in ice mass.

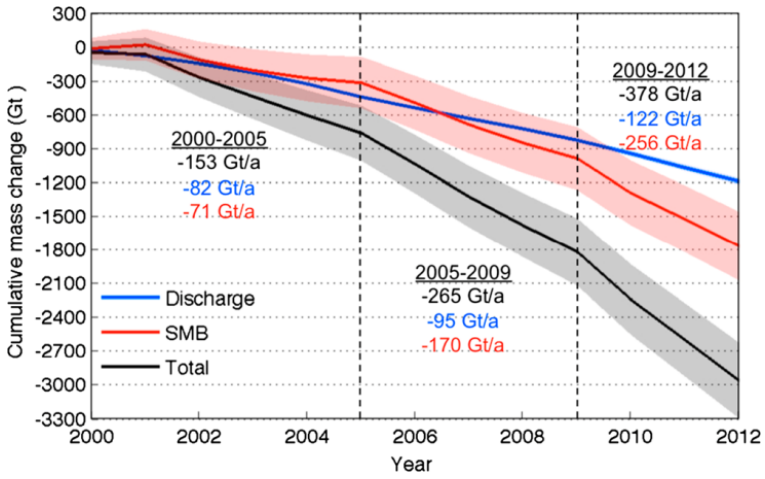

Figure 1.2. Cumulative mass change of the Greenland ice sheet (black), and its components due to changes in ice discharge with respect to 1996 (blue) and changes in surface mass balance with respect to the 1961–1990 mean (red) (Enderlin et al., 2014).

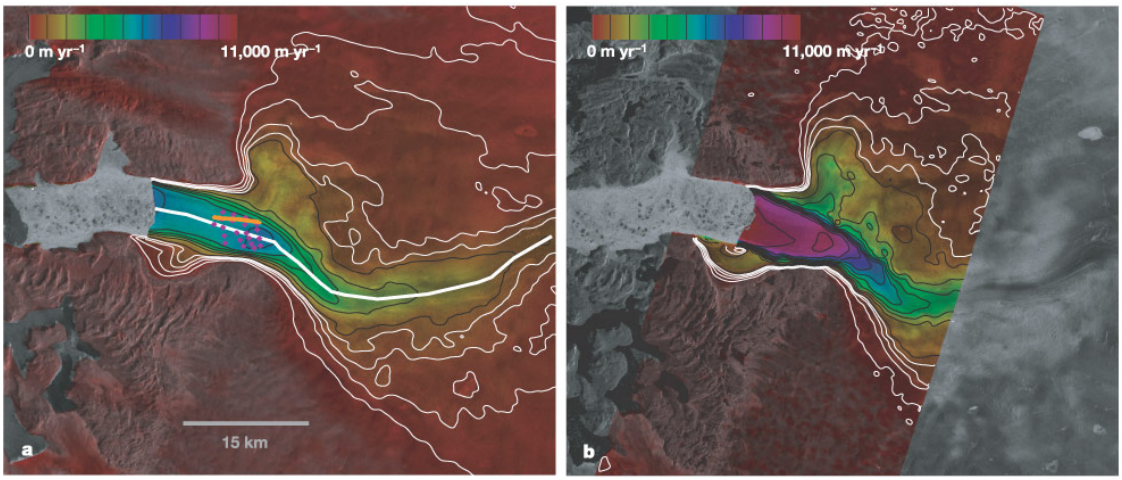

Figure 1.3. Ice flow speed of Jakobshavn Isbræ in (a) February 1992 (b) and October 2000 (Joughin et al., 2004). Speed is shown by the color scale illustrated on a synthetic aperture radar amplitude imagery.

1.2. The Southern Patagonia Icefield

The Northern and Southern Patagonia Icefields (NPI and SPI) cover areas of 3,950 (Rivera et al., 2007) and 12,550 km^2 (Skvarca et al., 2010), respectively, forming the largest temperate ice mass in the southern hemisphere (Warren and Sugden, 1993) (Fig. 1.4). Recent studies report that both icefields have been losing ice volume over decadal and longer time scales, contributing to SLR (Glasser et al., 2011; Rignot et al., 2003; Willis et al., 2012b). Rignot et al. (2003) reported that the volume loss of the icefields was equivalent to an SLR of 0.042 ± 0.002 mm a^{-1} from 1968/1975 to 2000, later increasing to 0.067 ± 0.004 mm a^{-1} in 2000–2012 (Willis et al., 2012b). Because many outlet glaciers in Patagonia terminate either in the ocean (western side) or freshwater lakes (mainly eastern side), calving glaciers greatly influence the SPI ice mass budget (Rignot et al., 2003).

Frontal variations of these calving glaciers have been measured for the period before 1944 (Davies and Glasser, 2012; Glasser et al., 2011; Masiokas et al., 2009) and for the period 1944–2005 (e.g. Aniya et al., 1997; Lopez et al., 2010). In particular, the measurements by Aniya et al. (1997) revealed that 65% of 48 outlet glaciers retreated between 1944/45 and 1985/86, losing a total area of 200 km^2 (Fig. 1.5). Lopez et al.

(2010) reported that the change in the frontal positions of 32 glaciers between 1945 and 2005 ranged from −11.6 to 8.3 km. These studies demonstrated a generally retreating trend of the SPI calving glaciers during the 20th century. Several calving glaciers in the SPI have changed rapidly over the last decade. These glaciers include Upsala Glacier, SPI's third largest calving glacier. Upsala Glacier retreated by 2.9 km from 2008 to 2011 (Sakakibara et al., 2013), and Jorge Montt Glacier retreated by 308 m a^{-1} in 2008–09 and 716 m a^{-1} in 2010–11 (Rivera et al., 2012b). Such abrupt changes cannot be attributed to climatic forcing alone. Therefore, ice dynamics is suspected as a driver of the rapid retreat.

Ice velocity was measured at some of the SPI calving glaciers. For example, remote sensing techniques have been used to observe the flow speed on Perito Moreno (Ciappa et al., 2010; Michel and Rignot, 1999; Rott et al., 1998; Stuefer et al., 2007), Upsala (Floricioiu et al., 2008, 2009; Sakakibara et al., 2013; Skvarca et al., 2003), and Jorge Montt Glaciers (Rivera et al., 2012a). In-situ ice velocity measurements have been performed at Perito Moreno (Sugiyama et al., 2011), Upsala (Naruse et al., 1995), and Pío XI Glaciers (Rivera et al., 1997). Muto and Furuya (2013) used satellite data to measure the velocity of eight calving glaciers in the SPI from 2002 to 2011. Some glaciers showed significant acceleration during the period of rapid frontal retreat, indicating the importance of ice dynamics in the abrupt glacier changes. Nevertheless, spatial and temporal patterns of ice speed in the SPI have been reported only for limited areas and a relatively short time period. The lack of data obscures the role of the ice dynamics in the rapid glacier changes in the Patagonian Icefields.

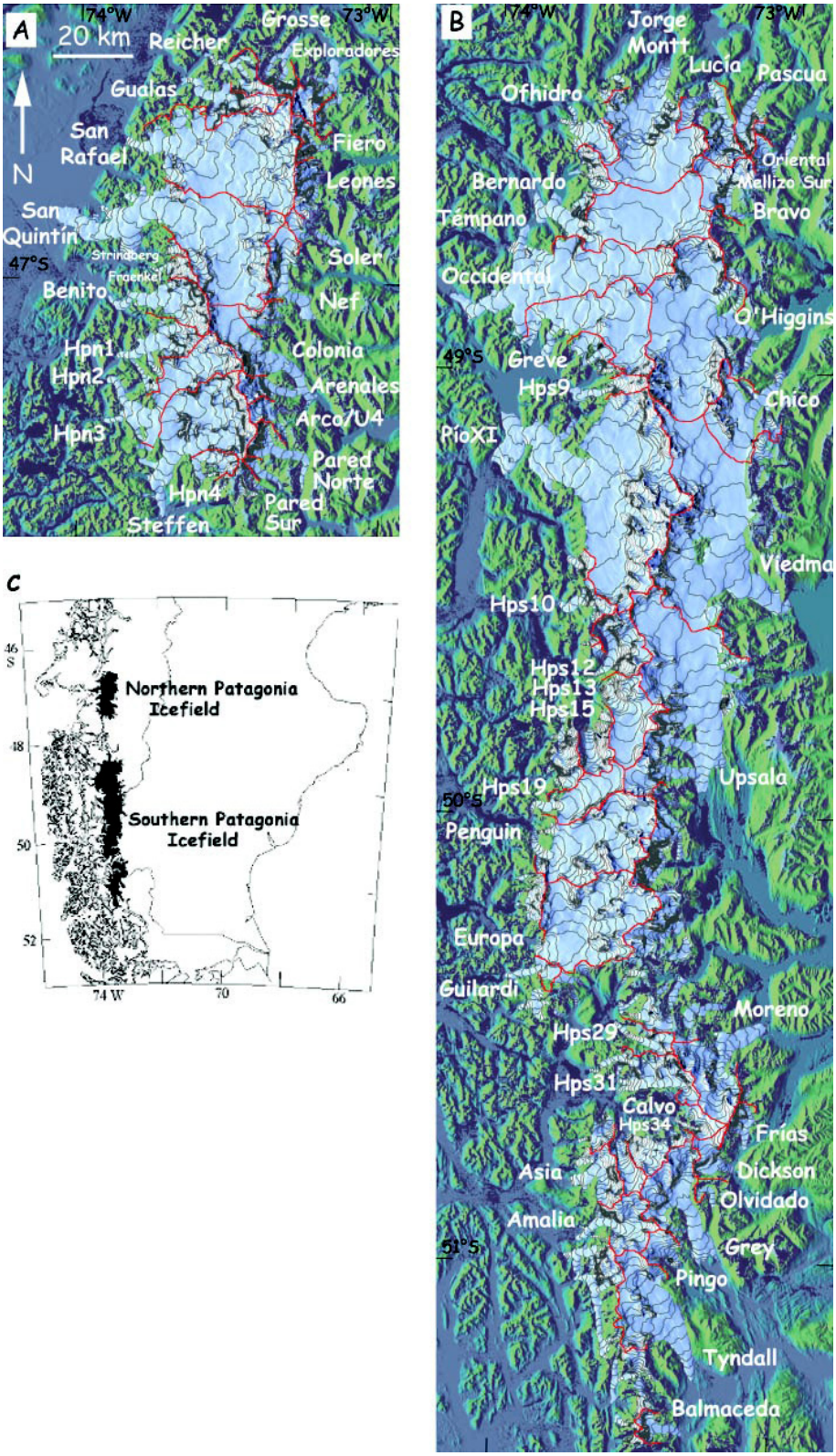

Figure 1.4. Location of glaciers in (a) the NPI and (b) the SPI and (c) location of the icefields in South America (Rignot et al., 2003).

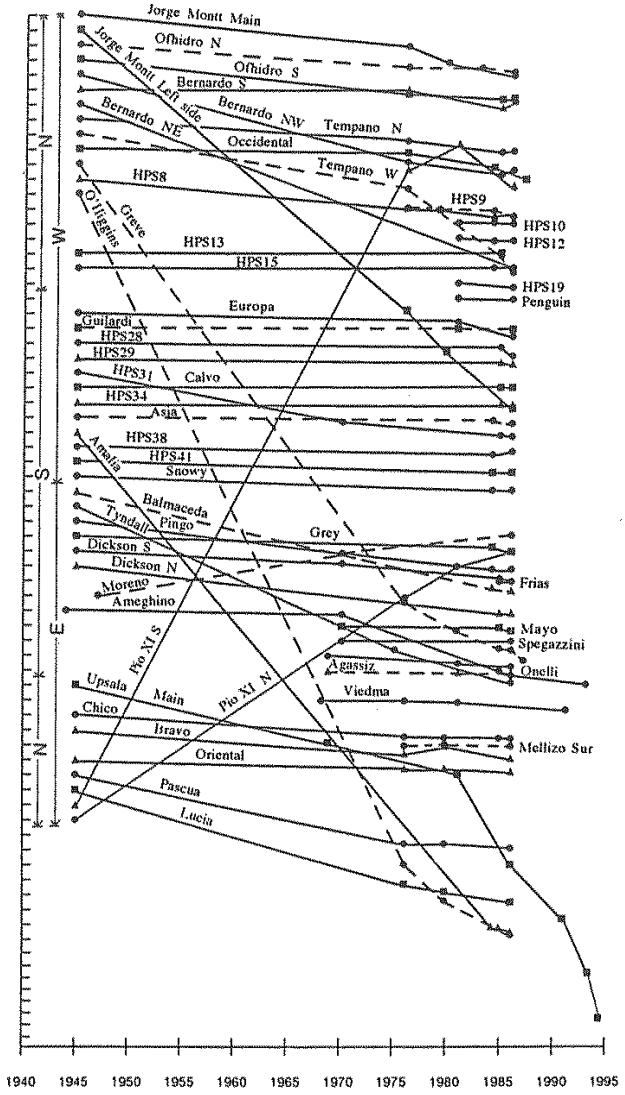

Figure 1.5. Variations in the surface area of outlet glaciers in the SPI. The ordinate is the change in glacier surface area (km^2/1 grid) (Aniya et al., 1997).

1.3. Northwestern Greenland

Marine-terminating outlet glaciers in Greenland have experienced significantly large changes since the beginning of the 21st century. Retreat, thinning, and acceleration of the glaciers have been reported in numerous observations (e.g. Howat and Eddy, 2011; Joughin et al., 2010; Moon and Joughin, 2008; Moon et al., 2012; Pritchard et al., 2009; Rignot and Kanagaratnam, 2006). Remarkable changes have occurred particularly at

large and fast-flowing glaciers (e.g. Jakobshavn, Helheim, and Kangerdlugssuaq Glaciers), which dominate ice discharge from the ice sheet (Howat et al., 2005, 2007, 2011; Joughin et al., 2004, 2008b; Luckman et al., 2006) (Fig. 1.6). Detailed observations showed that the glaciers accelerated when the termini retreated, suggesting reduction in the stresses resisting ice flowing into the ocean (Howat et al., 2008; Luckman et al., 2006).

The observed glacier changes are inhomogeneously distributed along the Greenland coast, and it is increasingly important to monitor the northwestern sector of the ice sheet. Rapid changes in marine-terminating glaciers were initially observed in southeastern Greenland and numerous studies were carried out in this region (e.g. Howat et al., 2008; Murray et al., 2010). The changes are spreading into northwestern Greenland since 2005, as demonstrated by the gravity measurement by the Gravity Recovery and Climate Experiment (GRACE) and a long-term crustal uplift monitoring using the global positioning systems (Khan et al., 2010) (Fig. 1.7). In contrast to the intensive research activities on the southern coast, relatively few studies were carried out on marine-terminating glaciers in northwestern Greenland. Recent studies reported significantly rapid retreat and acceleration of marine-terminating outlet glaciers in northwestern Greenland in the last decade (Howat and Eddy, 2011; Joughin et al., 2010; Moon and Joughin, 2008; McFadden et al., 2011). Kjær et al. (2012) studied glacier surface elevation changes and surface mass balance along the coast of Melville Bay in northwestern Greenland. This study demonstrated significantly large ice loss in this region and the importance of glacier dynamics in the recession of the ice sheet. However, these previous studies were carried out in subdecadal or longer temporal resolutions, and thus more frequent observations are needed to investigate the mechanisms of the changes in marine-terminating outlet glaciers.

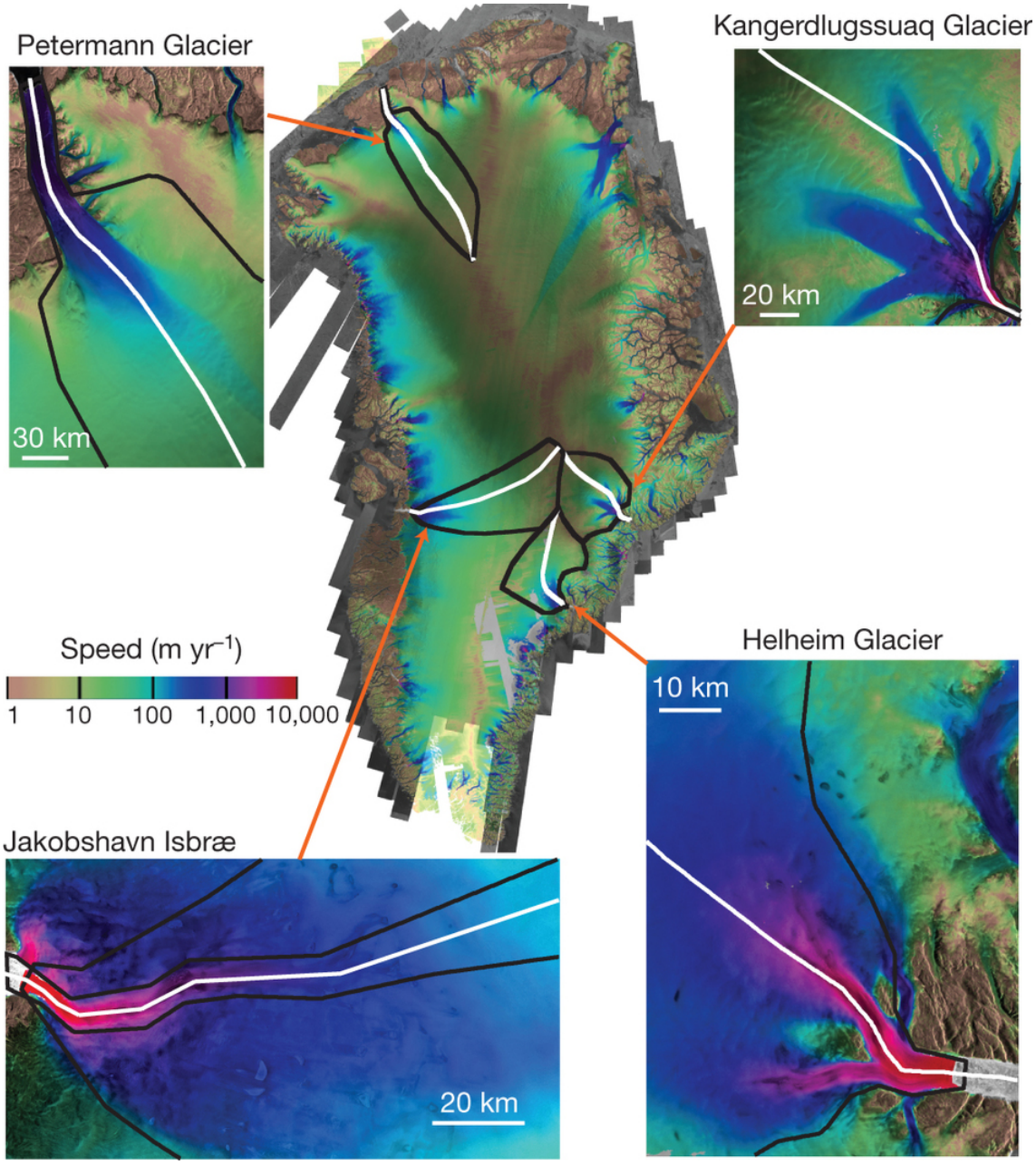

Figure 1.6. Velocity map of the Greenland ice sheet and the major outlet glaciers (Nick et al., 2013).

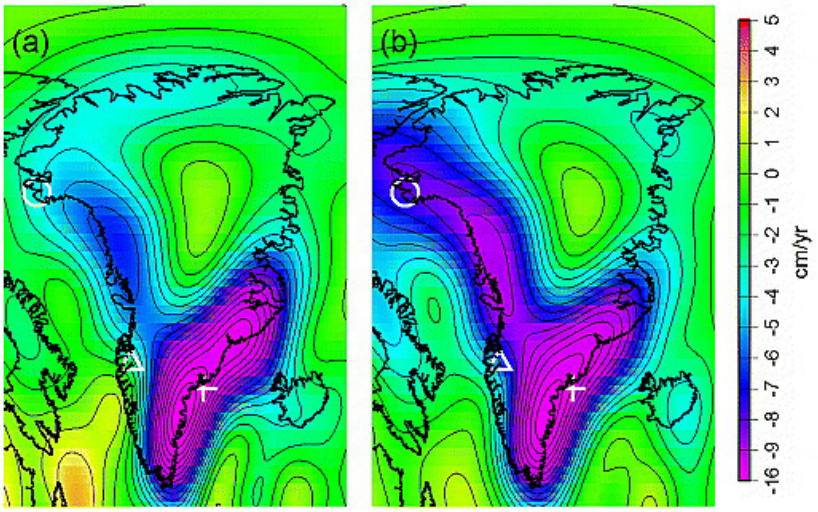

Figure 1.7. The rate of mass loss of the Greenland ice sheet determined from monthly GRACE gravity field solutions (water equivalent). (a) The mean rate between February 2003 and February 2007. (b) The mean rate between February 2003 and June 2009 (Modified from Khan et al., 2010).

1.4. Rapid retreat and flow acceleration of calving glaciers

Observations and numerical simulations reported in previous studies suggested that bed topography plays an important role in rapid retreat of calving glaciers (e.g. Howat et al., 2007; Joughin et al., 2008a; Nick et al., 2009; Vieli et al., 2002). Previous studies also demonstrated that terminus position is relatively stable or changes slowly when the bed is sloping in flow direction, whereas terminus on upslope bed tends to retreat rapidly (e.g. Howat et al., 2007; Vieli et al., 2001). This is because ice flux due to calving increases as ice front retreats over an up-sloping bed (Meier and Post, 1987, van der Veen, 1996). Increase in the ice flux induces thinning of the glacier, and this feedback between retreat and thinning causes further change at the front of a calving glacier. Therefore, a calving glacier terminating on up-sloping bed is considered to be unstable (Nick et al., 2009; Schoof, 2007). Another interpretation of the influence of bed topography on rapid retreat of a calving glacier is flotation of ice. Ice front approaches to flotation condition when the front retreats into deeper water. Flotation of a large portion of ice near the calving front allows crevasses to penetrate full thickness of the ice, and such englacial fractures trigger a large scale calving event and collapse of

glacier terminus (Joughin et al., 2008a; Meier and Post, 1987; van der Veen, 1996). These processes have been proposed as the drivers of the rapid retreat of calving glaciers. However, lack of measurements in the vicinity of calving front obscures the influence of basal topography on the glacier retreat and detailed mechanisms connecting the topography and glacier front dynamics.

Previous studies proposed several mechanisms as drivers of ice flow acceleration of a calving glacier. One mechanism is that meltwater input to the glacier bed, which potentially changes glacier dynamics as elevated subglacial water pressure enhances basal ice motion (e.g. Andersen et al., 2010; Meier and Post, 1987; Sole et al., 2011; Sugiyama et al., 2011). Because amount of meltwater increases as air temperature rises, currently warming atmospheric condition potentially drives glacier acceleration (e.g. Bartholomew et al., 2010; Doyle et al., 2013; Sundal et al., 2011; van de Wal et al., 2008; Zwally et al., 2002). The second mechanism is the change in the force balance near the terminus. Forces acting on the glacier change when the glacier retreats, thins, and loses floating tongues (Nick et al., 2009; Thomas, 2004). These geometrical changes of a glacier sometimes reduce resistive stress acting on the terminus (Howat et al., 2005; Joughin et al., 2004; Thomas, 2004). Initial speedup causes surface steepening because glacier terminus thins more rapidly than upper reaches. This steepening then drives further acceleration and it propagates upglacier (Howat et al., 2005; Joughin et al., 2003; Payne et al., 2004). Such a change in the stress regime is also affected by basal topography and besides the glacier, e.g. bed depression or non-uniform valley width in a fjord (Howat et al., 2007; Nick et al., 2009). Another link between glacier geometry and ice dynamics is that ice thinning reduces effective pressure and causes further speedup (Meier and Post, 1987; Pfeffer, 2007). Because speedup causes ice thinning, a positive feedback mechanism may also exist between the thinning and acceleration. To understand the general mechanism of calving glacier speed up, it is important to specify the most dominant process for flow acceleration observed at each individual glacier.

1.5. Calving laws

Frontal variation of a calving glacier is determined by the calving rate (including iceberg calving and ablation due to melting) and ice flow velocity. The change in the glacier length *dL* over time *dt* is given by

$$\frac{dL}{dt} = u - \dot{c}, \tag{1.1}$$

where *u* is flow velocity at the glacier front averaged over the depth, and $\dot{c}$ is the calving rate which is defined by the total volume of icebergs generated per unit time by the cross-sectional area of the front (Cuffey and Paterson, 2010). Here, ice melt in the water is implicitly included in the second term. Glacier length does not change when the calving rate is equal to the flow velocity. Frontal retreat occurs when the calving rate is larger than the flow velocity. Therefore, changes in the calving rate are very important for the length change of calving glaciers.

Despite its importance in calving glacier changes, the calving rate is very difficult to determine by observations. Thus, many different approaches have been proposed to compute the calving rate from other observable variables. In the earlier period of the study, the calving rate was often related to water depth at the terminus with empirical relationships (Brown et al., 1982; Meier and Post, 1987; Pelto and Warren, 1991). This approach has a problem for rapid retreat of calving glaciers. Because the calving rate of Columbia Glacier increased irrespective of water depth during its rapid retreat. To overcome the problem, the calving rate was related to the height of the calving front above hydrostatic equilibrium condition (van der Veen, 1996, 2002). Minimum thickness above hydrostatic equilibrium condition h_0 is defined by

$$h_0 = h - \frac{\rho_w}{\rho_i} d, \tag{1.2}$$

h and *d* are ice thickness and water depth at the front and ρ_w and ρ_i are densities of glacier ice and water in front of the glacier. Conversely, flotation level of the glacier is defined by water level which fulfills the hydrostatic equilibrium condition of the terminus. It is proposed from observations at Columbia Glacier that the calving rate increases when h_0 is less than 50 m (van der Veen, 1996). For example, thickness above flotation decreases as the glacier thins, and this results in increase in the calving rate. As

the calving rate increases, glacier front retreats according to Equation (1.1). This calving law was widely used for calving glacier models. Such models were able to reproduce observed rapid retreat of calving glaciers to some extent (Nick et al., 2009; Vieli et al., 2002). However, this criterion can be applied only to grounded termini and it is difficult to use for floating termini. More recently, a new approach was proposed with consideration of mechanical processes near the ice front. This method relates the calving rate to the depth of crevasses near the calving front. This concept can be implemented in a model by relating the crevasse depth to longitudinal stress near the terminus (Benn et al., 2007). The formation of crevasses is controlled by longitudinal stretching of ice, thus it can be computed from ice flow patterns. In this criterion, the position of the calving front was determined as the point where crevasse depth equals the ice height above water level in front of the terminus. A modeling study using this criterion was able to reproduce retreat of floating termini (Nick et al., 2010). However, this criterion does not represent the exact physical processes of crevasse penetration into the ice. Because evolution of a glacier in a model is largely dependent on the choice of a calving law, it is necessary to improve our understanding of processes controlling calving (Nick et al., 2010).

1.6. Objectives of this study

The objective of this study is to quantify changes in frontal positions and flow velocities of calving glaciers in the Southern Patagonia Icefield and northwestern Greenland. Then observed changes of the calving glaciers are analyzed to find the mechanisms controlling rapid retreat and flow acceleration. In order to achieve these objectives, this study aims

1. to measure ice front positions and flow velocities of calving glaciers in the SPI and northwestern Greenland by means of satellite image analysis.

2. to measure basal topography and glacier geometry of rapidly retreating Upsala Glacier in the SPI by means of field observation and satellite data analysis.

In Part 1, schemes of measurements of ice front positions and flow velocities are developed. These schemes are applied for 47 calving glaciers in the SPI and the

Prudhoe Land, northwestern Greenland. By means of these measurements, frontal variations and velocity changes for the studied glaciers are quantified over the last 20 years. Frontal variations are compared with velocity changes to investigate the influence of the ice dynamics on the glacier variation. Based on these results, causes of the recent glacier changes in the SPI and the Prudhoe Land are discussed, with special attention to the ice speed changes of rapidly retreating calving glaciers.

In Part 2, field observations and satellite data analysis were carried out at Upsala Glacier in the SPI, which has shown rapid retreat and acceleration since 2008. This detailed study on one of the largest calving glaciers in Patagonia aims to investigate changes in glacier geometry during the rapid retreat and flow acceleration. Basal topography of this glacier was measured by in-situ bathymetric survey at the proglacial lake, where lake bottom is recently uncovered from the terminus of the glacier. Surface elevations were measured using digital elevation models (DEMs) derived from satellite images. Changes in the glacier geometry were investigated with frontal retreat and flow velocity to find the mechanisms triggered the initial retreat in 2008, and controlled subsequent rapid retreat and flow acceleration.

Chapter 2

Satellite data analysis

In order to measure ice front positions and flow velocities, I analyzed satellite images acquired by Landsat series. The satellite images acquired by Landsat have longer-term archives and larger spatial coverage than other similar optical sensors. Ice front positions are manually delineated on false color images. Flow velocities are determined using feature tracking scheme applied for repeated images (Scambos et al., 1992). For the analyses I have coded the computer programs in this study. This was important to process a large amount of satellite images with optimal settings and parameters.

2.1. Satellite images

To measure glacier front positions and ice velocities, satellite images of Landsat 8 Operational Land Imager (OLI) (level 1T, with 15/30 m resolution, 2013–2014), Landsat 7 Enhanced Thematic Mapper Plus (ETM+) (level 1T, with 15/30 m resolution, 1999–2014), and Landsat 4 and 5 Thematic Mapper (TM) (level 1T, with 30 m resolution, 1984–2009) were used (Tables 2.1 and 2.2). These images are distributed by the United States Geological Survey (USGS). Failure of the scan-line corrector (SLC) on the ETM+ after 31 May 2003 resulted in strips of missing value; however, the geometric quality of the data, when properly masked, is as good as the pre-SLC failure data (Howat et al., 2010).

Table 2.1. Landsat images used for the measurements of calving glaciers in the SPI.

Satellite	Period	Resolution (m)	Band	Number	Path/Row
Landsat 4	1989–2007	30	3, 4, 5	7	
Landsat 5	1984–2009	30	3, 4, 5	197	230/95, 96; 231/94,
Landsat 7	1999–2014	30/15	3, 4, 5, 8	350	95, 96; 232/94, 95
Landsat 8	2013–2014	30/15	4, 5, 6, 8	61	

Table 2.2. Landsat images used for the measurements of calving glaciers in northwestern Greenland.

Satellite	Period	Resolution (m)	Band	Number	Path/Row
Landsat 4	1988	30	3, 4, 5	2	032, 033, 034, 035,
Landsat 5	1987–1998	30	3, 4, 5	15	036, 037, 038, 039 /
Landsat 7	1999–2014	30/15	3, 4, 5, 8	193	004; 029, 030, 031,
Landsat 8	2013–2014	30/15	4, 5, 6, 8	86	032, 033, 034 / 005

2.2. Ice front position measurement

Glacier front positions were mapped using false color composite images of bands 3–5 for Landsat 4/5/7 (30 m resolution) and bands 4–6 for Landsat 8 (30 m resolution) (McNabb and Hock, 2014). In each image, the ice fronts of the studied glaciers were manually delineated using geographic information system software QGIS. Mean displacement of the calving front was computed by dividing the areal change near the terminus between two successive images by the width of the ice front (Moon and Joughin, 2008) (Fig. 2.1). The main sources of uncertainty in this measurement are errors in manual delineation and accuracy of geo-location of the images. The relative positioning error introduced in the process of overlapping Landsat images was ±64 m, based on the horizontal displacement of off-ice surface features computed by the method described in Section 2.3.

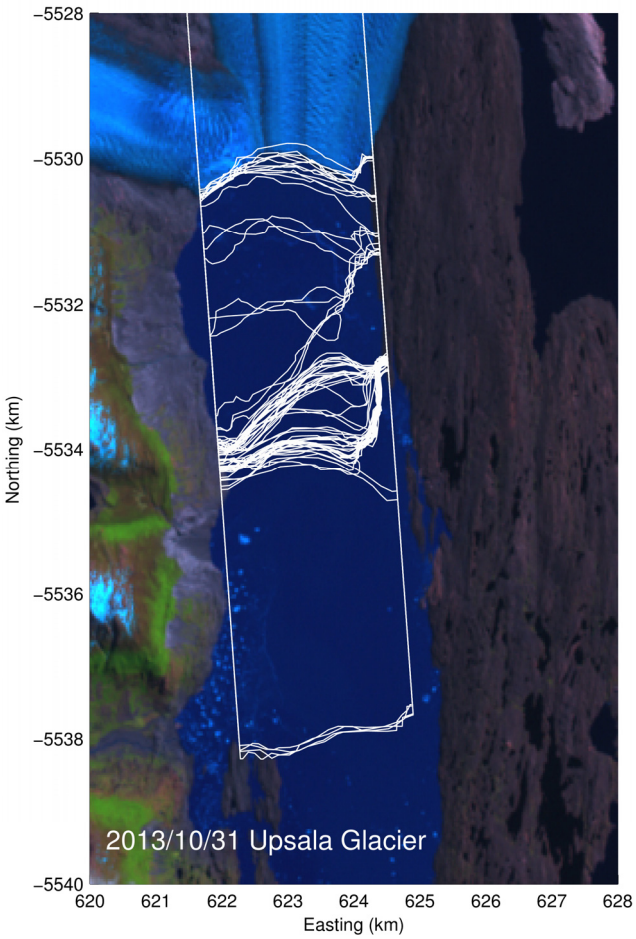

Figure 2.1. Ice front positions of Upsala Glacier from 1985 to 2014 delineated on satellite images. The two parallel lines along the glacier margins define the region considered for the areal change measurement. Background image is a false color composite of Landsat 8 OLI image acquired on 31 October 2013.

2.3. Ice velocity measurement

Ice speeds were measured by tracking displacement of glacier surface features on temporally separated satellite image pairs. To automatically track the surface features, a computer code of image matching algorithm based on the cross correlation of the image pairs was developed in this study (e.g. Scambos et al., 1992). Cross correlation is computed in the frequency domain by multiplying the Fourier transform of one image and the complex conjugated Fourier transform of the second image (McClellan et al., 2003). The cross correlation surface *CC* is given by

$$CC(x,y) = \mathrm{IFFT}\left(\mathrm{FFT}(f(x,y)) \times \mathrm{FFT}(g(x,y))^{*}\right), \tag{2.1}$$

where FFT($f(x,y)$) is the fast Fourier transform (FFT) of the intensity data within the matching window from the first image of an image pair, FFT($g(x,y)$) is the FFT of the intensity data within the matching window from the second image, the asterisk (*) denotes the complex conjugate, and IFFT is the inverse fast Fourier transform (Fig. 2.2). Fitch et al. (2002) developed a method called orientation correlation. Taking f as the matching window from the first image and g as that from the second image, the orientation images f_o and g_o are given by

$$f_o(x,y) = \mathrm{sgn}\left(\frac{\partial f(x,y)}{\partial x} + i\frac{\partial f(x,y)}{\partial y}\right), \tag{2.2}$$

$$g_o(x,y) = \mathrm{sgn}\left(\frac{\partial g(x,y)}{\partial x} + i\frac{\partial g(x,y)}{\partial y}\right), \tag{2.3}$$

$$\text{where } \mathrm{sgn}(x) = \begin{cases} 0 \text{ if } |x| = 0 \\ \frac{x}{|x|} \text{ otherwise} \end{cases}, \tag{2.4}$$

sgn is the signum function and i is the complex imaginary unit. To measure offset of the surface features, cross correlation surface was calculated using these orientation images in the frequency domain. This method is referred as the cross correlation on orientation images (CCF-O) method (Haug et al., 2010; Heid and Kääb, 2012). The CCF-O method was employed in this study because this scheme works better than conventional methods regardless of image contrast (Heid and Kääb, 2012). Another advantage of the CCF-O method is its ability to process the striped Landsat images which occurred after the SLC failure (Heid and Kääb, 2012). The offset measurement was achieved in a subpixel resolution by upsampling intensity data within matching windows by a factor of 16 in the frequency domain (Guizar-Sicairos et al., 2008).

For this measurement, band 3 images for Landsat 4/5 (30 m resolution) and band 8 images for Landsat 7/8 (15 m resolution) were used. The band 3 images were interpolated to 15 m resolution using a bi-cubic interpolation scheme. Sizes of the matching windows and spatial resolutions of the calculation used in this study are summarized in Table 2.3. The window size of f was adjusted to the same size as g by padding the surrounding area with zero. Image pairs used for the measurement were automatically selected according to the acquired date, spatial coverage, image quality

and cloud cover.

In total, I processed 3397 pairs of the Landsat images acquired from 1984 to 2014 with temporal separations of 16–365 days. Results obtained with a low signal-to-noise ratio (< 20), which occurred typically in snow-covered accumulation areas, were excluded. Displacement vectors based outside the glaciers were removed using digital glacier outlines, that are from the Global Land Ice Measurements from Space (GLIMS) (Bishop et al., 2004; Kargel et al., 2005; Raup et al., 2007) for the SPI and the Greenland Mapping Project Ice Cover Mask (Howat et al., 2014) for northwestern Greenland. Remaining vectors were filtered if they deviated by more than a certain angle or magnitude threshold from a median vector that was computed within either the 5×5 or 3×3 grid areas (Heid and Kääb, 2012; Kääb et al., 2005; Sakakibara and Sugiyama, 2014) (Table 2.3). To obtain a smooth flow field, the median values of 5×5 neighboring pixels in the displacement vector fields were taken (Howat et al., 2010) (Fig. 2.3).

Possible errors in a feature tracking method include (1) ambiguities in the cross-correlation peak, (2) co-registration errors, and (3) false correlations (Howat et al., 2010). Errors caused by (1) and (2) were estimated from the root mean square of horizontal displacement of off-ice surface pixels, where the displacement should be zero. Errors caused by (3) were minimized by applying the filters described above. The sum of the errors (1)–(2) computed for each image pair ranged from a few to 300 m a^{-1}, depending on image quality and temporal separation. Ice speed obtained by the satellite image analysis was validated by comparing data with in-situ global positioning system (GPS) measurements on Moreno, Upsala, and Viedma Glaciers in the SPI. The GPS measurements were performed during a field campaign in the SPI over a period between December 2012 and January 2013 (Table 2.4). These results showed that the ice speeds derived from satellite images well agreed with the field data obtained using the GPS.

Table 2.3. Sizes of the matching windows, spatial resolutions of the calculation, and filtering thresholds for the direction and magnitude filters.

Region	Window size (pixels)		Resolution	Filtering threshold	
	f	*g*	(pixels)	Direction (°)	Magnitude (m)
SPI	30×30	80×80	8×8	20	200
Northwestern Greenland	40×40	80×80	10×10	20	50

Table 2.4. Comparison between ice speeds measured using the Landsat images and those measured in the field at the same locations by GPS.

Site	Satellite image analysis		GPS measurement	
	Period	Speed (m a^{-1})	Period	Speed (m a^{-1})
Perito Moreno A	Oct 2012-Dec 2012	590±90	Jan 2013	549
Perito Moreno B	Dec 2012-Apr 2013	670±30	Jan 2013	648
Upsala	Oct 2012-Dec 2012	930±60	Jan 2013	893
Viedma	Aug 2012-Oct 2012	750±40	Jan 2013	755

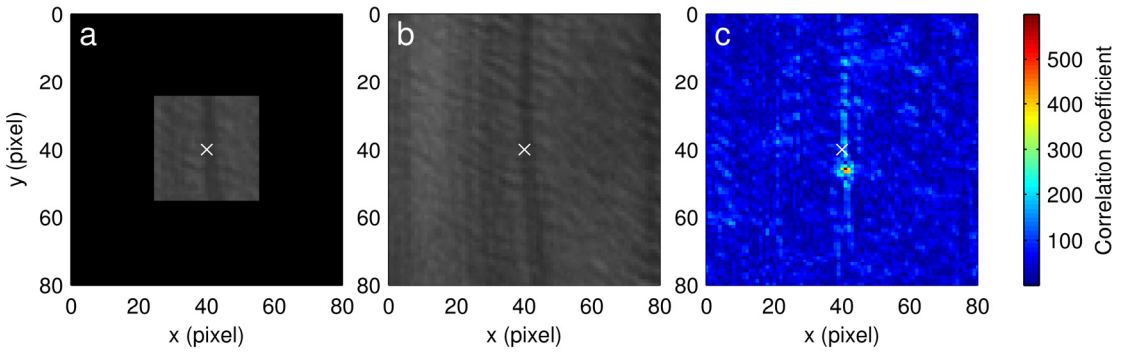

Figure 2.2. Matching windows defined on (a) the first image and (b) the second image and (c) cross correlation surface between the matching windows.

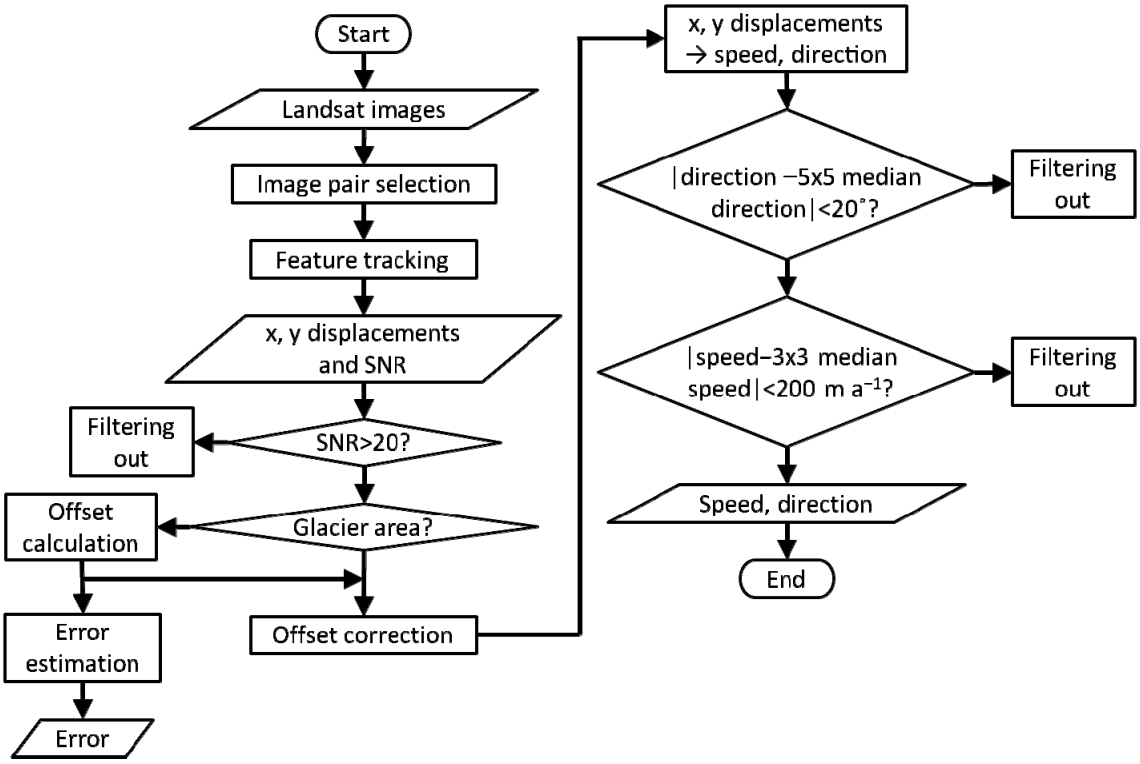

Figure 2.3. Work flow of the ice velocity measurement and post processing. Parameters shown in this figure are values applied for the measurements of calving glaciers in the SPI.

Chapter 3

Calving glaciers in the Southern Patagonia Icefield

In order to quantify changes in ice front position and flow velocity of calving glaciers in the SPI, I analyzed Landsat images acquired from 1984 to 2014. The procedures described in Chapter 2 were carried out on 32 termini of 28 calving glaciers in the SPI (Ofhidro, Bernardo, Greve, and Pío XI Glaciers have two termini). Total surface area of each studied glacier is greater than 100 km^2 as determined in Aniya et al. (1996) (Fig. 3.1). Using obtained ice front positions and flow speeds, changes in the calving glaciers are quantified. Based on these results, I discuss possible mechanisms driving recent glacier changes in the SPI are discussed. Particularly, the role of ice speed acceleration in the rapid retreat of calving glaciers is discussed in details.

3.1. Results

3.1.1. Ice front position

Among the 32 termini studied, only the two termini of Pío XI Glacier advanced between 1980s and 2014. Of the other 30 termini, 11 termini changed less than ±20 m a^{-1}, and 17 termini retreated by more than 20 m a^{-1} (Fig. 3.1 and Table 3.1). The results show a large variation in the magnitude of the glacier retreat. Jorge Montt, HPS12, and Upsala Glaciers retreated at rates greater than 200 m a^{-1}, which significantly exceed the mean and median retreat rates of 66 m a^{-1} and 26 m a^{-1} for the all termini. Excluding the three rapidly retreating glaciers, the mean retreat rate was 3 m a^{-1} for ocean-terminating glaciers and 57 m a^{-1} for lake-terminating glaciers. Temporal variations in the retreat rate were relatively small, as indicated by the change in the mean (median) retreat rate from 82 (28) m a^{-1} in 1984–1999 to 68 (33) m a^{-1} in 2000–2014 (Table 3.1).

Jorge Montt, HPS12, Upsala, and Pío XI Glaciers showed substantially greater and more complex frontal variations than the other glaciers (Fig. 3.2). The front position of Jorge Montt Glacier varied only slightly before 1987, but it rapidly retreated from 1987 to 2000 at a rate of 590 m a^{-1}. The retreat gradually slowed down between 2000 and

2010, followed by another rapid retreat at a rate of 700 m a^{-1} from 2010 to 2012. The total retreat distance from 1984 to 2014 was 11.9 km (396 m a^{-1}). The retreat rate of HPS12 Glacier was 320 m a^{-1} for 1984–2009, and it increased to 1030 m a^{-1} for 2009–2014. Upsala Glacier retreated at a rate of 90 m a^{-1} between May 2000 and January 2008 then the retreat rate suddenly increased to 880 m a^{-1} between January 2008 and May 2011. An even more rapid retreat (2000 m a^{-1}) occurred between November 2010 and May 2011 (Sakakibara et al., 2013). Unlike the other glaciers, Southern terminus of Pío XI Glacier consistently advanced, except for short retreat episodes such as 0.85-km retreat from 1999 to 2000. Total advance of the terminus from 1984 to 2014 was 1.65 km. This glacier has a second calving front further north, which also advanced, but the advance was smaller than the southern terminus.

Table 3.1. Cumulative displacement of the glacier front positions between 1984 and 2014. The rates are computed for periods of 1984–2014, 1984–1999 and 2000–2014. Positive values indicate glacier advance.

Glacier	1984–2014 (km)	1984–2014 (m a^{-1})	1984–1999 (m a^{-1})	2000–2014 (m a^{-1})
Jorge Montt	−11.87±0.11	−396±4	−543±8	−248±8
Ofhidro N	−1.68±0.11	−56±4	−37±8	−79±8
Ofhidro S	−2.15±0.11	−72±4	−83±8	−59±8
Bernardo E	NA	NA	NA	−68±8
Bernardo W	−1.68±0.11	−56±4	−33±8	−80±8
Tempano	−1.63±0.11	−54±4	−66±8	−42±8
Occidental	−4.27±0.11	−151±4	−47±9	−259±8
Greve W	−5.15±0.11	−172±4	−280±8	−66±8
Greve E	NA	NA	NA	−244±8
Pío XI N	1.27±0.11	42±4	51±8	50±8
Pío XI S	1.65±0.11	55±4	42±8	97±8
HPS12	−13.06±0.11	−437±4	−303±8	−665±8
HPS13	0.14±0.11	5±4	4±8	8±8
HPS15	0.07±0.11	2±4	5±8	−2±8
HPS19	0.23±0.11	8±4	NA	10±8
Penguin	0.21±0.11	7±4	10±8	10±8
Europa	−0.11±0.11	−4±4	NA	−1±8
Guilardi	−0.41±0.11	−14±4	−12±8	−12±8
HPS31	0.01±0.11	0±4	NA	0±8
Calvo	0.19±0.11	6±4	NA	6±8
HPS34	−0.22±0.11	−7±4	−14±9	−12±8
Asia	−0.89±0.11	−30±4	NA	0±8
Amalia	−0.62±0.11	−21±4	NA	−26±8
Tyndall	−2.82±0.11	−98±4	−92±8	−79±8
Grey	−2.07±0.11	−69±4	NA	−44±8
Perito Moreno	−0.04±0.11	−1±4	−6±7	15±8
Spegazzini	−0.01±0.11	0±4	−1±7	3±8
Upsala	−7.93±0.11	−260±4	−262±7	−258±8
Viedma	−1.44±0.11	−47±4	−28±7	−65±8
Chico	−0.97±0.11	−32±4	−24±7	−39±8
O'Higgins	−0.67±0.11	−22±4	−25±8	−6±8
Lucia	−3.26±0.11	−109±4	−150±8	−66±8
Mean		−66	−82	−68
Median		−26	−28	−33

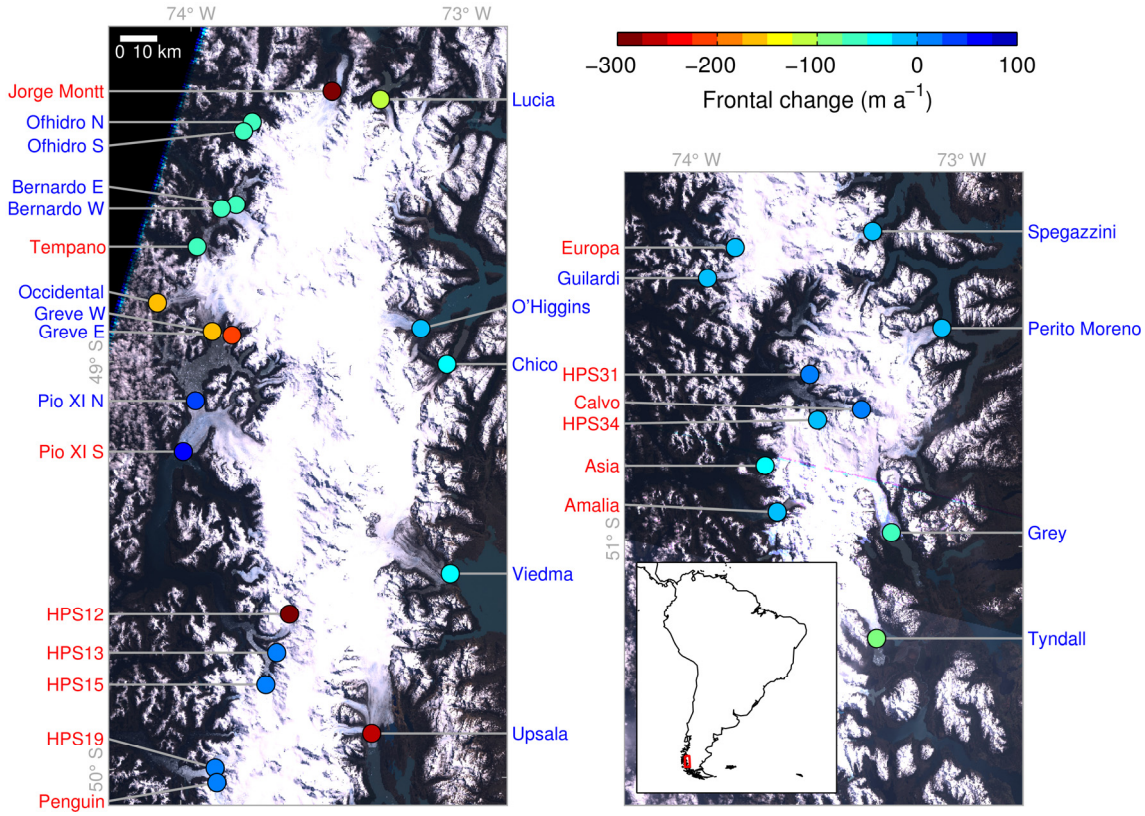

Figure 3.1. Rates of change in the ice front positions from 1984 to 2014 (advance is positive). Names of ocean-terminating glaciers are indicated in red, whereas lake-terminating glaciers are in blue. Background is a true color mosaic Landsat 7 ETM+ image acquired on 14 October 2001. The left panel indicates northern half of the SPI, and the right panel indicates the southern half. The inset shows the location of the SPI in South America.

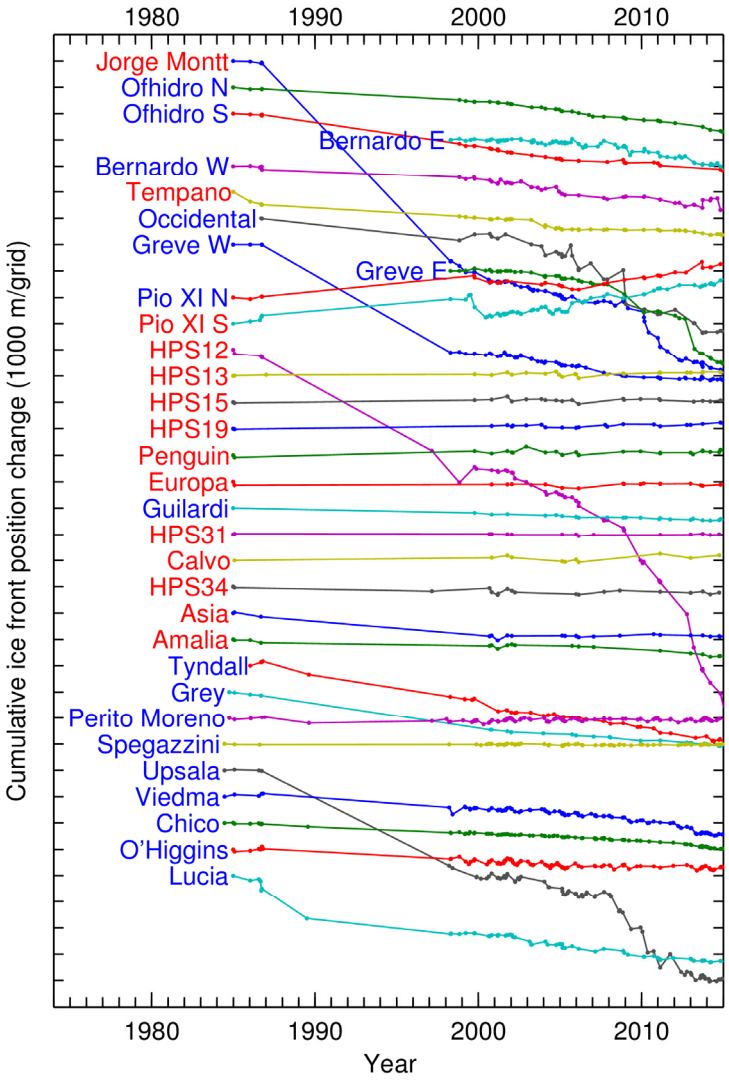

Figure 3.2. Cumulative changes in the ice front positions of the studied glaciers from 1984 to 2014. Upward change in the ordinate represents glacier advance. Names of ocean-terminating glaciers are indicated in red, whereas lake-terminating glaciers are in blue.

3.1.2. Ice speed

Figure 3.3 shows the distribution of the mean ice speed over the SPI in 1984–2014 obtained from Landsat 4 and 5 TM, 7 ETM+, and 8 OLI image pairs. Within lower 5 km of the termini, ice speed ranged between 148 and 5970 m a^{-1} (Table 3.2 and Fig. 3.4). In general, ocean-terminating glaciers flow faster than lake-terminating glaciers. The mean of maximum speed was 2565 m a^{-1} for ocean-terminating glaciers and 886 m a^{-1} for

lake-terminating glaciers. The ocean-terminating glaciers are located on the western side of the icefield (e.g., Jorge Montt, Pío XI, and Penguin Glaciers). Flow speed of these glaciers often exceeds 2000 m a^{-1}. Between 1984 and 2014 ice speed of the studied glaciers changed by the mean and the median rates of 1.1 and −2.4 m a^{-2}, respectively (Table 3.2). Excluding glaciers which largely accelerated such as Jorge Montt, HPS12, and Upsala Glaciers, the mean and the median changing rates are −7.3 and −3.4 m a^{-2}. This shows that the majority of the glaciers decelerated during the period, whereas Jorge Montt, HPS12, Upsala Glaciers accelerated at rates significantly greater than the other glaciers from 1984 to 2014 (Figs 3.4 and 3.5).

Between 1986 and 2000, ice speeds near the front of Jorge Montt Glacier increased from 3620 m a^{-1} to 4380 m a^{-1} (Fig. 3.6a). After the increase, the glacier gradually slowed down until 2009. Then, ice speed within 30-km of the 1984 front increased in 2012 by 200–1970 m a^{-1} and the speed stayed at this level until 2014. Between 1986 and 2000, ice speed of HPS12 Glacier increased from 480 m a^{-1} to 960 m a^{-1} at 8-km from the 1985 front (Fig. 3.6b). The lowest ~10 km further accelerated in 2008 reaching a maximum speed of 3400 m a^{-1} near the front. Near the front of Upsala Glacier, ice speed decelerated from 2080 m a^{-1} to 1660 m a^{-1} in 2000–2002, then accelerated from 1660 to 1990 m a^{-1} in 2004–2007 (Fig. 3.6c). When the glacier started to retreat in 2008, the speed near the front suddenly increased by 110 m a^{-1}, reaching a peak speed of 3840 m a^{-1} at the end of 2009. The lowest reaches of the southern terminus of Pío XI Glacier, the ice speed increased from 2000 m a^{-1} to 4050 m a^{-1} between 1986 and 2000, then gradually decreased with small fluctuations, reaching its lowest level in 2009 (Fig. 3.6d).

Table 3.2. The minimum and maximum ice flow speeds within 5 km from the front and acceleration of the 32 studied termini over a period between 1984 and 2014. The speeds are averaged over a period between 1984 and 2014. The acceleration is the average within 5 km from the front.

Glacier	Minimum (m a^{-1})	Maximum (m a^{-1})	Acceleration (m a^{-2})
Jorge Montt	1378	2550	46
Ofhidro N	236	650	3
Ofhidro S	280	622	−2
Bernardo E	204	336	2
Bernardo W	219	335	6
Tempano	312	720	−12
Occidental	297	367	3
Greve W	719	2050	−13
Greve E	389	585	20
Pío XI N	591	691	14
Pío XI S	534	931	−92
HPS12	880	2040	139
HPS13	3350	3730	0
HPS15	1150	2390	0
HPS19	1800	3100	−8
Penguin	5620	5970	−6
Europa	1152	1880	−7
Guilardi	148	230	−3
HPS31	1920	3200	−16
Calvo	3100	4640	NA
HPS34	1540	1930	6
Asia	400	1340	−8
Amalia	890	1490	3
Tyndall	358	407	−2
Grey	404	1030	−21
Perito Moreno	556	701	−5
Spegazzini	301	1430	−13
Upsala	989	1808	53
Viedma	488	675	9
Chico	150	405	−7
O'Higgins	2070	3040	−50
Lucia	331	580	−4
Mean	1024	1620	1.1
Median	545	1185	−2.4

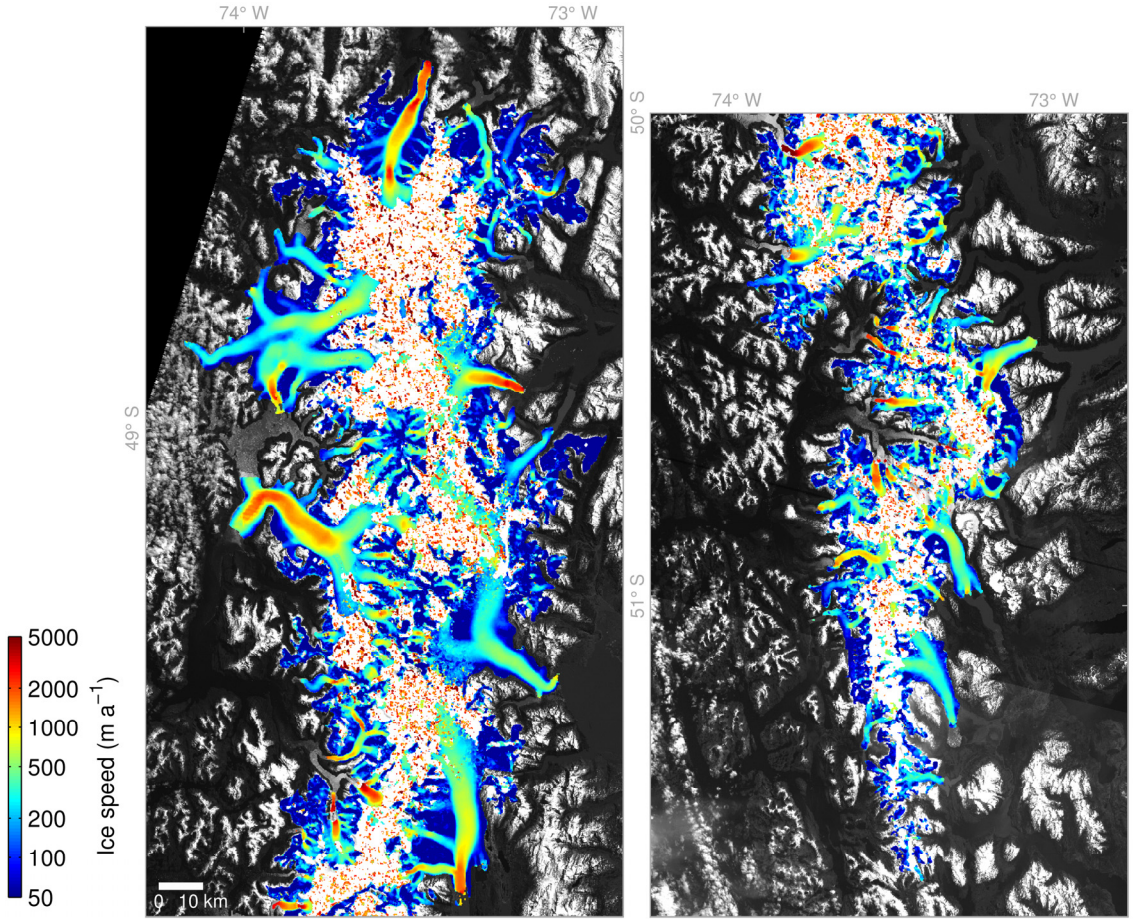

Figure 3.3. Ice speed distributions over the SPI in 1984–2014. Background is a mosaic Landsat 7 ETM+ image acquired on 14 October 2001. The speed at each location equals the mean of all measurements available within the period. The left panel indicates northern half of the SPI, and the right panel indicates the southern half.

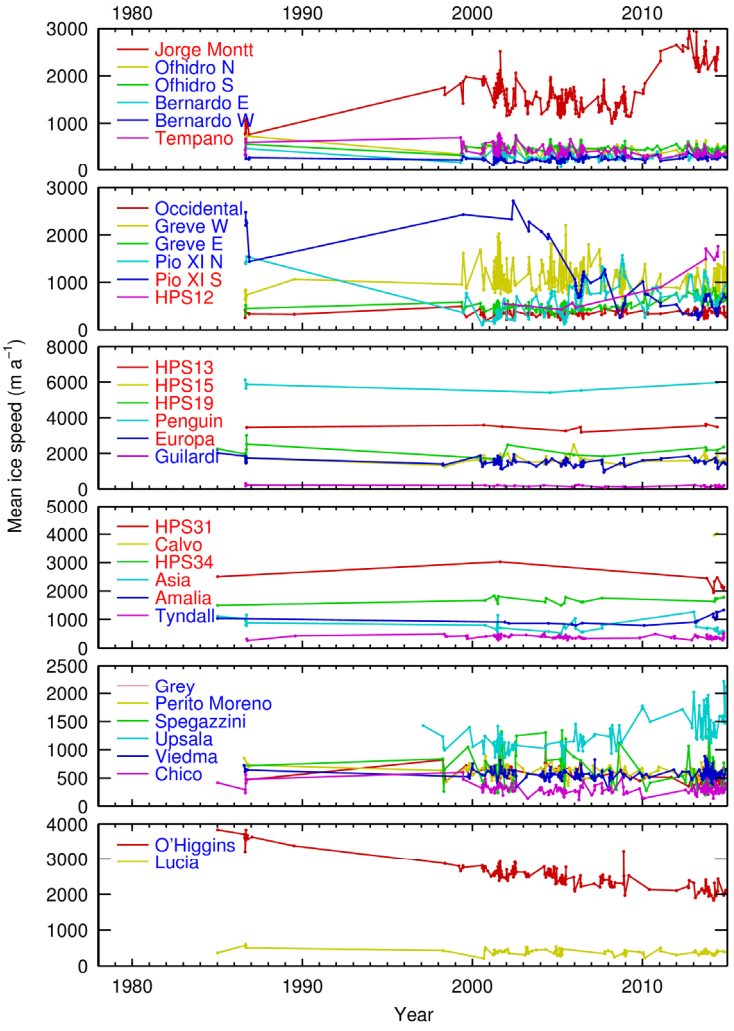

Figure 3.4. Ice speeds for the studied termini from 1984 to 2014. The speeds are averaged within 5 km from the front.

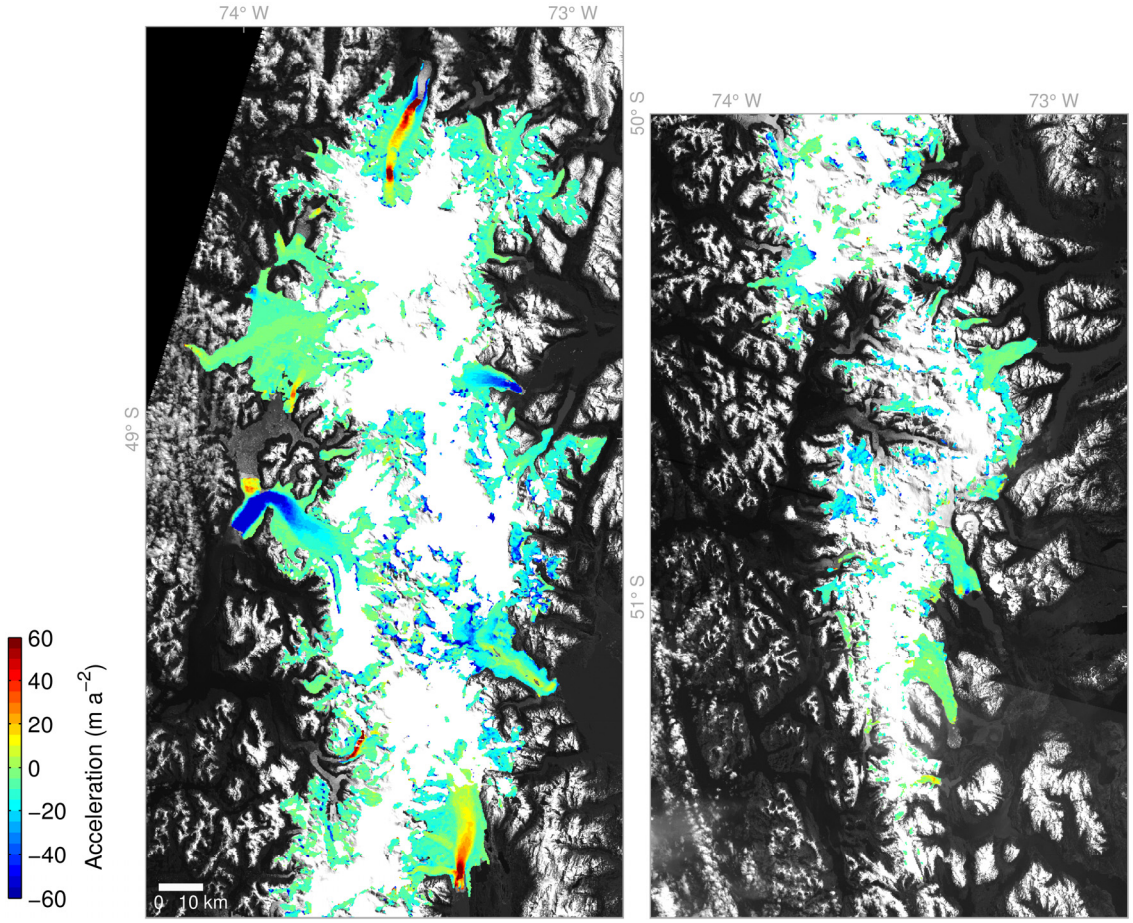

Figure 3.5. Flow acceleration over the SPI in 1984–2014. Background is a mosaic Landsat 7 ETM+ image acquired on 14 October 2001.

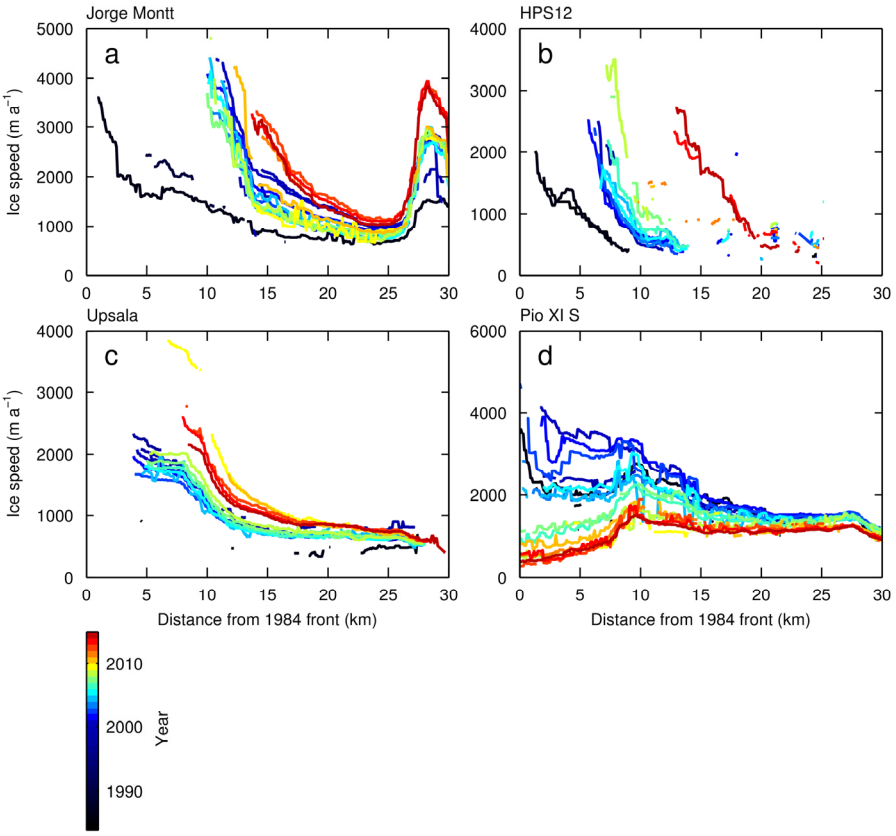

Figure 3.6. Ice speed along the central flowline and its temporal variations at (a) Jorge Montt, (b) HPS12, (c) Upsala, and (d) the southern terminus of Pío XI Glaciers. (See Figure 3.7 for the same plots for all other glaciers.)

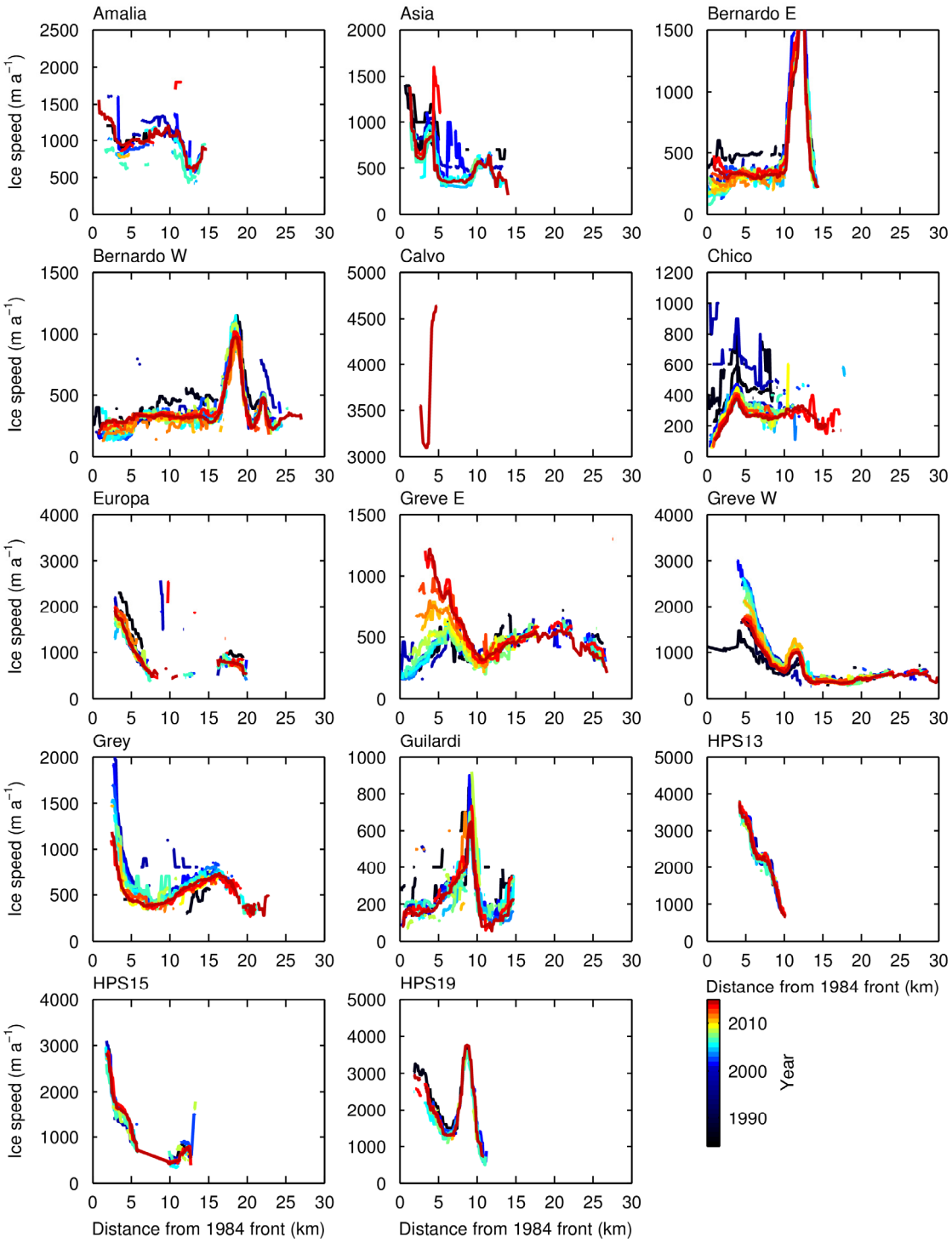

Figure 3.7. Same plot as Figure 3.6 but for all the other glaciers.

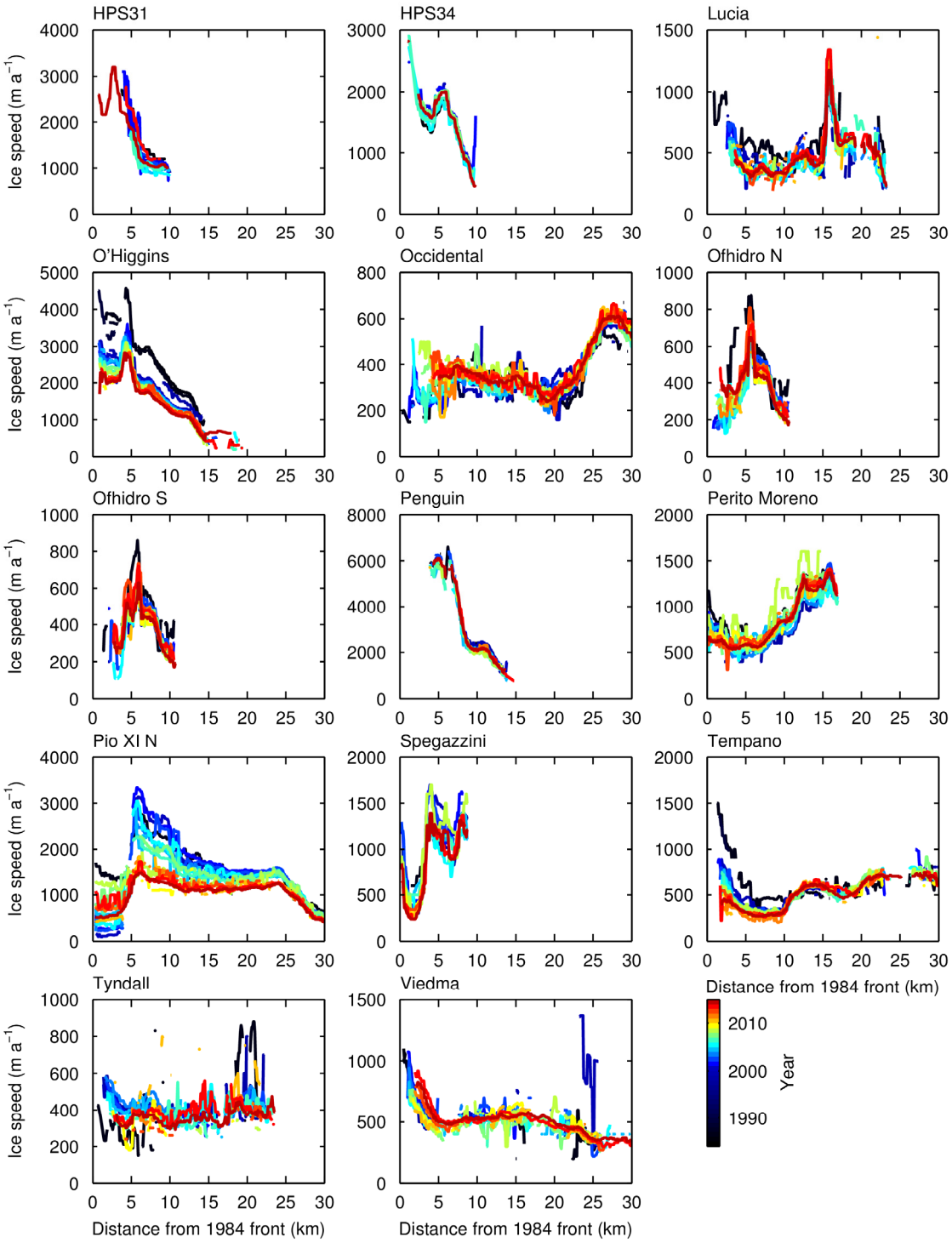

Figure 3.7. (Continued.)

3.2. Discussion

3.2.1. General trends in frontal variations and speed changes

Most of the calving glaciers in the SPI have been retreating over the last 30 years (Figs 3.1 and 3.2), in agreement with areal changes recently reported by Davies and Glasser (2012). Aniya et al. (1997) reported that 65% of the SPI glaciers had lost ice-covered area from 1944/45 to 1985/86. Thus, results of this study indicate that the retreating trend has continued for more than 60 years.

At some of the glaciers, however, patterns of frontal variations significantly changed after 1986. For instance, the retreat rate of O'Higgins Glacier was the greatest in Patagonia for the period 1944–1986 (Aniya et al., 1997), but this glacier retreated at a rate of only 22 m a^{-1} from 1984 to 2014. Similarly, Amalia Glacier retreated at a rate of 278 m a^{-1} in 1945/45–1985/86 (Aniya et al., 1997), whereas the retreat rate from 1984 to 2014 was only 21 m a^{-1}. Compared to these two glaciers, Jorge Montt and Upsala Glaciers retreated faster during a period from 1984 to 2014 as compared to the earlier period. These observations demonstrate that the glaciers in the SPI have been retreating in general, but their rates are spatially and temporally not uniform.

In general, greater retreat rate was observed in the lake-terminating glaciers than the ocean-terminating glaciers (Figs 3.1 and 3.2). This trend is agreed with the glacier variations over the period between 1944 and 1986 reported by Aniya et al. (1997). Aniya et al. (1997) proposed that accumulation area ratio (AAR), which is the ratio of accumulation area to total area, and surface slope of the glaciers caused the difference in glacier variation between the lake-terminating glaciers and the ocean-terminating glaciers. The ocean-terminating glaciers have large AAR (>0.8) and relatively steep surface gradient, resulting in their stable frontal positions (Aniya et al., 1997). This situation likely causes the contrast of frontal variation between lake-terminating glaciers and ocean-terminating glaciers observed between 1984 and 2014.

Changes in the frontal positions are associated with the observed ice speed variations near the terminus. Figure 3.8 compares the magnitude of the frontal variation with flow acceleration over a period between 1984 and 2014 at each glacier. Figure 3.8 illustrates

a relationship between frontal retreat and glacier acceleration. However, this trend arises from the outliers, the three glaciers with the largest retreat. If these rapidly changing glaciers are excluded, the remaining calving glaciers in the SPI are generally decelerating over the study period (Table 3.2 and Fig. 3.8). Except for Pío XI Glacier, the glaciers fall into one of three categories: stable front position without significant ice speed change, gradual retreat with deceleration, and rapid retreat with large acceleration (Fig. 3.8).

A likely driver of the retreat trend lasting for more than 60 years is the warming climate as suggested by Rignot et al. (2003). According to meteorological stations south of 46°S, the climate has warmed 0.4–1.4 °C since the beginning of the last century (Rosenblüth et al., 1995). This warming trend increases in higher latitudes, especially in the eastern side of the Andes. Ibarzabal y Donangelo et al. (1996) found a warming by 0.3 °C in the period 1940–1990 at the weather station in El Calafate (50°30'S). Reanalysis data at 50°S, 75°W also show a warming of 0.5 °C at 850 hPa between 1960 and 1999 (Rasmussen et al., 2007). As a result of this 0.5 °C warming, the melt rate in the ablation areas of the Patagonia icefields has increased by 0.5 m water equivalent according to the estimation by Rasmussen et al. (2007).

The mass balance of Patagonian glaciers is characterized by an extraordinary amount of snowfall in the accumulation area (e.g., Schwikowski et al., 2013; Shiraiwa et al., 2002). Although data from meteorological stations between 51 and 53°S indicate little variation from 1950 to 2000 (Aravena and Luckman, 2009), reanalysis data in the Patagonian icefields show that solid precipitation has decreased about 5% from 1960 to 1999 (Rasmussen et al., 2007). This decrease can be explained by a shift of some precipitation from snow to rain under the rising temperatures. Such an influence of warming on precipitation probably play an important role in the future mass balance of Patagonian icefields, as suggested by a recent modeling study (Schaefer et al., 2013). Since no significant change was observed in accumulation in Patagonia, the long-term retreat trend is most likely due to an increase in melting arising from the warming climate.

In contrast to the influence of atmospheric warming, roles of the ocean and lakes in

glacier retreat is scarcely understood in the Patagonian Icefields (Moffat, 2014). The only observation investigating water circulation and properties in front of calving glacier in the Patagonian Icefields was carried out at Jorge Montt Glacier. The observation indicated that local, along-fjord wind forcing is crucial for modulating the supply of warm water to the glacier front (Moffat, 2014). This process can be important in the melting at the glacier front. To better understand roles of the ocean and lakes in glacier variations of the Patagonian glaciers, long-term observation of water in front of the glaciers is needed.

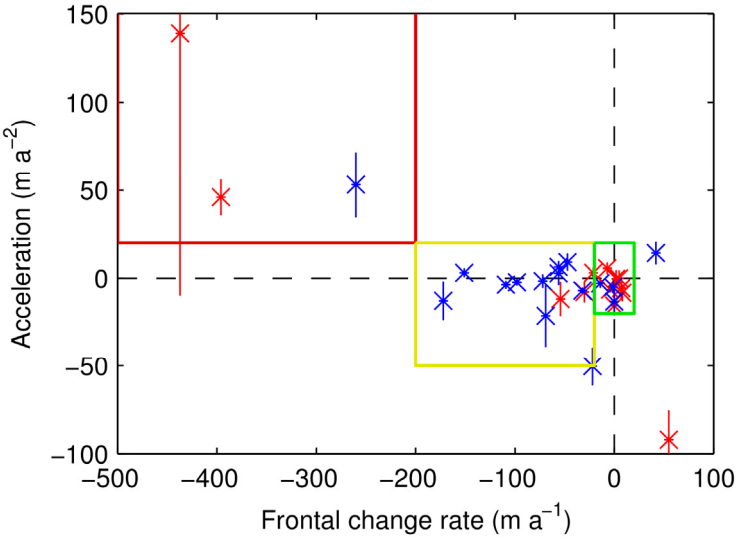

Figure 3.8. Front position change v.s. flow acceleration between 1984 and 2014. Color codes are the same as in Figure 3.1. The ordinate indicates mean acceleration within 5 km from the front and error bar indicates the standard deviation. The three categories: stable front position without significant ice speed change, gradual retreat with deceleration, and rapid retreat with large acceleration, are indicated by green, yellow, and red boxes, respectively.

3.2.2. Acceleration associated with rapid glacier retreat

In most cases, the observed warming trend can explain the retreat of the glaciers in the SPI. However, the exceptionally rapid retreat of Jorge Montt, HPS12, and Upsala Glaciers requires additional interpretation. Their retreat rates exceeded 200 m a^{-1} and

sometimes reached 500 m a^{-1} (Fig. 3.9). These rapidly retreating glaciers also showed large ice speed variations as compared to the other glaciers (Figs 3.6 and 3.7). Comparisons of the front position and ice speed changes demonstrate that the rapid retreats are associated with large ice flow accelerations (Fig. 3.9). To understand the connections between rapid retreat and ice flow acceleration, I look into more details of the front position and ice speed variations in these three glaciers.

Over a period between 2000 and 2008, ice speed of Jorge Montt Glacier at 2.0 km from the 2014 front decelerated from 2100 m a^{-1} to 1670 m a^{-1} with seasonal variations. This deceleration was accompanied by 0.8-km retreat (Fig. 3.10a). Then the ice speed sharply increased by 1560 m a^{-1} from 2009 to 2012. This acceleration coincided with a rapid terminus retreat by 2 km. The elevated speed continued until 2014, while the retreat rate slowed down. Ice speed at 1.3 km from the 2014 front of HPS12 Glacier sharply increased from 910 m a^{-1} to 2020 m a^{-1} in coincident with 3.9-km retreat from 2011 to 2014 (Fig. 3.10b). Ice speed at 3.0 km from the 2014 front of Upsala Glacier indicated no significant changes from 2000 to 2004 (Fig. 3.10c). Then the speed gradually increased from 960 m a^{-1} to 1180 m a^{-1} until 2008, and the front positions were stable during this period. After 2008, glacier rapidly accelerated by 840 m a^{-1} over the next two years, which coincided with the onset of a rapid retreat.

These observations strongly suggest important roles of glacier dynamics in the abrupt changes of the three calving glaciers. The rapid retreats were often accompanied by flow acceleration, and the timing of acceleration closely agrees with the rapid retreat, particularly at Jorge Montt Glacier in 2010 and at Upsala Glacier in 2008 (Figs 3.10a and 3.10c). The magnitude of the speedup was greater near the fronts (Figs 3.6a and 3.6c). This results in more enhanced stretching flow regime in the lower reaches, which should have caused dynamic thinning, i.e. thinning due to compressive vertical strain.

According to recent studies, acceleration was commonly observed in rapidly retreating calving glaciers in Greenland. The acceleration was often attributed to a reduction in the resistive stress, which is expected to occur when a glacier terminus retreats and force balance of the glacier is altered (Howat et al., 2007). Such changes in the force balance are caused by loss of ice near the glacier front, retreat from a bedrock

bump, and ice detachment from the fjord walls after thinning (Howat et al., 2005; Joughin et al., 2004; Thomas, 2004). Calving flux increases when a glacier accelerates, which leads to thinning and subsequent retreat (Howat et al., 2005; Joughin et al., 2004). Moreover, thinning near the terminus steepens ice surface, which causes further acceleration in that region, and the acceleration propagates upglacier as the geometry changes (Howat et al., 2005; Joughin et al., 2003; Payne et al., 2004). I assume that the dynamically controlled glacier retreat observed in Greenland also occurred at the three rapidly retreating glaciers in the SPI.

In 2008, Upsala Glacier suddenly went from a relatively stable phase to a rapidly retreating and fast-flowing phase. The transition is not due to a climatic forcing because no noticeable change was observed in air temperature at a nearby weather station (Fig. 3.12) (Sakakibara et al., 2013). According to previous studies of this glacier, the spatial pattern of bedrock topography probably controls the changes in its retreat rate (Naruse and Skvarca, 2000; Skvarca et al., 2002). Numerical modeling of calving glaciers showed that a transition from a stable condition to rapid retreat takes place when the front retreats over a bedrock rise into deeper water (Nick et al., 2009; Vieli et al., 2002). The rapid retreat and ice speed increase of Jorge Montt after 2010 was also attributed to the seabed geometry (Rivera et al., 2012b). Thus, it is likely that the underlying glacier bed topography plays a key role in the rapid changes of both freshwater and tidewater calving glaciers in the SPI.

Between 2000 and 2012, rapid thinning at rates exceeding 20 m a^{-1} was observed in Jorge Montt, HPS12, and Upsala Glaciers (Willis et al., 2012b). These rates significantly exceeded the SPI mean thinning rate of 1.8 ± 0.1 m a^{-1} (Willis et al., 2012b). According to my analysis, these three glaciers accelerated during the same period in the terminus areas where large thinning rates were reported. Such acceleration near the terminus should have enhanced the stretching ice flow regime. For example, near the calving front of Upsala Glacier, the longitudinal tensile strain rate increased from 0.19 to 0.34 a^{-1} after the rapid retreat in 2008 (Sakakibara et al., 2013). The increase in the tensile strain results in vertical compression, i.e. thinning of the glacier due to ice dynamics. Presumably, the dynamic thinning caused by flow acceleration plays an important role in the mass loss of the SPI. The ice mass loss from Upsala

Glacier from 2000 to 2012 corresponds to 15% of the total loss from the SPI (Willis et al., 2012b).

Results of my analysis suggest that dynamical changes of the calving glaciers contributed to the mass loss of the SPI. Flow acceleration on the rapidly retreating glaciers was greater near the ice front, the acceleration enhanced stretching of ice along the glacier and induced dynamic thinning. In turn this thinning due to changes in flow regime played an important role in the rapid retreat. Both of the flow acceleration and the rapid retreat increased the ice discharge. This increase in the ice discharge likely accounted for a large portion of the ice mass loss of the SPI over the last several decades.

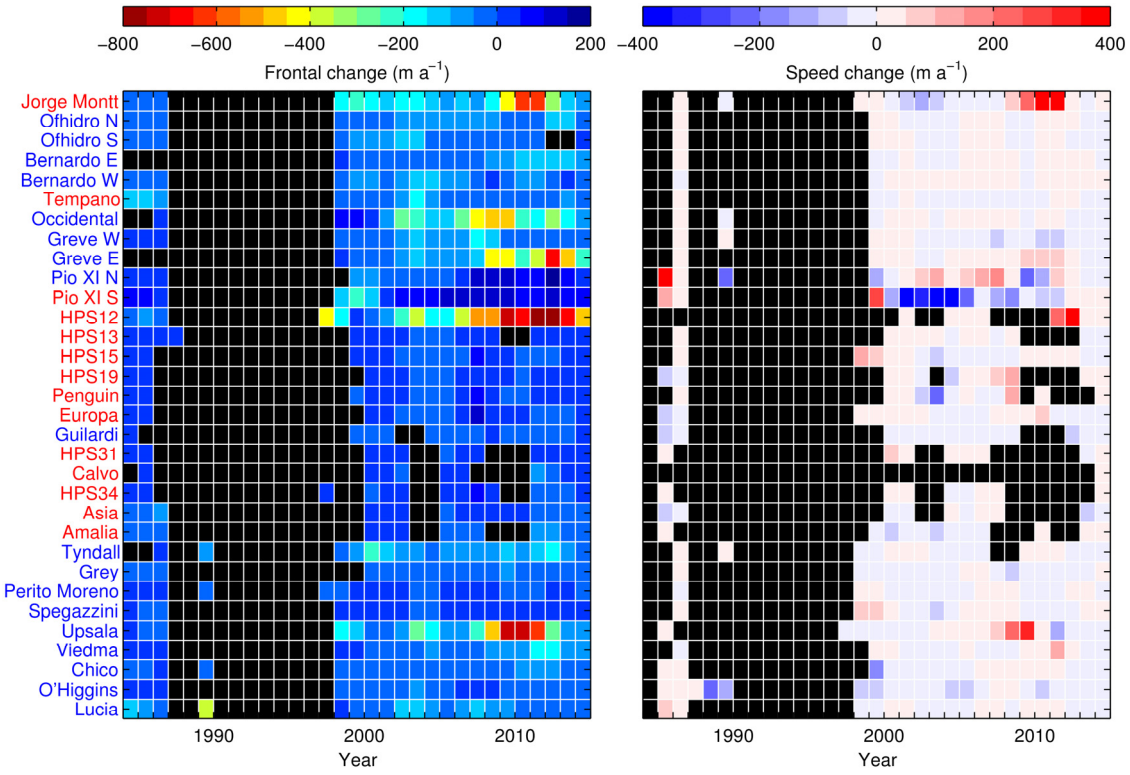

Figure 3.9. Annual changes in frontal position and ice speed within 5 km from the termini of the SPI calving glaciers from 1984 to 2014. Black indicates no data available.

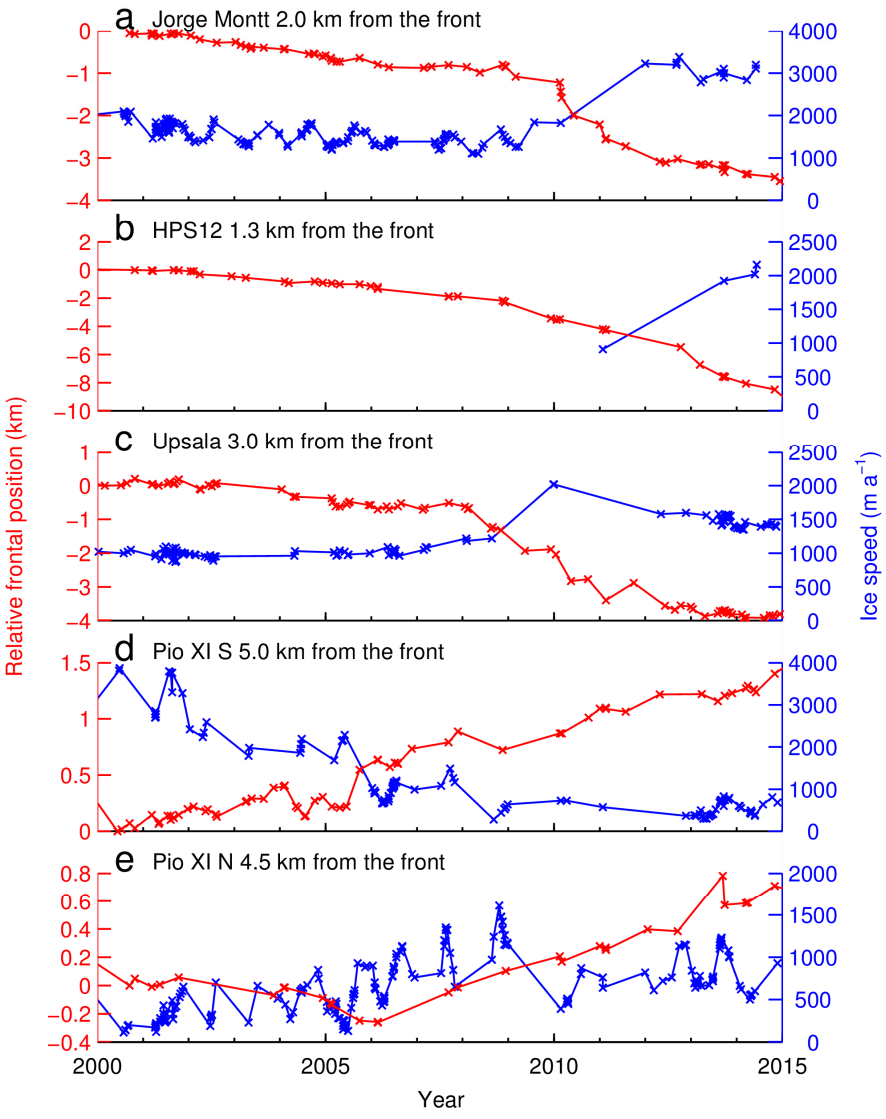

Figure 3.10. Front position and ice speed for selected glaciers from 2000 to 2014. (a) Ice speeds at 2.0 km from the front of Jorge Montt Glacier, (b) at 1.3 km from the front of HPS12 Glacier, (c) at 3.0 km from the front of Upsala Glacier, (d) at 5.0 km from the southern front of Pío XI Glacier, and (e) at 4.5 km from the northern front of Pío XI Glacier. (See Figure 3.11 for the same plots for all other glaciers.)

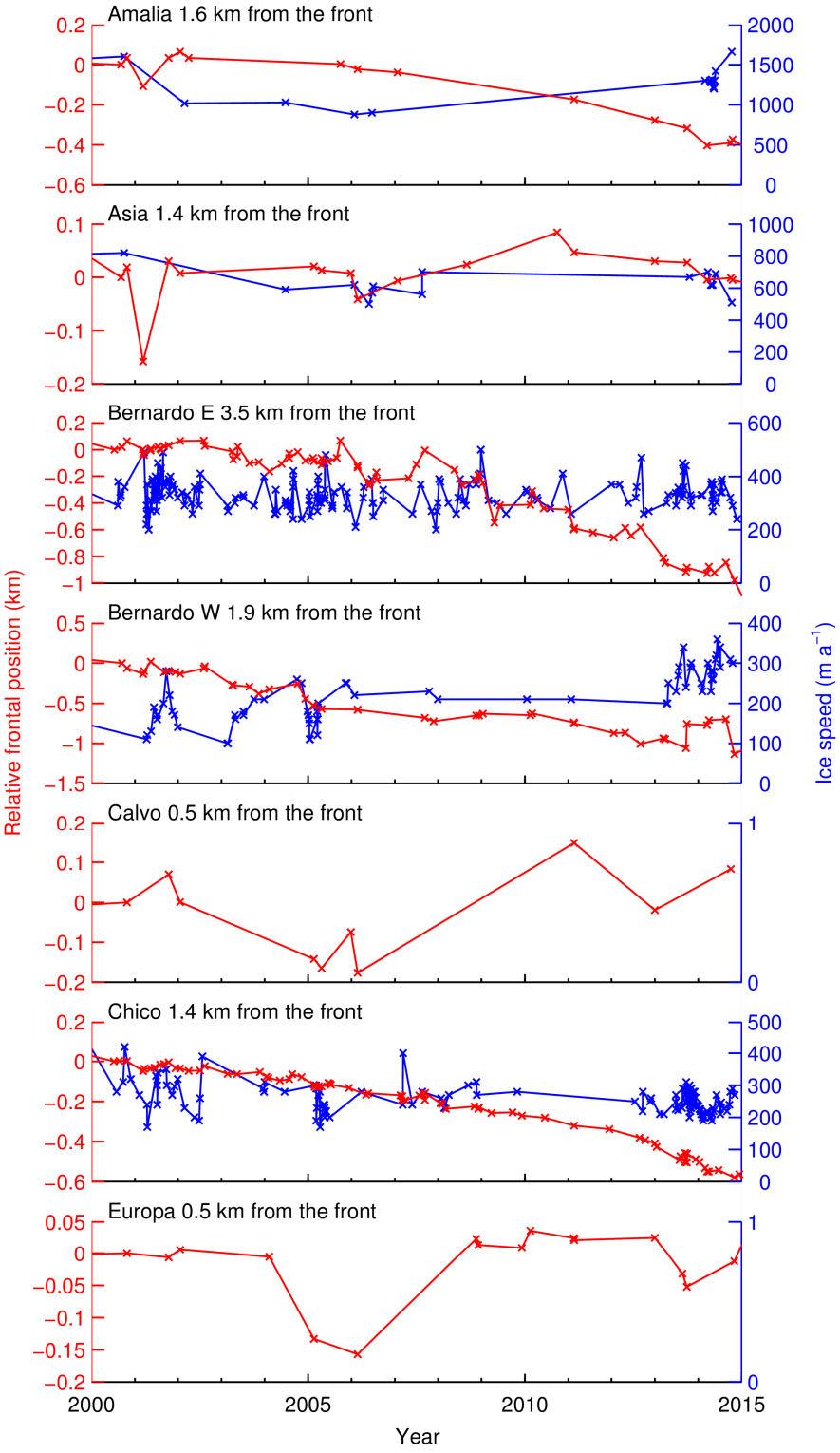

Figure 3.11. Same plot as Figure 3.10 but for all the other glaciers.

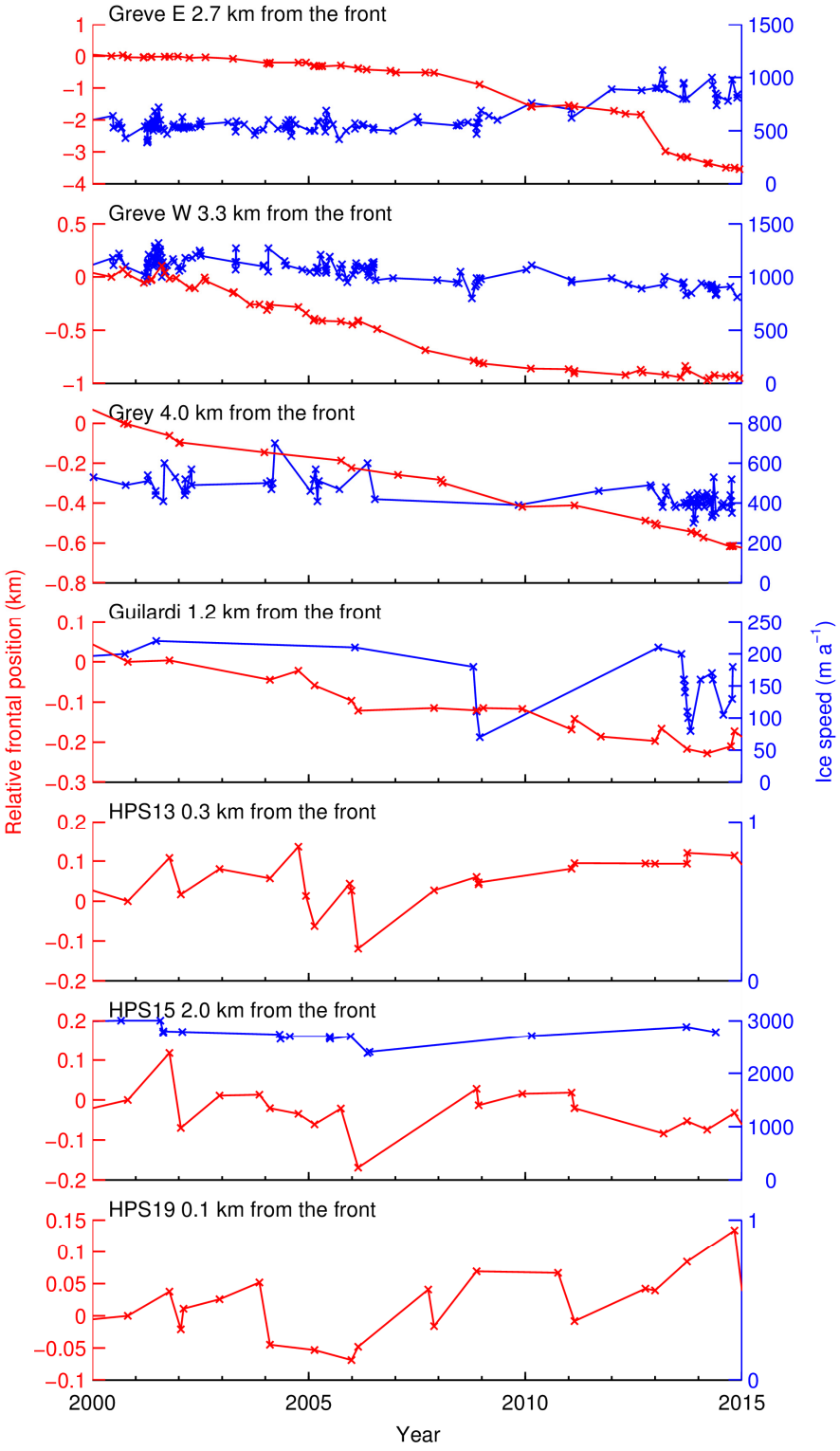

Figure 3.11. (Continued.)

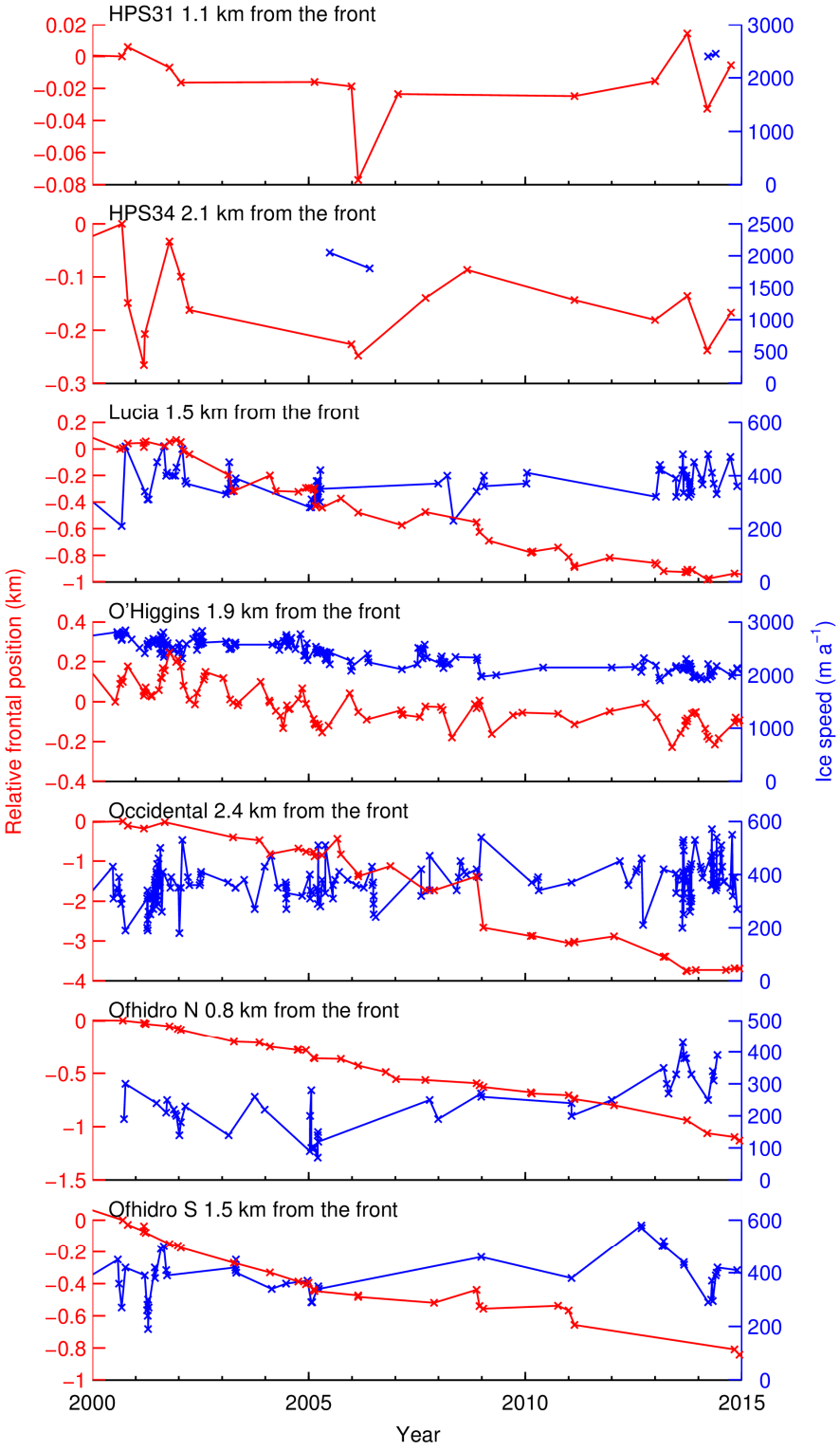

Figure 3.11. (Continued.)

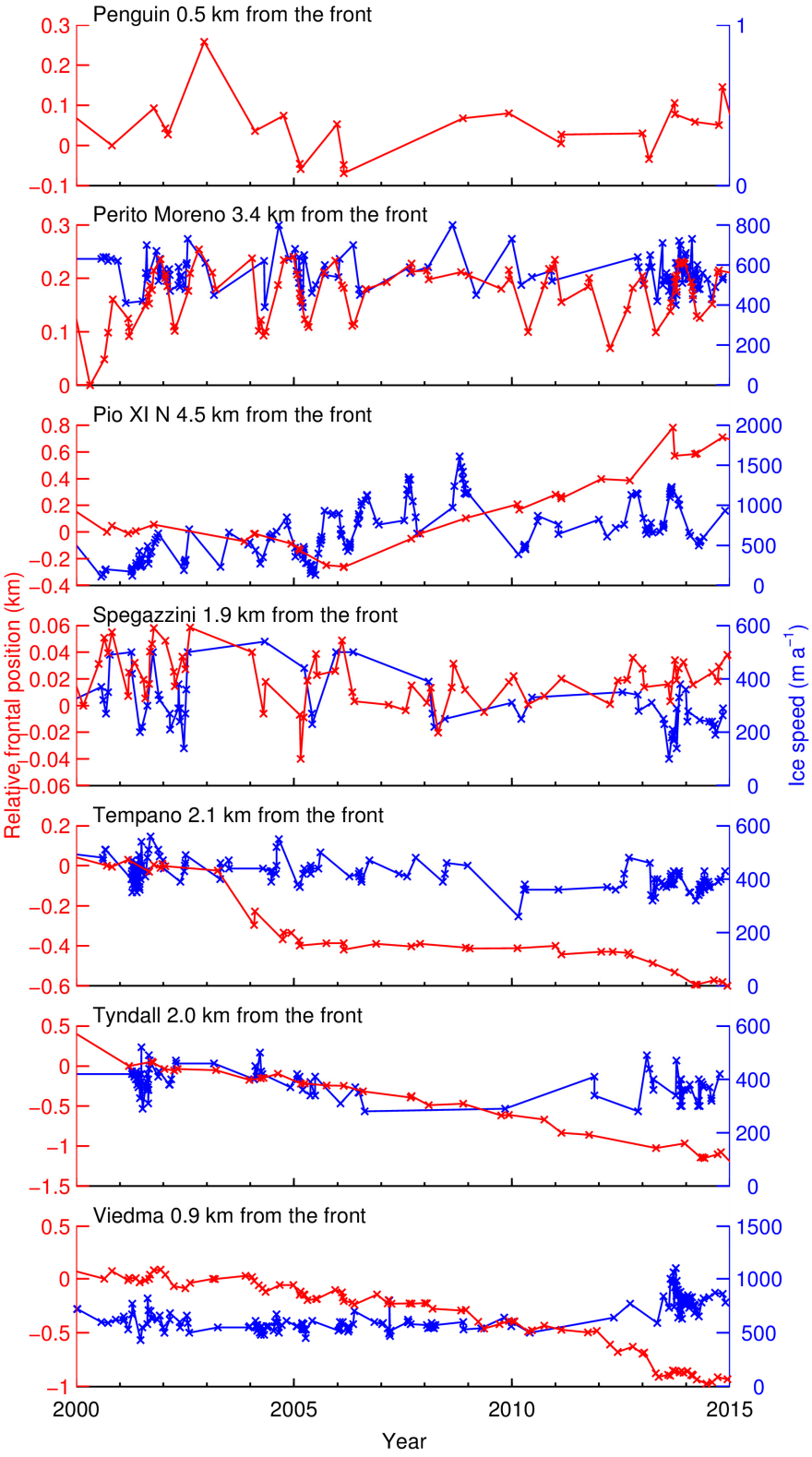

Figure 3.11. (Continued.)

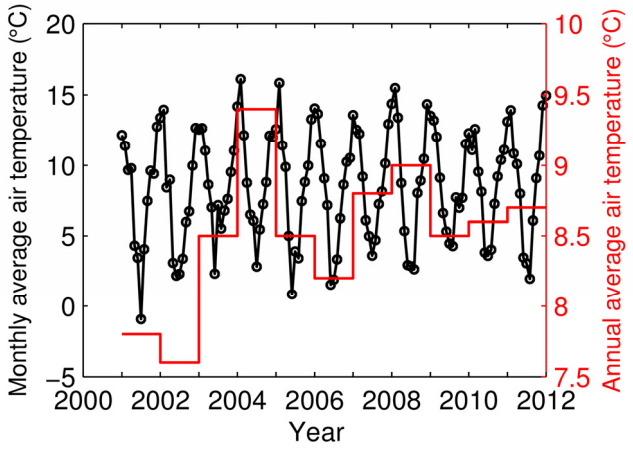

Figure 3.12. Monthly and annually averaged air temperatures from 2001 to 2012 at Estancia Cristina, located about 12 km from Upsala Glacier (Sakakibara et al., 2013).

3.2.3. Advance of Pío XI Glacier

Pío XI Glacier, the largest glacier in South America, is the only glacier that advanced during the studied period. Its southern terminus began advancing in 2000, its northern terminus in 2006 (Fig. 3.2). According to Rivera et al. (1997), this glacier advanced four times during the 20th century (1926–28, 1945–51, 1976–81, and 1992–94).

The ice speed of both branches of Pío XI Glacier showed large, complex variations. In the southern branch, the glacier rapidly slowed down between 2000 and 2008, as shown by the deceleration from 3870 m a^{-1} to 640 m a^{-1} at 5.0 km from the 2014 front (Fig. 3.10d). The southern terminus progressively advanced during these periods. The northern branch's ice speed changes were different from these observations in the southern branch. During the retreat of the northern terminus before 2006, the ice speed slightly increased (Fig. 3.10e). After the glacier began to advance in 2006, the speed increased from 930 m a^{-1} to 1470 m a^{-1} at 4.5 km from the 2014 front until 2009. Then the speed dropped by 600 m a^{-1} though the front was advancing (Fig. 3.10e). Seasonal speed variations were recognized in the northern branch, where the annual peak speed occurs in early summer.

Rivera et al. (1997) suggested that an advance of Pío XI Glacier is the glacier's response to a positive precipitation anomaly. That is, the front position is controlled by

decadal variations in snowfall over a large accumulation area with a delay time of 10–25 years. Figures 3.10d and 3.10e showed the complex frontal and ice speed variations of Pío XI Glacier. These variations are probably due to mass balance fluctuations in its large accumulation area, and also to complex glacier geometry and bed conditions near the calving fronts.

3.3. Summary

By using Landsat images, I quantified the ice front positions and velocities of the 32 termini of 28 calving glaciers in the SPI over a period between 1984 and 2014. The measurement enabled to produce the first icefield-wide velocity map over the SPI. Among the all studied termini, only the two termini of Pío XI Glacier advanced, 11 termini changed less than ±20 m a^{-1}, and 17 termini retreated by more than 20 m a^{-1} between 1984 and 2014. 53% of the studied termini retreated over the period, and the mean and median retreat rates for all fronts were 66 m a^{-1} and 26 m a^{-1}, respectively. Jorge Montt, HPS12, and Upsala Glaciers rapidly retreated at a rate more than 200 m a^{-1} and the total retreat distances of these glaciers were greater than 7 km during a period between 1984 and 2014. Within 5 km from the termini of the studied glaciers, ice speed ranged between 148 and 5970 m a^{-1}. Between 1984 and 2014 the mean and median ice speed changes were 1.1 and −2.4 m a^{-2}, respectively. These results indicate that glaciers in the SPI were decelerating in general, but the mean rate was influenced by rapid speed changes of several glaciers. Ice speed of Jorge Montt, HPS12, and Upsala Glaciers accelerated at a rate exceeding 40 m a^{-2} in the same period. This acceleration was significantly greater than those of the other glaciers. These three glaciers also showed rapid retreat. The timing of acceleration closely agreed with the rapid retreats and the magnitude of the acceleration was greater near the fronts.

Except for Pío XI Glacier, the glaciers fall into one of three categories: stable front position without significant ice speed change, gradual retreat with deceleration, and rapid retreat with large acceleration. The overall retreat trend was probably due to the long-term warming trend. Nevertheless, results of this study demonstrated that the extraordinary large retreats in the three glaciers (Jorge Montt, HPS12, and Upsala Glaciers) were not directly controlled by the warming trend, but instead driven by

glacier dynamics. Magnitude of the acceleration was greater near the front, which enhanced the stretching flow regime along the glacier in the lower reaches. I assume that this increase in the longitudinal straining induced dynamic thinning near the glacier terminus. Such dynamically controlled rapid retreat observed in several calving glaciers plays a key role in the recent volume decrease of the SPI.

Chapter 4

Calving glaciers in northwestern Greenland

In order to quantify changes in ice front position and flow velocity of calving glaciers along the coast of the Prudhoe Land in northwestern Greenland (Fig. 4.1), I analyzed Landsat images acquired from 1987 to 2014. The procedures described in Chapter 2 were applied to all 19 calving glaciers situated in this region. Using obtained ice front positions and flow speeds, changes in the calving glaciers are quantified. Based on the results, I discuss possible mechanisms of recent glacier changes in the Prudhoe Land, particularly the mechanism of ice speed changes in the rapidly retreating calving glaciers is investigated. In addition, frontal variations and ice speed changes are compared with atmospheric temperature records.

4.1. Results

4.1.1. Ice front position

Satellite data analysis shows that all the glaciers along the coast of the Prudhoe Land retreated over the study period (Fig. 4.2). Cumulative displacement from 1980s to 2014 measured at each individual glacier ranged from −5.35 ± 0.11 km (Tracy Glacier) to −0.23 ± 0.11 km (Meehan Glacier), and the median and mean displacements were −0.63 and −1.02 km, respectively. Retreat trend of the calving glaciers was observed after 2000 as represented by the median (mean) displacement rates of 1 (1) m a^{-1} in 1980s–1999 and −39 (−66) m a^{-1} in 2000–2014 (Table 4.1). Among the studied glaciers, Heilprin, Tracy, Farquhar, Melville, Bowdoin, and Diebitsch Glaciers retreated by more than 1 km from the 1980s to 2014.

Tracy Glacier retreated most rapidly during the study period (Fig. 4.2). The glacier showed terminus advance between 1987 and 1999, and then the terminus retreated by 4.4 km from 1999 to 2007. The retreat rate slightly decreased after 2007, but it increased again in 2011 and retreated by 1.0 km from 2011 to 2014. The retreat distance from 1999 to 2014 was 5.7 km. Farquhar Glacier shared its terminus with Tracy Glacier

until 2002, but they lost contact to each other in 2002 after the disintegration of the terminus. Farquhar Glacier retreated further by 0.9 km from 2002 to 2007. Heilprin Glacier showed a slight advance from 1987 to 1999, which is consistent with the observation at Tracy Glacier. Heilprin Glacier began to retreat in 1999 and lost the lower 1.9 km between 1999 and 2014. This retreat rate was smaller than that of Tracy Glacier over the same period, but one of the highest among the studied glaciers. Bowdoin Glacier retreated by 0.2 km from 1999 to 2008. After this relatively stable period, this glacier rapidly retreated by 1.1 km from 2008 to 2013. Diebitsch Glacier retreated by 0.6 km from 1997 to 2004. Then the front slightly advanced until 2006, which was followed by another retreat of 1.0 km from 2006 to 2014 (Fig. 4.2).

Table 4.1. Cumulative displacement of glacier fronts between 1987 and 2014, and displacement rates in the periods from the 1980s to 1999 and from 2000 to 2014. Positive values indicate glacier advance. 'NA' indicates no data available.

Glacier	1980s–2014 (km)	1980s–1999 (m a^{-1})	2000–2014 (m a^{-1})
Heilprin	−1.38±0.11	50±10	−111±8
Tracy	−5.35±0.11	63±10	−350±8
Farquhar	−1.26±0.11	NA	−111±9
Melville	−1.31±0.11	−90±10	−27±8
Sharp	−0.45±0.11	−1±10	−31±8
Hart	−0.62±0.11	−3±10	−35±8
Hubbard	−0.73±0.11	−11±10	−39±8
Bowdoin	−1.27±0.11	5±10	−84±8
Sun	−0.94±0.11	−9±10	−57±8
Verhoeff	−0.40±0.11	7±10	−29±8
Meehan	−0.23±0.11	NA	−27±8
Morris Jesup	−0.86±0.11	NA	−51±8
Diebitsch	−1.58±0.11	NA	−97±8
Clements	−0.55±0.11	NA	−38±8
Bamse	−0.62±0.11	NA	−41±8
Bu	−0.36±0.11	NA	−26±8
Chield	−0.39±0.11	NA	−25±8
Dodge	−0.46±0.11	NA	−29±8
Storm	−0.63±0.11	NA	−41±8
Mean	−1.02	1	−66
Median	−0.63	1	−39

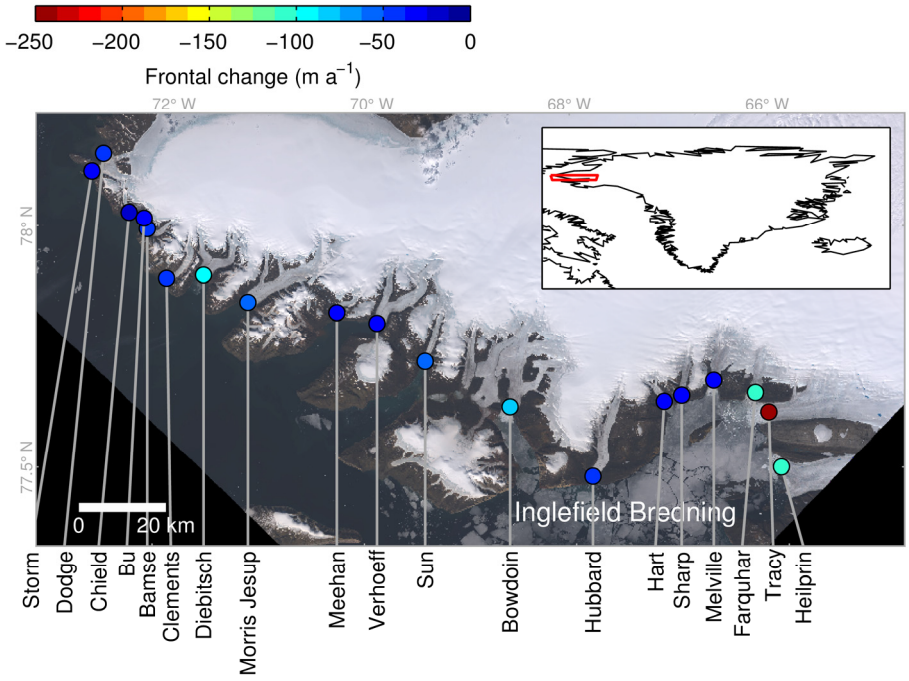

Figure 4.1. Locations of the studied glaciers along the coast of the Prudhoe Land. The color of the markers indicates the displacement rate of the ice front positions from 2000 to 2014 (advance in positive). Background is a true color mosaic Landsat 8 OLI image acquired on 9 July 2014. The inset shows the location of the study area in Greenland.

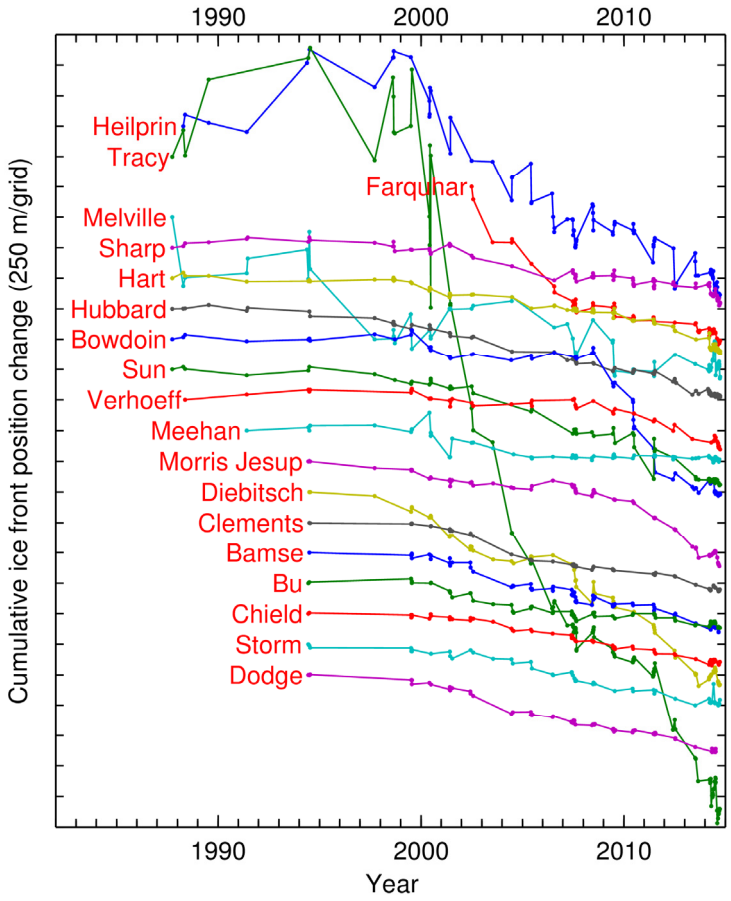

Figure 4.2. Cumulative changes in the ice front positions of the studied glaciers from 1980s to 2014. Upward change in the ordinate represents glacier advance.

4.1.2. Ice speed

Figure 4.3 shows the mean ice speed distributions over the studied glaciers in 1987–2014. Ice speed within 5 km from the front of each individual glacier ranges from 14 m a^{-1} to 1814 m a^{-1} (Table 4.2). Relatively fast ice flow (> 500 m a^{-1}) was observed near the front of Heilprin, Tracy, Farquhar, Melville, and Sharp Glaciers, which drain into the eastern part of the Inglefield Bredning (< 67W°) (Fig. 4.3). Among 17 glaciers with data available for the period from 2000 to 2014, 5 glaciers accelerated by more than 5 m a^{-2}, whereas 12 glaciers showed no significant change (speed change was less than ±5 m a^{-2}) (Fig. 4.4 and Table 4.2). The speed change from 2000 to 2014 averaged over the glaciers was 6.4 m a^{-2}, but this number is influenced by the acceleration of several glaciers (Heilprin, Tracy, Farquhar, Bowdoin, and Diebitsch Glaciers) and thus

does not represent the general trend.

Ice speed of Heilprin Glacier was relatively stable before 2000. In this period, the speed at 2 km from the 1987 front was fluctuated only within a range 1050–1190 m a^{-1}. Between 2000 and 2014, ice speeds near the front gradually increased from 1290 m a^{-1} to 1505 m a^{-1}. In the same period the speed at 10 km from the 2000 front increased from 610 m a^{-1} to 750 m a^{-1} (Fig. 4.5a). At Tracy Glacier, ice speed at 7 km from the 2000 front was relatively stable before 2000 within a range 940–970 m a^{-1}. Then the speed increased in 2000–2007 from 950 m a^{-1} to 1580 m a^{-1}, followed by further acceleration from 1580 m a^{-1} to 2030 m a^{-1} in 2011–2014 (Fig. 4.5b). Similarly, Farquhar Glacier largely accelerated in 2000–2014 near the front from 460 m a^{-1} to 830 m a^{-1} (Fig. 4.5c). Bowdoin Glacier showed no significant speed change between 1987 and 1999. After this relatively stable period, the glacier accelerated significantly in 1999–2005 from 158 m a^{-1} to 344 m a^{-1}. This large acceleration was followed by slowdown, and then another acceleration began in 2013 (Fig. 4.5d). These speed variations at Bowdoin Glacier are similar to those at Diebitsch Glacier located at 80 km west. This glacier substantially accelerated between 1999 and 2006 (from 99 m a^{-1} to 243 m a^{-1}) (Fig. 4.5e), which was followed by slowdown and another acceleration.

Table 4.2. The minimum and maximum ice flow speeds of the 19 studied glaciers, which sampled from the locations within 5 km from the termini. Acceleration over the same period is also listed. The speeds are averaged over a period between 2000 and 2014. The acceleration is averaged over the 5 km from the termini. 'NA' indicates no data available.

Glacier	Minimum (m a^{-1})	Maximum (m a^{-1})	Acceleration (m a^{-2})
Heilprin	997	1406	15
Tracy	1613	1814	81
Farquhar	428	794	5
Melville	756	1283	−1
Sharp	317	505	1
Hart	87	102	1
Hubbard	58	94	−1
Bowdoin	213	303	11
Sun	21	36	0
Verhoeff	74	127	−4
Meehan	14	28	−1
Morris Jesup	87	113	−4
Diebitsch	100	177	7
Clements	26	35	−1
Bamse	45	86	0
Bu	NA	NA	NA
Chield	NA	NA	NA
Dodge	10	19	0
Storm	16	27	0

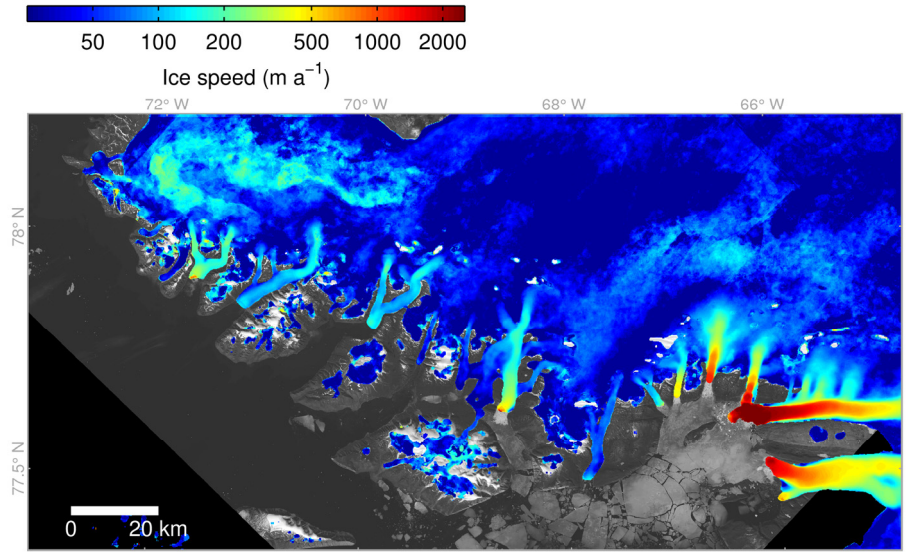

Figure 4.3. Ice speed distributions over the Prudhoe Land in 1987–2014. Background is a Landsat 8 OLI image acquired on 9 July 2014. The speed at each location equals the mean of all measurements available within the period.

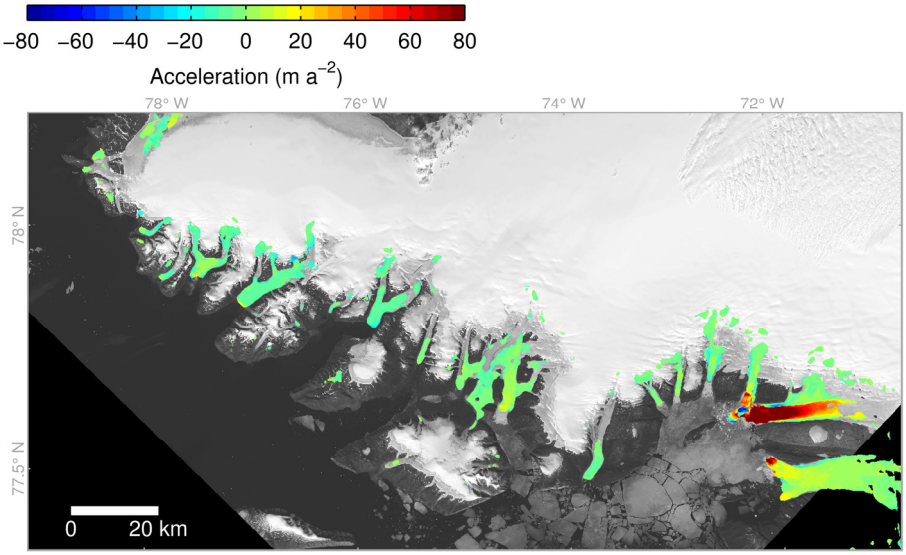

Figure 4.4. Flow acceleration over the Prudhoe Land in 2000–2014. Background is a Landsat 8 OLI image acquired on 9 July 2014.

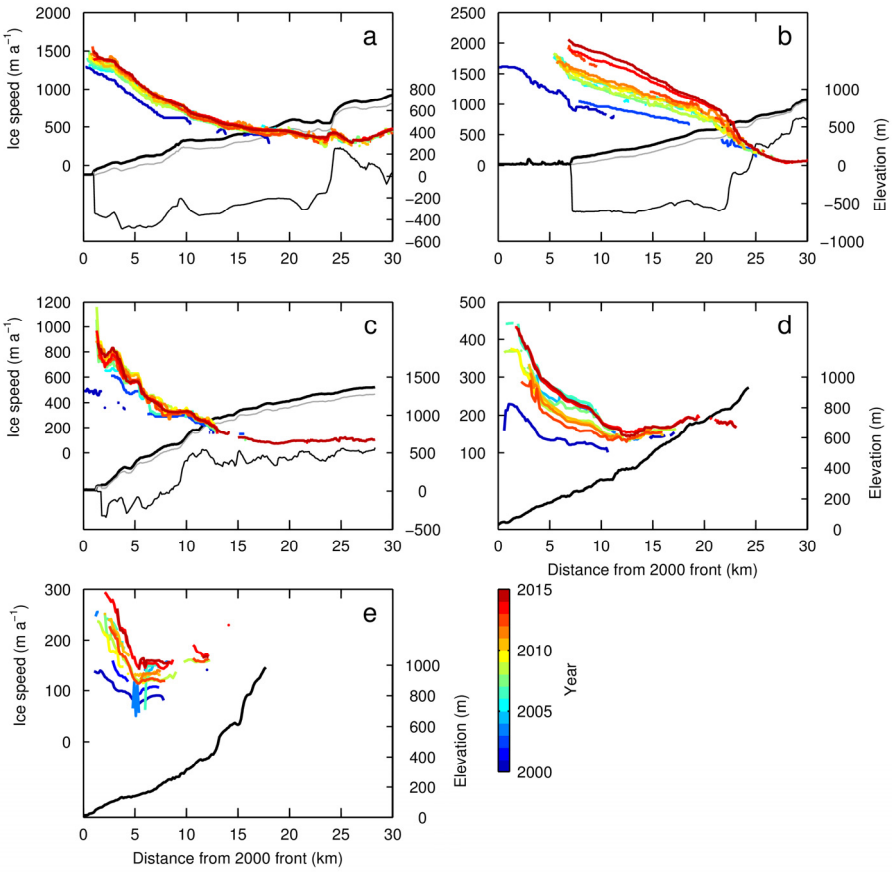

Figure 4.5. Ice speed along the central flowline and its temporal variations at (a) Heilprin, (b) Tracy, (c) Farquhar, (d) Bowdoin, and (e) Diebitsch Glaciers. Thick and thin black curves indicate surface and bed elevations, respectively. Gray line indicates flotation level defined by water level which fulfills the hydrostatic equilibrium condition of the glacier ice. The flotation level was calculated using the bed and surface elevations, assuming that ice density is 910 kg m^{-3} and water density in front of the glacier is 1025 kg m^{-3}. (See Figure 4.6 for similar plots for all other glaciers.)

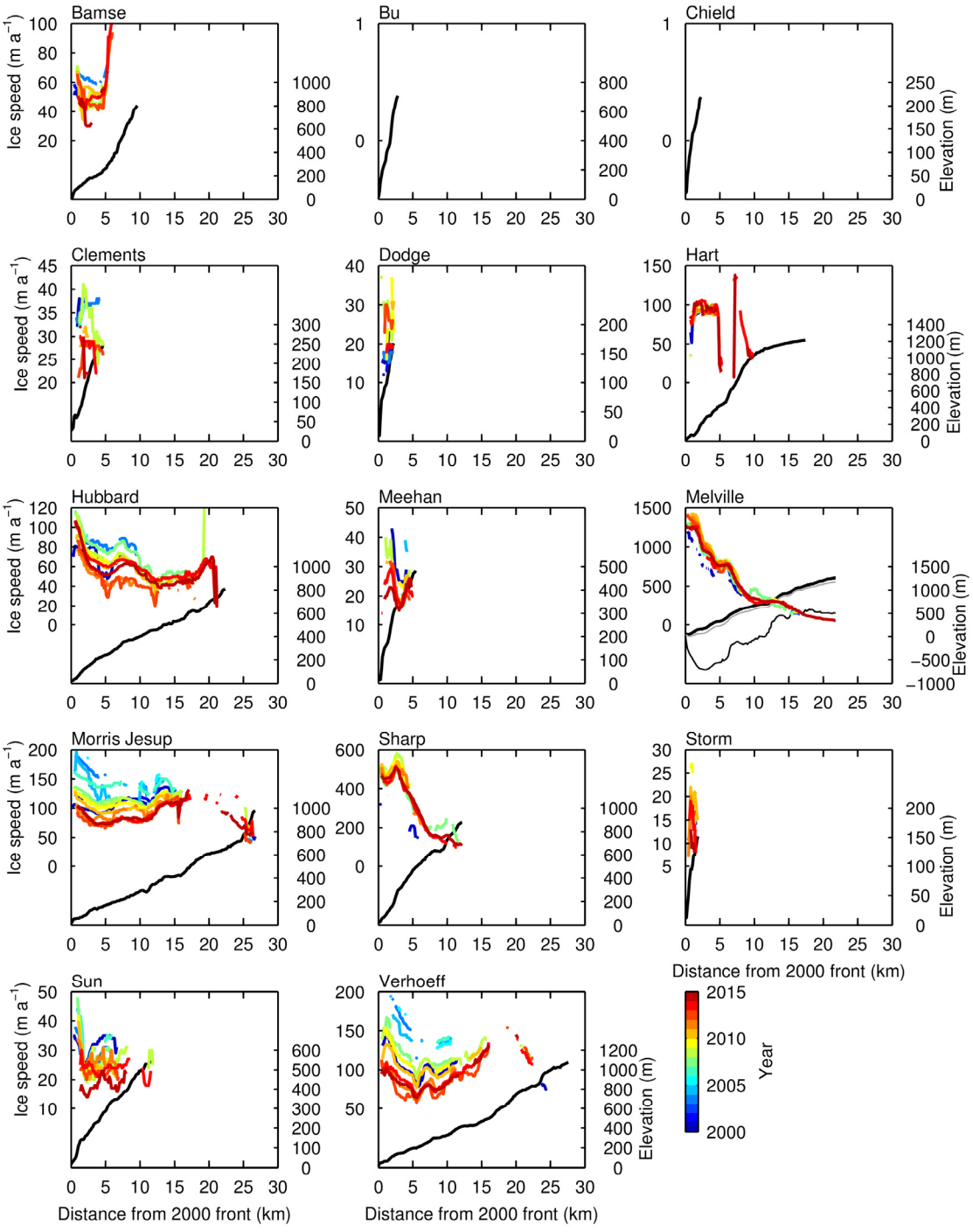

Figure 4.6. Same plots as Figure 4.5 for all other glaciers.

4.2. Discussion

4.2.1. Driver of the frontal variations

All of the studied glaciers showed frontal retreat over the period between 2000 and 2014, and most of the glaciers began retreat around 2000 (Fig. 4.2). This general trend is represented by an increase in the mean retreat rate from −1 m a^{-1} in 1987–1999 to 66 m a^{-1} in 2000–2014 (Table 4.1). Climatic forcing is a possible driver of the glacier retreat after 2000, because rapid warming trend is reported in the Arctic (e.g. Carr et al., 2013). Atmospheric warming causes more negative surface mass balance, which results in ice thinning near the calving front and increases calving events (van der Veen, 1996, 2002). Moreover, increased amount of surface meltwater fills crevasses near the calving front and triggers calving by the process of hydrofracturing (Sohn et al., 1998). Thus, I compare the observed frontal variations with summer air temperature to investigate a driver of the recent glacier retreat in the Prudhoe Land.

Daily mean air temperatures at Pituffik (Thule Air Base; 76.53°N, 68.75°S; 59 m a.s.l.), approximately 100 km south of the study site, were obtained from the National Climatic Data Center. Figure 4.7 shows the mean and median rates of frontal position change for all the studied glaciers from 1997 to 2014 and June–August mean temperature at Pituffik from 1985 to 2014. To investigate the general trend of glacier change in the region, extremely rapid retreats (> 200 m a^{-1}) observed in Heilprin, Tracy, Farquhar, Melville, and Bowdoin Glaciers were excluded from this analysis. The mean retreat rate increased from 31 m a^{-1} in 2000 to 61 m a^{-1} in 2003. Then, it decreased until it reached 23 m a^{-1} in 2007, which was followed by another increase to 88 m a^{-1} in 2012 (Fig. 4.7). From these results, It is found that the glaciers retreated at relatively high rates (>50 m a^{-1}) during two periods, namely 2003–2004 and 2011–2012. June–August mean temperature increased between 1996 and 1999 from 1.4°C to 4.5°C. This rapid warming was consistent with the significant increase in glacier runoff from 1996 to 1998, reported in northwestern Greenland (Fettweis, 2007). The warm temperature conditions continued until 2003. Rapid warming was also observed between 2004 and 2007, where summer temperature increased from 3.5°C to 5.5°C. The temperature was maintained at the elevated level until 2012 (Fig. 4.7). The relatively

high retreat rates from 2007 to 2012 coincided with the final phase of the warm summer periods. It indicates that the rapid retreat lagged to the warming by several years. This lag is also observed in the relationship between 5-year running mean of the June–August temperature and the mean retreat rate. It is likely that cumulative effect of warming on melting triggered the frontal retreat of the glaciers in the Prudhoe Land. Surface melting increases under warming conditions particularly in the lower reaches, and this enhanced melting induces ice thinning. Ice near the front tends to get afloat as the ice becomes thinner, and calving rate increases under such a condition (van der Veen, 1996, 2002). Another mechanism that connects warming and active calving is deepening of crevasses due to increase in surface meltwater (Benn et al., 2007; Sohn et al., 1998; van der Veen, 1998). Because of the foregoing analysis and discussion, the warming in summer period is suggested as a possible driver for the frontal retreat of the glaciers in the Prudhoe Land.

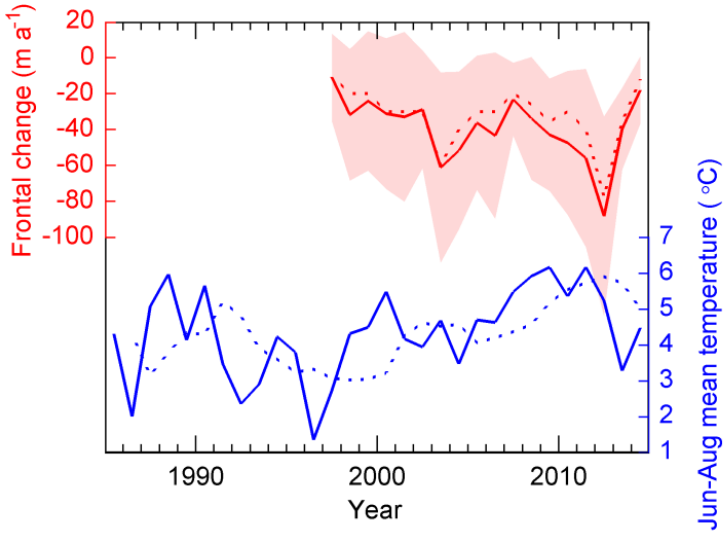

Figure 4.7. Mean (red line) and median (red dotted line) rates of frontal position change for studied glaciers from 1997 to 2014 with the shaded rim indicating the standard deviation. June–August mean temperature (blue) at Pituffik from 1985 to 2014. The blue dotted line indicates the 5-year running mean of the temperature.

4.2.2. Role of ice dynamics in rapid glacier retreat

The generally retreating trend since 2000 is likely due to the warming trend as explained

above. However, retreat rates of Heilprin, Tracy, Farquhar, Bowdoin, and Diebitsch Glaciers (84–358 m a^{-1} for 2000–2014) were significantly larger than the mean of all the studied glaciers (66 m a^{-1}), and thus cannot be attributed to the warming alone. These rapidly retreating glaciers are distributed randomly over the studied region (Fig. 4.1). This suggests that these rapid retreats were controlled by factors independently affecting each glacier.

Figure 4.8 shows a relationship between the changes in ice speed and frontal position over a period between 2000 and 2014. All the rapidly retreating glaciers (> 80 m a^{-1}) (Heilprin, Tracy, Farquhar, Bowdoin, and Diebitsch Glaciers) accelerated during the period (Fig. 4.8). This relationship between rapid retreat and acceleration suggests that the rapid retreats were driven by the ice dynamics rather than surface mass balance. The most likely interpretation of the relationship between the retreat and acceleration is the dynamic thinning (e.g. Thomas et al., 2003). Figure 4.5 shows that speedup of the rapidly retreating glaciers was greater near the front, which implies that a stretching flow regime was enhanced by the speedup. The increase in the tensile strain along the glacier results in vertical compression, i.e. thinning of the glacier due to ice dynamics. Between 2003 and 2008, Tracy Glacier thinned at a rate of −7.29 m a^{-1}, whereas the thinning rate of nearby Heilprin Glacier was −0.77 m a^{-1} (Pritchard et al., 2009). Pritchard et al. (2009) attributed this contrasting behavior of the two largest glaciers in this study site to more enhanced dynamic thinning at Tracy Glacier. During this period, more than five times greater acceleration at Tracy Glacier (81 m a^{-2}) than Heilprin (15 m a^{-2}) Glacier was observed. This evinces that ice dynamics played a dominant role in the rapid retreat of several glaciers. Most likely, thinning due to flow acceleration contributed to the rapid retreat because most of the fronts of the rapidly retreating glaciers reaching flotation. Flotation level at the glacier front of Heilprin, Tracy, and Farquhar Glaciers were nearly equal to the sea level (Figs 4.5a, 4.5b, and 4.5c). In addition to these glaciers, the flotation level at the front of Bowdoin Glacier almost reached the sea level because of glacier thinning (Sugiyama et al., 2015). Ice front of the rapidly retreating glaciers were mostly in nearly floating conditions, suggesting that calving enhanced by ice flotation controls the retreat of these glaciers. This hypothesis agrees with the idea proposed by van der Veen (1996). van der Veen (1996) proposed

that frontal position is controlled by the ice thickness above flotation and ice thinning at the terminus triggers rapid frontal retreat.

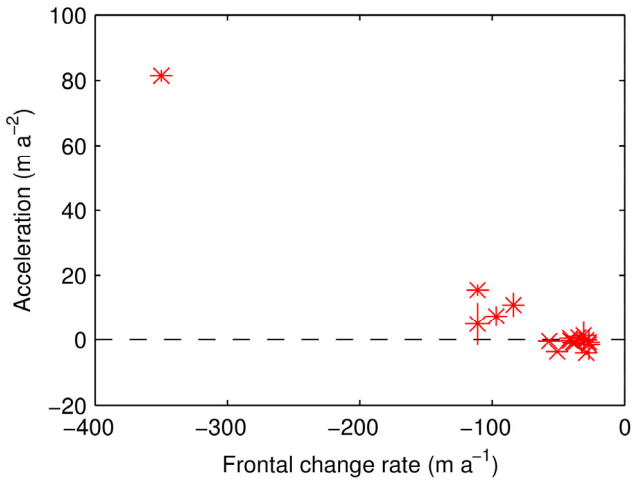

Figure 4.8. Rate of ice speed change v.s. rate of frontal position change at the studied glaciers from 2000 to 2014. The speed change is an average within 5 km from the 2014 front. Error bar indicates the standard deviation of the acceleration within 5 km from the front.

4.2.3. Mechanism of ice acceleration

Here, I examine two previously proposed mechanisms as possible drivers of the flow acceleration observed in this study. The first mechanism is that frontal retreat alters the force balance near the terminus, and this change in the mechanical condition induces flow acceleration (e.g. Howat et al., 2005, 2007; Joughin et al., 2004). In the observational data in the Prudhoe Land, relationships between variations in ice front position and flow speed were found. Figure 4.9 shows relative frontal position and annual ice speed for selected glaciers. To investigate changes in ice flow near the terminus, ice speed was taken at fixed location roughly one width from the front, with adjustments to minimize missing data. Tracy Glacier accelerated twice in 2000–2006 (from 910 m a^{-1} to 1410 m a^{-1} at 1.9 km from the 2014 front) and in 2010–2014 (from 1420 m a^{-1} to 1890 m a^{-1}) (Fig. 4.9b). The first speedup coincided with disintegration of the glacier tongue shared with Farquhar Glacier, which occurred in the summer 2001. The ice front of Tracy Glacier retreated by 3.3 km over the same period. This

disintegration affected ice speed of Farquhar Glacier as well. Ice speed at 0.8 km from the front of Farquhar Glacier increased in 2000–2006 from 360 m a^{-1} to 790 m a^{-1} (Fig. 4.9c). The second speedup of Tracy Glacier in 2010–2014 occurred when the retreat rate was relatively high (280 m a^{-1} in 2010–2014). These results show close agreement of the timings between high retreat rate and the rapid speedup, and suggest that the frontal retreat rapidly changed the ice dynamics. For example, rapid retreats of Greenlandic outlet glaciers were often associated by ice speedup (e.g. Howat et al., 2008; Joughin et al., 2010). Rapid removal of terminus ice causes reduction in the resistive stress acting on ice flowing into the ocean, and this change in the stress condition resulted in flow acceleration (Howat et al., 2005, 2007; Joughin et al., 2004).

Bowdoin Glacier showed a relatively small flow speed change from 1988 to 2000 (+37 m a^{-1}). Then ice speed at 1.8 km from the front increased in 2000–2005 from 171 m a^{-1} to 344 m a^{-1} (Fig. 4.9d). The ice front of Bowdoin Glacier stayed at almost same position over a period between 1980s and the late 1990s, but retreated a short distance around 2000. Thus, the onset of the retreat of Bowdoin Glacier closely agreed with the acceleration. Flow speed at 1.2 km from the front of Diebitsch Glacier increased in 1999–2006 from 87 m a^{-1} to 232 m a^{-1} (Fig. 4.9e). Ice front retreated by 0.3 km in 1999–2002. The magnitude of the retreat was relatively small in these two glaciers, but flow acceleration occurred when the frontal position retreated. It is likely that the ice dynamics near the termini of Bowdoin and Diebitsch Glaciers was sensitive to small changes in the frontal positions.

The second mechanism of acceleration is that basal ice motion enhanced by increased amount of meltwater input to the glacier bed. When surface melt increases and greater amount of meltwater reaches to the glacier bed, basal ice motion is potentially enhanced (e.g. Andersen et al., 2010; Meier and Post, 1987; Sole et al., 2011; Sugiyama et al., 2011). The rapidly retreating glaciers in the Prudhoe Land accelerated in the early 2000s (Fig. 4.9). The summer air temperature significantly increased in 1996–1998 and this warm condition was kept until 2003 (Fig. 4.7). Larger amount of meltwater was likely produced in summers between 1998 and 2003. This meltwater drained to the bed and probably increased basal water pressure. The speed change was observed on Tracy Glacier over a region within ~25 km from the glacier front. The bed elevation was

below sea level in this region, and similar condition was observed at Heilprin and Farquhar Glaciers (Figs 4.5a, 4.5b, and 4.5c). Thus, the glacier accelerated in the region where the bed elevation is below sea level. This agreement suggests that basal conditions play a key role in the significant changes in the flow speed i.e., physical conditions of the glacier bed below sea level is necessary to generate significantly large flow acceleration. A possible interpretation is that relatively high basal water pressure exerted by sea water facilitates greater acceleration when meltwater reached to the bed in summer time.

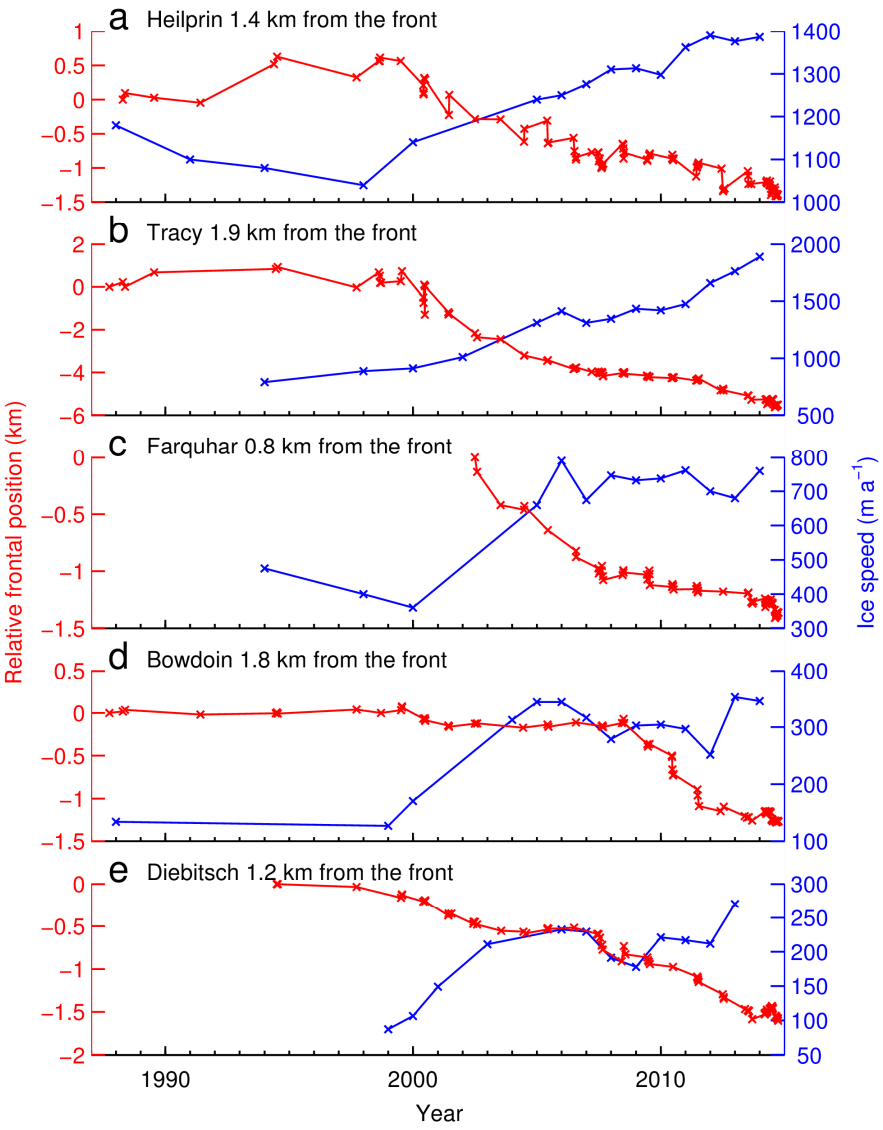

Figure 4.9. (a) Relative frontal position (red) and annual ice speed at a fixed location roughly one width from the front of Heilprin Glacier over a period between 2000 and 2014. (b) same as (a) except for Tracy Glacier. (c) Farquhar Glacier. (d) Bowdoin Glacier. (e) Diebitsch Glacier. (See Figure 4.10 for similar plots for all other glaciers.)

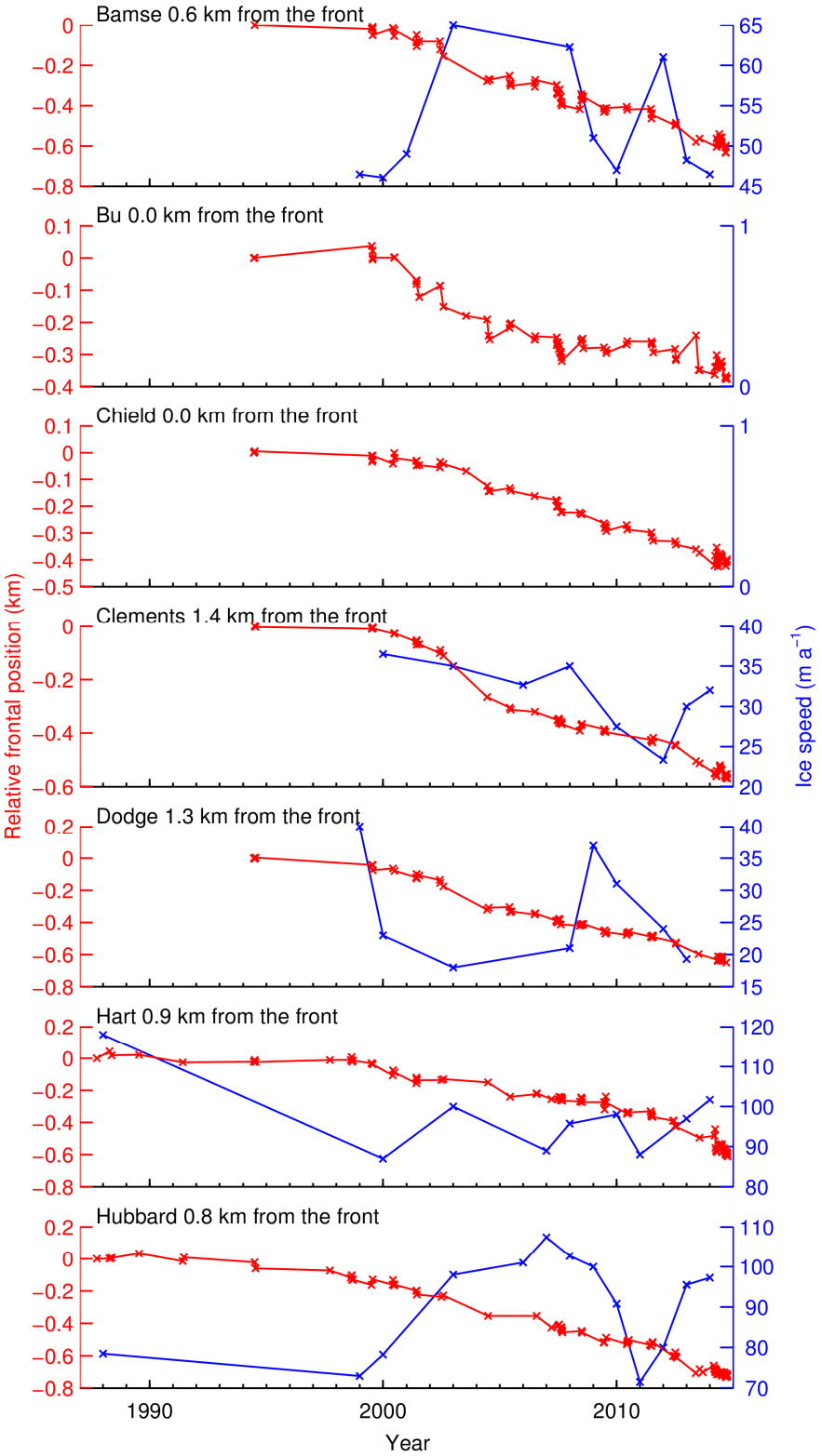

Figure 4.10. Similar plots of Figure 4.9 for all other glaciers.

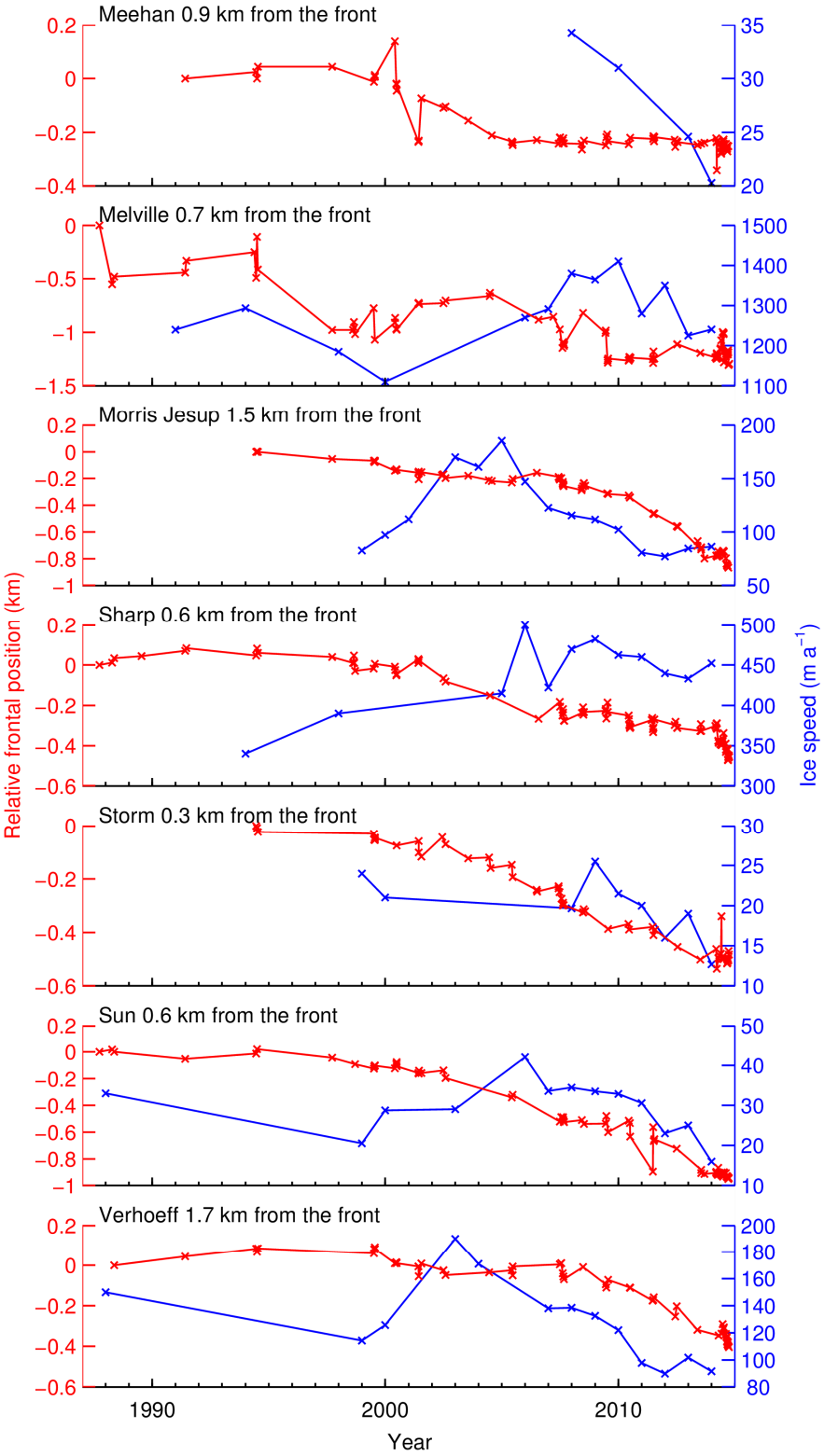

Figure 4.10. (Continued.)

4.3. Summary

Ice front positions and velocities of 19 calving glaciers along the coast of the Prudhoe Land, northwestern Greenland were measured using the Landsat images acquired from 1987 to 2014. All of the studied 19 glaciers retreated by 5.35 to 0.23 km between the 1980s and 2014, having a mean and median retreat distance of 1.02 and 0.63 km, respectively. Heilprin, Tracy, Farquhar, Melville, Bowdoin, and Diebitsch Glaciers retreated by more than 1 km in the same period. Most of the glaciers began to retreat around 2000, as indicated by the change in the median (mean) retreat rate from −1 (−1) m a^{-1} in 1980s–1999 to 39 (66) in 2000–2014. Within 5 km from the front of the studied glaciers, ice speed ranged between 14 and 1814 m a^{-1}. Many of the studied glaciers accelerated in the early 2000s. Heilprin, Tracy, Farquhar, Bowdoin, and Diebitsch Glaciers accelerated at a rate of 5–81 m a^{-2} between 2000 and 2014. There was correlation between retreat rate and acceleration for the studied glaciers. Flow acceleration was accompanied by rapid retreats of Tracy Glacier.

A possible driving force of the glacier retreat which began in 2000 is atmospheric warming, as represented by the increase in the summer temperature, observed in the late 1990s. The magnitude of the acceleration correlates the retreat rate as shown by the rapid retreat and flow acceleration at Heilprin, Tracy, Farquhar, Bowdoin, and Diebitsch Glaciers. The magnitude of the acceleration was greater near the front, enhancing the stretching flow regime along the glaciers and induced dynamic thinning in the lower reaches. The termini of Heilprin, Tracy, and Bowdoin Glaciers located where the flotation levels equal to the sea levels, suggesting that lowering in flotation level due to ice thinning resulted in frontal retreat. The rapid retreat of Heilprin, Tracy, Farquhar, Bowdoin, and Diebitsch Glaciers is likely enhanced by dynamic thinning due to flow acceleration.

Chapter 5

Mechanisms controlling rapid retreat and acceleration of Upsala Glacier

In order to measure bed topography and glacier geometry of a rapidly retreating calving glacier, field observations and satellite data analysis were carried out at Upsala Glacier in the SPI (Fig. 5.1). Bottom topography of the proglacial lake was surveyed in front of the glacier, where the lake expanded its area after the rapid retreat since 2008. Digital elevation models (DEMs) derived from satellite images were used to investigate evolution of the glacier geometry during the rapid retreat. Based on these results, I discuss mechanisms controlling rapid retreat and flow acceleration of calving glaciers.

5.1. Methods

5.1.1. Lake bottom topography measurement

Water depth was measured in a fjord called Brazo Upsala within 0.5 to 5 km from the 2014 glacier front (Fig. 5.2). The measurements were carried out in December 2013 and October 2014 from a boat equipped with ultrasonic echo water depth sounders (Lowrance HDS5 Gen-2 with an Airmar P319 transducer and Elite-5 Chirp with a Lowrance HDI-STH-TD transducer). Accuracy of the depth measurement was estimated by comparing the sounder data with those obtained by a depth sensor lowered to the bed with a string. Grounding of the depth sensor was confirmed by manual inspection. According to the calibration measurements at five locations with depth ranging 309 to 553 m, the root-mean-square deviation between the sounder and the depth sensor data was 15 m. The boat speed was 10 km h^{-1}, and water depth and horizontal coordinates every second were sampled. The coordinates were obtained with a GPS mounted on the echo sounder based on a single point-positioning technique. Errors in the GPS single positioning are typically expected to be several meters in the horizontal direction. After removing outliers, all available depth data were interpolated to 50 m grid points using bi-cubic interpolation to generate a bathymetric map of the lake.

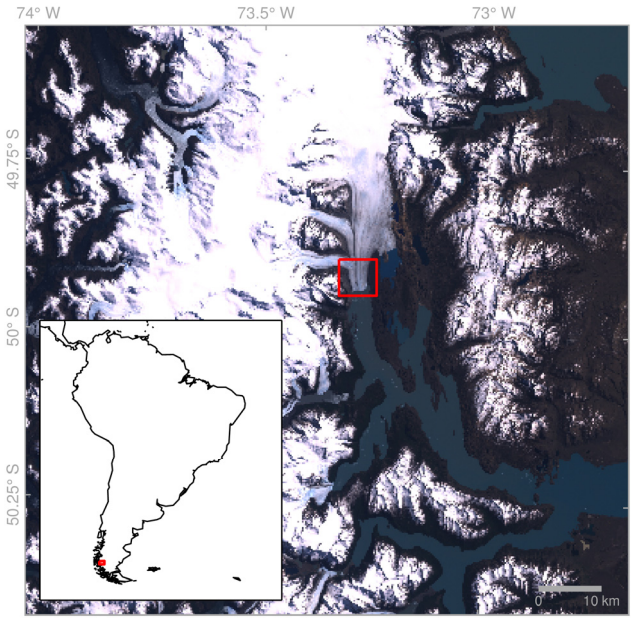

Figure 5.1. A satellite image showing a central part of the SPI including Upsala Glacier (Landsat 7, 14 October 2001). The red box indicates the area shown in Figures 5.2, 5.3, and 5.7. The inset shows the location of the glacier in South America.

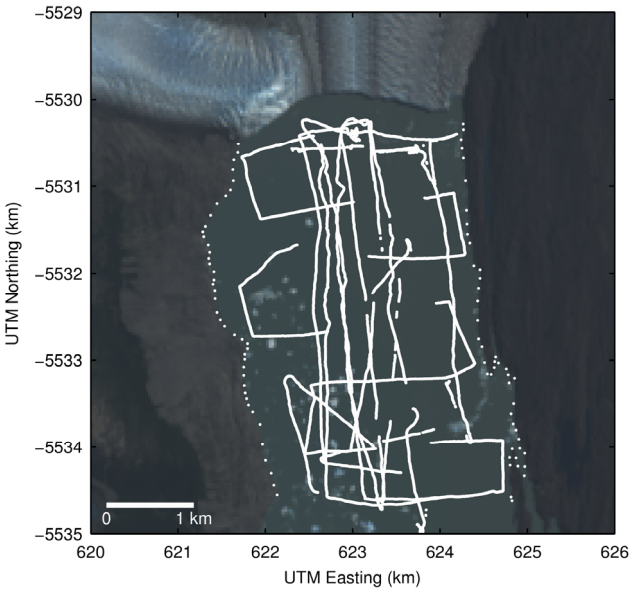

Figure 5.2. Tracks of water depth measurements in Brazo Upsala. Background is a Landsat 8 OLI band 8 image acquired on 12 February 2014.

5.1.2. Surface elevation analysis

Glacier surface elevations within 15 km from the 2000 glacier front were extracted from three different digital elevation models (DEMs). First, I used Advanced Spaceborne Thermal Emissivity and Reflection Radiometer (ASTER) DEMs distributed by the Land Processes Distributed Active Archive Center (LP DAAC). The ASTER DEMs have 30 m resolution and a vertical accuracy of ±7–15 m (Kääb, 2005; San and Suzen, 2005). Second, I generated DEMs by processing stereo pairs of satellite images obtained by Panchromatic Remote-sensing Instruments for Stereo Mapping (PRISM) mounted on Advanced Land Observation Satellite (ALOS). The PRISM DEMs have a resolution of 10 m and a vertical accuracy of ±9.3–11.8 m (Sakakibara et al., 2013). Third, I also utilized Shuttle Radar Topography Mission (SRTM) DEM based on interferometric synthetic aperture radar measurements in February 2000. This data set covers an area from 60°N to 57°S latitude (http://eros.usgs.gov/) with a 3 arc second resolution and a geocoding accuracy of ±12.6 m (Farr et al., 2007). The horizontal resolution of the DEM after a projection on the studied area was 76 m.

Elevations of ASTER and PRISM DEMs were calibrated with that of SRTM DEM (Willis et al., 2012a, 2012b). First, all values above 3500 m, which are above the peak elevation of Co Fitz Roy (3405 m), the highest mountain within the study area, were removed from the ASTER and PRISM DEMs to reduce the effect of clouds. Elevations within bedrock area were extracted from all the DEMs using a mask created from the GLIMS SPI glacier outlines in 2001, provided by the US National Snow and Ice Data Center (Bishop et al., 2004; Kargel et al., 2005; Raup et al., 2007). Then, SRTM bedrock elevations were subtracted from the ASTER and PRISM bedrock elevations. Such pixels with absolute differences of more than 100 m were discarded because they are due to DEM errors and clouds. Pixels with values deviated more than two standard deviations from the mean were also discarded, to further reduce the influence of clouds on the elevation data. The resulted elevation difference within the bedrock area was fitted with a linear function of east-west and north-south coordinates. This trend approximated by the linear equation was assumed as an artificial offset between the DEMs and the SRTM elevation data, and subtracted from the elevation difference within the bedrock area. This procedure was repeated 10 times. Then the trends

calculated for each image scene were combined into a single plane, which was removed from original ASTER and PRISM DEMs used for ice surface elevation change measurements. To reduce errors, pixels showing elevation changes < −40 or > 5 m a^{-1} were removed. Root mean square errors (RMSEs) between SRTM and ASTER DEMs, and SRTM and ALOS DEMs over the bedrock area were calculated to estimate the accuracies of the DEMs. The mean of RMSEs computed for all the ASTER and PRISM DEMs used in this study was 15.2 m.

5.2. Results

5.2.1. Ice front position and bed topography

Figure 5.3 shows the lake bathymetry in front of Upsala Glacier. Lake depth was ~590 m along the center line of the lake. A 100 m high bedrock rise was located at 3 km from the glacier front. The trough inclined ~0.8° down-glacier from the just upstream of the bedrock rise to the front. Slope angle of the side walls was typically 20°.

Ice front retreated from 16 January 2004 to 23 March 2005 back to approximately the location of the bedrock rise (Fig. 5.3). The front stayed at nearly the same position until 20 February 2008. Then, the eastern half of the front rapidly retreated and the glacier center retreated from the bedrock rise between 20 February 2008 and 14 August 2008. The western half subsequently retreated between 2 November 2008 and 13 May 2009. After this spatially nonuniform retreat from February 2008 to May 2009, retreat rate became more uniform across the glacier front until 25 August 2012. After this, the ice front was almost stable from 2012 to 2014 (Fig. 5.3). In contrast to the relatively small retreat (0.8 km) from 2000 to 2008, the retreat distance from 2008 to 2012 was large (3.2 km) (Fig. 5.4).

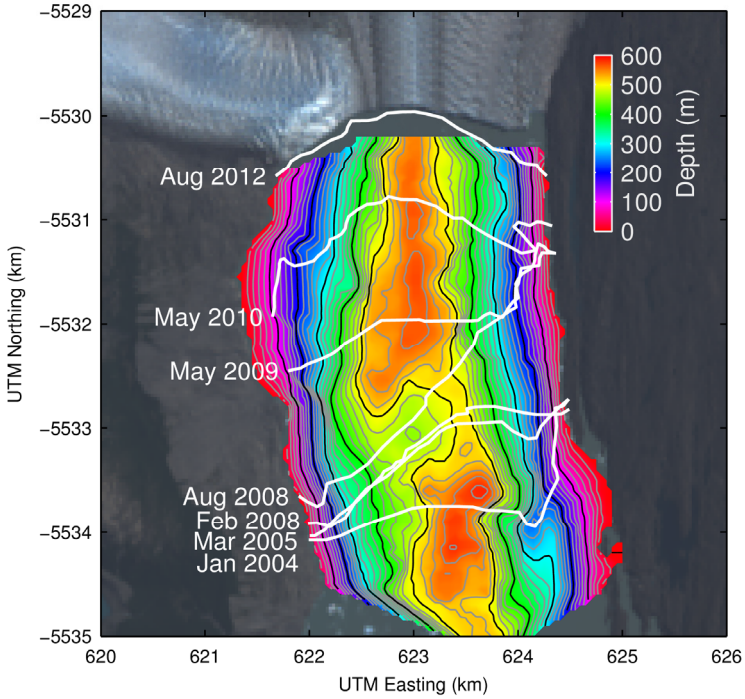

Figure 5.3. Frontal margins of Upsala Glacier and color-coded bathymetry of Brazo Upsala. Background is a Landsat 8 OLI band 8 image acquired on 12 February 2014.

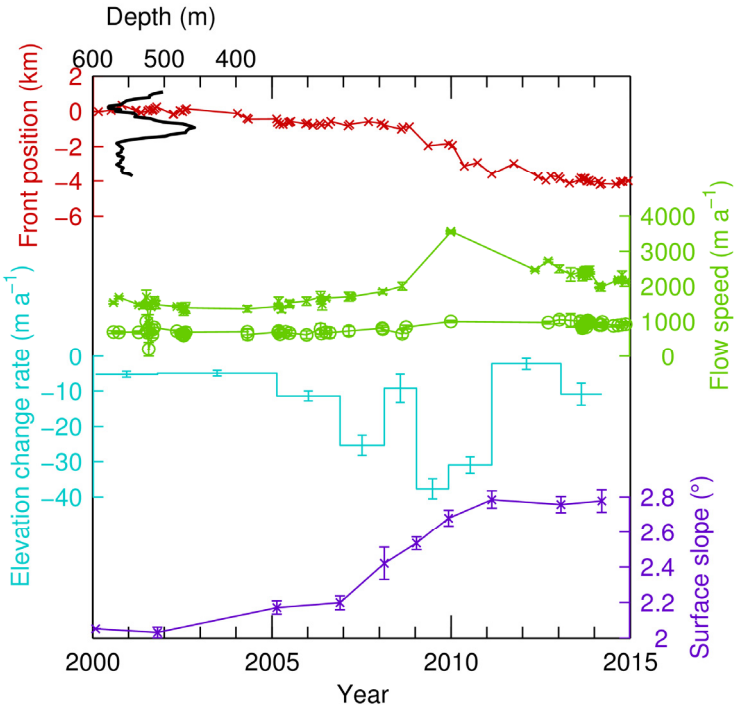

Figure 5.4. Cumulative changes in ice front positions of Upsala Glacier from 2000 to 2014 (red). Ice speeds at 4.5 (x) and 12.5 (o) km from the front along the centerline (green). Mean rate of elevation change within 4.5–12.5 km from the front along the centerline (cyan). Mean surface slope angle within 4.5–12.5 km from the front along the centerline (purple). Depth along the centerline is indicated as black line. Its horizontal distance is indicated in ordinate of the cumulative changes in the ice front positions.

5.2.2. Ice speed

Ice speed at 4.5 km from the front decreased from 1540 m a^{-1} to 1360 m a^{-1} in 2000–2002 and then the speed was almost stable at this level until 2004. The speed gradually increased from 1430 m a^{-1} to 1850 m a^{-1} from February 2005 to February 2008 when just before the rapid frontal retreat. The peak speed of 3570 m a^{-1} was observed in December 2009. After this, the speed decreased to 2340 m a^{-1} in April 2013 (Fig. 5.4). Ice speed at 12.5 km from the front indicates the similar changes but the magnitude was smaller than the speed at 4.5 km. Ice speed at 12.5 km from the front increased from 700 m a^{-1} to 1000 m a^{-1} between February 2005 and December 2009

(Fig. 5.4).

5.2.3. Surface elevation

Figure 5.5 shows glacier surface elevation along the centerline of Upsala Glacier. Mean rate of elevation change within 4.5–12.5 km from the 2000 front along the centerline was −5 m a^{-1} from February 2000 to February 2005. It decreased to −11 m a^{-1} in a period between February 2005 and November 2006. Over a period between November 2006 and February 2008, the rate was −25 m a^{-1}. From 2008 to 2011, the rate was sometimes below −30 m a^{-1}. It increased to a rate of −5 m a^{-1} between March 2011 and January 2013 (Fig. 5.4). Surface slope slightly increased from 2.05° to 2.20° from February 2000 to November 2006. Then it rapidly increased to 2.79° in March 2011. This slope angle was kept till 2014 (Figs 5.4 and 5.5).

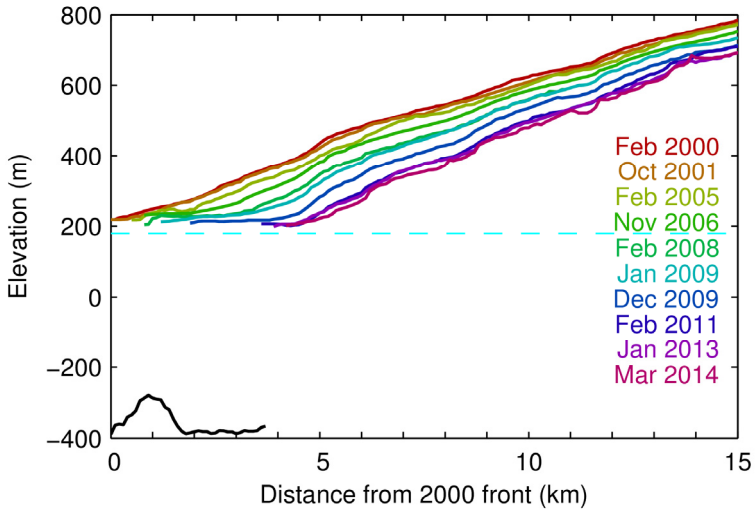

Figure 5.5. Glacier surface elevation along the centerline. The cyan and black lines indicate the lake level and bed elevation, respectively.

5.3. Discussion

5.3.1. Influence of the bed topography on the frontal retreat

The ice front gradually retreated from 2004 to 2005, but the retreat stopped and the front position was at the location of the bedrock rise from March 2005 to February 2008. The

ice near the glacier front thinned by 12 m a^{-1} from 2005 to 2006. Then the glacier thinned further by 25 m a^{-1} from 2006 to 2008, during the period when the front terminated at the bedrock rise location (Figs 5.4 and 5.5). Flow acceleration of 420 m a^{-1} at 4.5 km from the 2000 front was greater than that of 80 m a^{-1} at the 12.5 km from 2005 to 2008 (Fig. 5.4). This change in flow regime indicates increase in stretching flow. This change in the flow regime, i.e. enhancement in longitudinally stretching flow, likely contributed to the thinning in the vicinity of the terminus. A modeling study also reproduced dynamic thinning over the bed slope behind a bump (Vieli et al., 2002).

Flotation level is defined as water level which fulfills the hydrostatic equilibrium condition of glacier ice. It was calculated using the bed and surface elevations, assuming that ice density is 910 kg m^{-3} and lake water density is 1000 kg m^{-3}. Differences between the flotation level and the lake level are shown in Figure 5.6. The ice thinning lowered the flotation level within ~2 km from the front to the lake level between November 2006 and February 2008 (Figs 5.6a and 5.6b). However, the flotation level over the bedrock rise was above the lake level in February 2008 when just before the onset of the rapid retreat (Fig. 5.6b). These results suggest that the bedrock rise suppressed frontal retreat. Due to this suppression of the frontal retreat, large area of the terminus reached flotation. Thus, both of the stagnant ice front by the bedrock rise and the ice thinning resulted in expansion of the terminus area where the ice reached flotation. These relationships among the bed topography, thinning, and terminus flotation are similar to those reported for rapidly retreating glaciers in Greenland (Howat et al., 2008; Joughin et al., 2008a).

After February 2008, the ice front rapidly retreated by 3 km until August 2012 (Fig. 5.4). Frontal retreat was spatially nonuniform across the glacier front during this period (Fig. 5.3). The eastern half over the 1 km from the front disintegrated between February and August 2008 (Fig. 5.6b). Within this region, flotation level was more than 10 m below the lake level in 2008. After this event, flotation level in the western half is below the lake level in January 2009, and the western half retreated from January to May 2009 (Fig. 5.6c). Similar sequence of thinning and retreat was observed between December 2009 and May 2010 (Fig. 5.6d). These observations indicate that ice front began retreat after several months since ice became thinner than the hydrostatic equilibrium condition

(Figs 5.6b, 5.6c, and 5.6d). Consequently, terminus area with the ice fulfilling the hydrostatic equilibrium condition progressively disintegrated and resulted in the rapid frontal retreat between 2008 and 2012. These results well agreed with observations reported for the rapid retreat of Columbia Glacier in Alaska. A study on this glacier reported that during the rapid retreat the terminus retreated back to the points where flotation level of ice near the calving front is approximately equal to the sea level (Meier and Post, 1987).

A tabular iceberg was observed in front of the glacier in a Landsat image acquired on 29 September 2010 (Fig. 5.7). Production of tabular icebergs is a strong indication of floating termini (Amundson et al., 2010). Floating termini allow crevasses to penetrate the full thickness of the ice and induce calving (Joughin et al., 2008a). Terminus elevation profile of Upsala Glacier was very flat in 2009–2011 (Fig. 5.5), which also suggests that the ice was close to a floating condition. Therefore, it is likely that the terminus was near to flotation between 2009 and 2011. Thus, I suggest the following processes as a mechanism of the rapid retreat of Upsala Glacier after 2008. As the terminus retreated into the bedrock depression, terminus thinned until it reached flotation. Once ice reached flotation, full-thickness crevasses were formed at several hundred meters from the front, which resulted in the rapid frontal retreat.

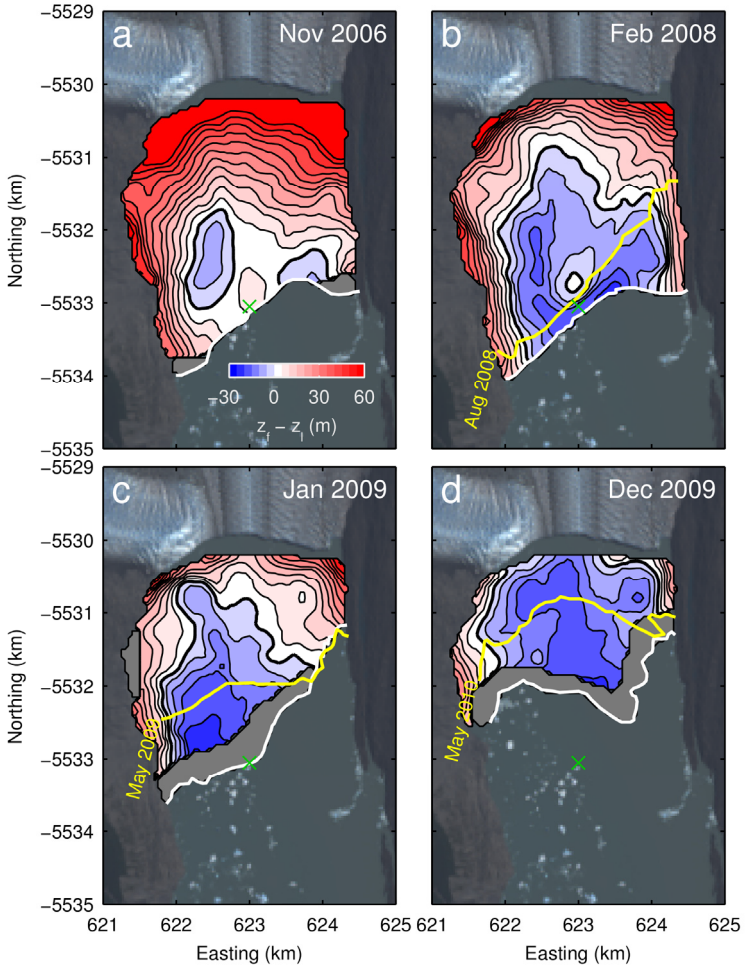

Figure 5.6. Contour maps of difference between the flotation level and the lake level within the terminus on (a) 26 November 2006, (b) 20 February 2008, (c) 14 January 2009, and (d) 7 December 2009. The difference is shown with 5 m contours and thick line indicates the boundary between the positive and negative values. Floating condition is achieved in the area shown as blue but not in the area shown as red. Yellow line shows the ice front position several months after the time of the contour map. Green cross indicates location of the bedrock rise. Background is a Landsat 8 OLI band 8 image acquired on 12 February 2014.

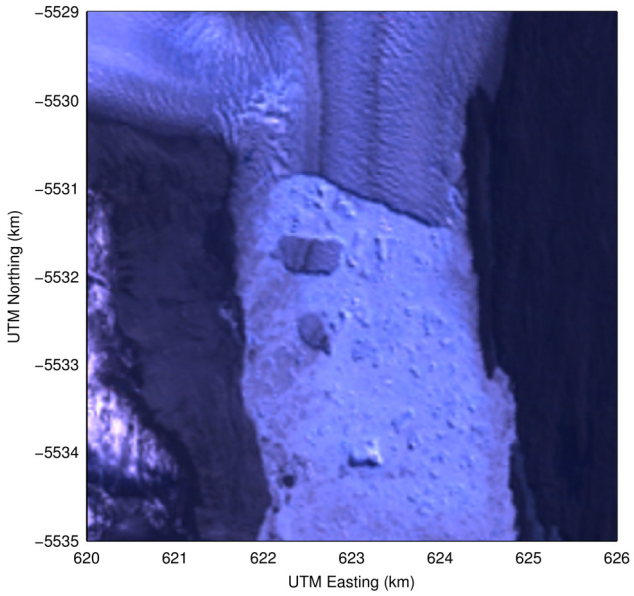

Figure 5.7. A Landsat 8 OLI true color image around terminus of Upsala Glacier acquired on 29 September 2010.

5.3.2. Feedback between acceleration, thinning, and retreat

Ice speed was relatively uniform until 2004, and then the speed significantly increased between 2006 and 2010 (Fig. 5.4). During the period of the acceleration, surface slope increased from 2.20° to 2.68° within 4.5–12.5 km from the front. Ice within ~12.5 km from the front thinned at a rate more than 20 m a^{-1} during this period (Fig. 5.4). Thus, ice thinning and surface steepening coincided with the speedup.

Flow speed at the base u_b and surface u_s are given by

$$u_b = k\frac{\tau_b^n}{P_e^m}, \tag{5.1}$$

$$u_s = u_b + \frac{2A}{n+1}\tau_b^n H, \tag{5.2}$$

k and m are empirical parameters, n is the exponent in Glen's flow law with the most plausible value of $n = 3$, P_e is the effective pressure, A is the creep parameter, and H is the ice thickness (Bindschadler, 1983; Cuffey and Paterson, 2010). Basal shear stress τ_b is defined by

$$\tau_b = f'\rho g H \sin\alpha, \tag{5.3}$$

where f' is the correction factor, ρ is the density of ice, g is gravitational acceleration,

and α is the surface slope (Cuffey and Paterson, 2010). According to these three equations, surface speed is proportional to H and α. Therefore, both of these changes in H and α should have influenced flow speed by changing τ_b. However, the role of H in sliding is complicated because it affects both τ_b and P_e, and these variables have contrasting effects on the sliding (Pfeffer, 2007).

Here, I investigate a role of the steepening in the acceleration. If it is assumed that surface speed is proportional to α and $n = 3$, the steepening from 2.20 to 2.68° (+22%) yields corresponding speedup of 81% between November 2006 and December 2009 (Fig. 5.4). For a comparison, the mean rate of the speedup from 2006 to 2009 was 76% within 4.5–12.5 km from the front. According to these calculations, the steepening accounts for most of the observed speedup. Assuming that the mean thickness within 4.5–12.5 km from the front is similar to the thickness at 3.5 km from the front, the ice thinned by 10% between November 2006 and December 2009 (Fig. 5.4). Thinning tends to decrease flow speed because basal shear stress decreases. On the other hand, it can increase flow speed because the effective pressure at the bed decreases (Pfeffer, 2007). Although it is difficult to accurately calculate the influence of the thinning on the ice flow, the magnitude of the relative rate of the ice thickness change is more than 2 times smaller than the rate of slope change. In addition, it is proposed that influence of changes in effective pressure on the ice flow is square root of n smaller than that of driving stress (Bindschadler, 1983). These results suggest that the slope change caused most of the speedup between 2006 and 2009.

Thinning rate was greater than 10 m a^{-1} from 2005 to 2011 and even greater (> 30 m a^{-1}) from 2009 to 2011 (Fig. 5.4). This extremely large thinning was likely due to compressive vertical straining caused by increase in horizontal stretching resulted from flow acceleration. Along the glacier centerline, longitudinal strain rate at 4.5–12.5 km increased from 0.12 a^{-1} to 0.32 a^{-1} between 2007 and 2010. This increase is due to more enhanced acceleration near the terminus as compared to the upper reaches. Thinning rate decreased to 5 m a^{-1} after March 2011 when ice speed decreased in the lower reaches (Fig. 5.4). Because the thinning rate increases downglacier (Fig. 5.5), there is a possibility that the ice thinning caused surface steepening and thus enhanced flow acceleration. This feedback mechanism among the speedup, thinning, and steepening

was reported in Greenland (e.g. Joughin et al., 2012; Howat et al., 2005, 2007). In addition to this feedback, it is likely that the thinning due to flow acceleration caused ice flotation and triggered the rapid frontal retreat of Glacier Upsala.

5.4. Summary

Field observations and satellite data analysis were performed at Upsala Glacier in the SPI to investigate mechanisms controlling the rapid retreat and the flow acceleration. Lake bathymetry within a region from 0.5 to 5 km from the 2014 front of Upsala Glacier was measured by echo sounders in December 2013 and October 2014. From these measurements a bedrock rise having a height of 100 m was found in the middle of a trough having a depth of ~590 m in the lake. The frontal position and the flow speed were measured using Landsat images acquired from 2000 to 2015. In addition to the Landsat data, SRTM, ALOS, and ASTER DEMs were used to measure the surface elevations. The frontal position was stagnant over the bedrock rise from March 2005 to February 2008. Then the front rapidly retreated by 3 km until 2012. The ice thinned by more than 30 m a^{-1} between 2009 and 2011. Ice speed at 4.5 km from the front increased by 1860 m a^{-1} between 2007 and 2010. This speedup was coincident with an increase in surface slope from 2.20° to 2.79° between 2006 and 2011.

The terminus over the bedrock rise thinned under a condition of the stagnant front between 2005 and 2008, and its flotation level within the terminus reached the lake level in front of the glacier in February 2008. After this, the terminus fulfilling the hydrostatic equilibrium condition progressively detached from the glacier front. This disintegration of the ice resulted in the rapid retreat between 2008 and 2012. The thinning in the lower reaches steepened surface slope and increased flow speed between 2006 and 2011. This flow acceleration stretched the ice and induced ice thinning. These results suggest that there was positive feedback between flow acceleration and ice thinning. It is likely that the feedback enhanced the frontal retreat since 2008. Thus, the basal topography and the feedback between flow acceleration and ice thinning play crucial roles in the rapid retreat of Upsala Glacier.

Chapter 6

Conclusion

6.1. Ice front variations and velocity changes

Satellite image analysis was carried out to quantify changes in ice front positions and velocities of calving glaciers in the Southern Patagonia Icefield (SPI) and along the coast of the Prudhoe Land, northwestern Greenland. The analysis was conducted over periods more than 20 years with annual to seasonal resolutions. Special focus of the study was rapid frontal retreat and flow acceleration of the calving glaciers.

Ice front positions and velocities of 32 termini of 28 calving glaciers in the SPI were measured using Landsat images acquired from 1984 to 2014. Among the 32 termini studied, only the two termini of Pío XI Glacier advanced, 11 termini indicated no significant changes, and 17 termini retreated from 1980s and 2014. This result indicates that 53% of the studied termini retreated over the study period, and the mean retreat rate was 66 m a^{-1} for all studied termini. Jorge Montt, HPS12, and Upsala Glaciers rapidly retreated at rates more than 200 m a^{-1} in the same period. Ice speed near the front of all studied glaciers ranged between 148 and 5970 m a^{-1}. Ice speed of the three rapidly retreating glaciers significantly accelerated. According to detailed analysis of the frontal variations and ice speed changes, I revealed that the timing of the acceleration closely agreed with the rapid retreats.

Ice front positions and velocities were also measured for 19 calving glaciers along the coast of the Prudhoe Land, northwestern Greenland, using Landsat images acquired from 1987 to 2014. All 19 studied glaciers retreated by 5.34 to 0.23 km between the 1980s and 2014. The mean and median retreat distances were 1.02 and 0.63 km, respectively. Heilprin, Tracy, Farquhar, Melville, Bowdoin, and Diebitsch Glaciers retreated by more than 1 km in the same period. Most of the glaciers began to retreat around 2000, as indicated by change in the median (mean) retreat rate from −1 (−1) m a^{-1} in 1980s–1999 to 38 (66) in 2000–2014. Within 5 km from the fronts, ice speed ranged between 14 and 1814 m a^{-1}. Many of the studied glaciers accelerated in the early 2000s. Heilprin, Tracy, Farquhar, Bowdoin, and Diebitsch Glaciers accelerated at a rate

of 5–81 m a^{-2} between 2000 and 2014. There was correlation between retreat rate and acceleration for studied glaciers.

These results indicated that calving glaciers in the SPI and in northwestern Greenland are in a generally retreating trend. It is suggested that the primary cause of the generally retreating overall trend is negative mass balance due to increase in air temperature. However, the rapid frontal retreats were not directly controlled by the warming. The rapid retreat of calving glaciers was accompanied by flow acceleration in both of the study areas. For these rapid retreating glaciers, magnitude of the flow acceleration was greater near the front. This change in the flow regime enhanced stretching flow along the glaciers and induced dynamic thinning near the termini. The results of the satellite data analysis suggested that thinning due to the flow acceleration is the driver of the observed rapid retreat.

6.2. Mechanisms controlling rapid retreat and acceleration

Field observations and satellite data analysis were carried out at Upsala Glacier in the SPI to investigate mechanisms controlling rapid retreat and flow acceleration of calving glaciers. During field campaigns in 2013 and 2014, bottom topography of the proglacial lake was measured in front of the glacier, where the lake expanded its area after the rapid retreat began in 2008. The lake bottom topography and the glacier surface elevations were analyzed over the period of the retreat and flow acceleration of Upsala Glacier.

From lake bathymetric survey a bedrock rise was found at the valley center 3 km from the glacier front, where the lake was 590 m deep. The glacier front was stable at the location of the bedrock rise from March 2005 to February 2008. Then the front rapidly retreated by 3 km by 2012. Ice thinned by more than 30 m a^{-1} between 2009 and 2011. Ice speed at 4.5 km from the front increased by 1860 m a^{-1} between 2007 and 2010. This speedup coincided with steepening of the glacier surface from 2.20 to 2.79° between 2006 and 2011.

The glacier thinned near the terminus between 2005 and 2008, while the ice front position was stable at the lake bottom bump location. As a result of this thinning,

floatation level which calculated from the glacier surface elevation and bottom elevations, became below the lake level. When this threshold was reached, ice front got afloat and rapid retreat began in August 2008. After August 2008, ice progressively detached from the glacier front as soon as that portion of ice became thinner than the floating condition. This disintegration resulted in the rapid retreat between 2008 and 2012. Since the thinning was more significant in the lower reaches, surface slope steepened and ice speed increased between 2006 and 2011. This flow acceleration stretched the ice along the glacier and it induced thinning due to vertical compression. This positive feedback between flow acceleration and ice thinning enhanced the frontal retreat since 2008.

Thus, my interpretation on the rapid retreat of Upsala Glacier since 2008 is as follows. The glacier gradually retreated and thinned under the warming climate condition until the ice front retreated to the lake bed bump. Then, the ice behind the calving front thinned to near flotation, while the terminus position remained at the same location. As the ice reached hydrostatic equilibrium condition, crevasses penetrated to the bed of the glacier and full-thickness calving occurred. Because of the active calving the glacier went for rapid retreat in 2008. The thinning near the terminus steepens ice surface, which took a vital role in the flow acceleration. The acceleration caused further thinning because ice discharge increased by enhanced calving due to the increased flow speed. This study demonstrated that a calving glacier dynamically changes its thickness, length, and flow speed in a cycle consists of thinning near the terminus, rapid frontal retreat, and flow acceleration. Once a glacier gets into this cycle, positive feedbacks act among the processes and the glacier is further destabilized.

6.3. Future prospects of the study

I developed techniques to measure ice front position and flow velocity of calving glaciers with long-term and high temporal resolutions. It is beneficial to carry out similar measurements for calving glaciers in other regions in the world. For example, calving glaciers in the Canadian Arctic is a possible study area because observational data for calving glaciers are lacking. As this area locates close to northwestern Greenland, it is assumed that calving glaciers in these regions are influenced by a

similar warming condition. By comparing changes in calving glaciers in the Canadian Arctic and those in northwestern Greenland, we can better understand response of calving glaciers to a similar climate conditions but in different geometrical settings.

This study suggested an important role of rapid changes of calving glaciers in regional ice mass loss. As a next step of this study, it is necessary to quantify ice mass discharged by calving glaciers to the ocean and lakes. The ice discharge through a calving glacier is estimated as product of ice density, calving rate, cross-sectional area at the front. By comparing changes in the ice discharge and those in the surface mass balance, we can quantify relative importance of mass loss due to calving to the total mass loss in a region. These data should contribute to better understand processes controlling the regional ice mass loss, such as changes in glacier dynamics of calving glaciers and changes in the climate. This improves the future projection of glacier contributions to SLR.

Based on the observations and the analysis conducted at Upsala Glacier, I proposed possible mechanisms controlling rapid retreat and flow acceleration of calving glaciers. The next challenge is to implement my findings in a numerical glacier model to simulate rapid retreat and flow acceleration of calving glaciers. By including observational facts revealed in this study, numerical simulations on glacier dynamics and evolution should improve our understanding of future changes in calving glaciers.

References

Amundson, J. M., M. Fahnestock, M. Truffer, J. Brown, M. P. Lüthi, and R. J. Motyka (2010), Ice mélange dynamics and implications for terminus stability, Jakobshavn Isbræ, Greenland, *J. Geophys. Res.*, **115**, F01005, doi:10.1029/2009JF001405

Andersen, M. L., T. B. Larsen, M. Nettles, P. Elosegui, D. van As, G. S. Hamilton, L. A. Stearns, J. L. Davis, A. P. Ahlstrøm, J. de Juan, G. Ekström, L. Stenseng, S. A. Khan, R. Forsberg, and D. Dahl-Jensen (2010), Spatial and temporal melt variability at Helheim Glacier, East Greenland, and its effect on ice dynamics, *J. Geophys. Res.*, **115**, F04041, doi:10.1029/2010JF001760.

Aniya, M., H. Sato, R. Naruse, P. Skvarca, and G. Casassa (1996), The use of satellite and airborne imagery to inventory outlet glaciers of the Southern Patagonia Icefield, South America, *Photogramm. Eng. Remote Sens.,* **62**(12), 1361–1369.

Aniya, M., H. Sato, R. Naruse, P. Skvarca, and G. Casassa (1997), Recent glacier variations in the Southern Patagonia Icefield, South America, *Arct. Alp. Res.*, **29**(1), 1–12.

Aravena, J. C., and B. H. Luckman (2009), Spatio-temporal rainfall patterns in Southern South America, *Int. J. Climatol.*, **29**, 2106–2120.

Bartholomew, I., P. Nienow, D. Mair, A. Hubbard, M. A. King, and A. Sole (2010), Seasonal evolution of subglacial drainage and acceleration in a Greenland outlet glacier, *Nat. Geosci.*, **3**, 408–411, doi:10.1038/ngeo863.

Benn, D. I., C. R. Warren, and R. H. Mottram (2007), Calving processes and the dynamics of calving glaciers, *Earth Sci. Rev.*, **82**, 143–179, doi:10.1016/j.earscirev.2007.02.002.

Bindschadler, R. (1983), The importance of pressurized subglacial water in separation and sliding at the glacier bed, *J. Glaciol.*, **29**(101), 3–19.

Bishop, M. P., et al. (2004), Global Land Ice Measurements from Space (GLIMS): Remote sensing and GIS investigations of the Earth's cryosphere, *Geocarto Int.*, **19**(2), 57–84, doi:10.1080/10106040408542307.

Brown, C. S., M. F. Meier, and A. Post (1982), Calving speed of Alaska tidewater glaciers, with application to Columbia glacier, *U. S. Geol. Surv. Prof. Pap.* **1258-C**, 13 pp.

Carr, J. R., C. R. Stokes, and A. Vieli (2013), Recent progress in understanding marine-terminating Arctic outlet glacier response to climatic and oceanic forcing: Twenty years of rapid change, *Progress in Physical Geography*,

doi:10.1177/0309133313483163.

Carr, J. R., C. Stokes, and A. Vieli (2014), Recent retreat of major outlet glaciers on Novaya Zemlya, Russian Arctic, influenced by fjord geometry and sea-ice conditions, *J. Glaciol*., **60**(219), 155–170, doi:10.3189/2014JoG13J122.

Ciappa, A., L. Pietranera, and F. Battazza (2010), Perito Moreno Glacier (Argentina) flow estimation by COSMO SkyMed sequence of high-resolution SAR-X imagery, *Remote Sens*. *Environ*., **114**, 2088–2096.

Church, J. A., P. U. Clark, A. Cazenave, J. M. Gregory, S. Jevrejeva, A. Levermann, M. A. Merrifield, G. A. Milne, R. S. Nerem, P. D. Nunn, A. J. Payne, W. T. Pfeffer, D. Stammer, and A. S. Unnikrishnan (2013), Sea Level Change, in *Climate Change 2013: The Physical Science Basis. Contribution of Working Group I to the Fifth Assessment Report of the Intergovernmental Panel on Climate Change,* edited by Stocker, T.F., D. Qin, G.-K. Plattner, M. Tignor, S.K. Allen, J. Boschung, A. Nauels, Y. Xia, V. Bex and P.M. Midgley, Cambridge University Press, Cambridge, United Kingdom, and New York, NY, USA.

Cuffey, K., and W. S. B. Paterson (2010), The Physics of Glaciers, 4th ed., Elsevier, Burlington, Mass.

Davies, B. J., and N. F. Glasser (2012), Accelerating shrinkage of Patagonian glaciers from the Little Ice Age (~AD 1870) to 2011, *J. Glaciol*., **58**(212), 1063–1084, doi:10.3189/2012JoG12J026.

Doyle, S. H., A. L. Hubbard, C. F. Dow, G. A. Jones, A. Fitzpatrick, A. Gusmeroli, B. Kulessa, K. Lindback, R. Pettersson, and J. E. Box (2013), Ice tectonic deformation during the rapid in situ drainage of a supraglacial lake on the Greenland Ice Sheet, *Cryosphere*, **7**, 129–140, doi:10.5194/tc-7-129-2013.

Enderlin, E. M., I. M. Howat, S. Jeong, M. J. Noh, J. H. van Angelen and M. R. van den Broeke (2014), An improved mass budget for the Greenland ice sheet, *Geophys*. *Res*. *Lett*., **41**, 866–872, doi:10.1002/2013GL059010.

Farr, T. G., P. A. Rosen, E. Caro, R. Crippen, R. Duren, S. Hensley, M. Kobrick, M. Paller, E. Rodriguez, L. Roth, D. Seal, S. Shaffer, J. Shimada, J. Umland, M. Werner, M. Oskin, D. Burbank, and D. Alsdorf (2007), Shuttle Radar Topography Mission, *Rev*. *Geophys*., **45**, RG2004, doi:10.1029/2005RG000183.

Fettweis, X. (2007), Reconstruction of the 1979–2006 Greenland ice sheet surface mass balance using the regional climate model MAR, *Cryosphere*, **1**, 21–40, doi: 10.5194/tc-1-21-2007.

Fitch, A. J., A. Kadyrov, W. J. Christmas, and J. Kittler (2002), Orientation Correlation,

in: British Machine Vision Conference, 133–142.

Floricioiu, D., M. Eineder, H. Rott, and T. Nagler (2008), Velocities of major outlet glaciers of the Patagonia Icefield observed by TerraSAR-X, *Proceedings of '2008 IEEE International Geoscience and Remote Sensing Symposium'*, Boston, U.S..

Floricioiu, D., M. Eineder, H. Rott, N. Yague-Martinez, and T. Nagler (2009), Surface velocity and variations of outlet glaciers of the Patagonia Icefields by means of TerraSAR-X, *Proceedings of '2009 IEEE International Geoscience and Remote Sensing Symposium'*, Cape Town, South Africa.

Gardner, A. S., G. Moholdt, J. G. Cogley, B. Wouters, A. A. Arendt, J. Wahr, E. Berthier, Re. Hock, W. T. Pfeffer, G. Kaser, S. R. M. Ligtenberg, T. Bolch, M. J. Sharp, J. O. Hagen, M. R. van den Broeke, and F. Paul (2013), A reconciled estimate of glacier contributions to sea level rise: 2003 to 2009, *Science*, **340**(6134), 852–857, doi:10.1126/science.1234532.

Glasser, N. F., S. Harrison, K. N. Jansson, K. Anderson, and A. Cowley (2011), Global sea-level contribution from the Patagonian Icefields since the Little Ice Age maximum, *Nature Geosci.*, **4**(5), 303–307, doi:10.1038/ngeo1122.

Guizar-Sicairos, M., S. T. Thurman, and J. R. Fienup (2008), Efficient subpixel image registration algorithms, *Opt. Lett.*, **33**, 156–158, doi:10.1364/OL.33.000156.

Haug, T., A. Kääb, and P. Skvarca (2010), Monitoring ice shelf velocities from repeat MODIS and Landsat data – a method study on the Larsen C ice shelf, Antarctic Peninsula, and 10 other ice shelves around Antarctica, *Cryosphere*, **4**(2), 161–178, doi:10.5194/tc-4-161-2010.

Heid, T., and A. Kääb (2012), Evaluation of existing image matching methods for deriving glacier surface displacements globally from optical satellite imagery, *Remote Sens. Environ.*, **118**, 339–355, doi:10.1016/j.rse.2011.11.024.

Howat, I. M., and A. Eddy (2011), Multi-decadal retreat of Greenland's marine-terminating outlet glaciers, *J. Glaciol.*, **57**(203), 389–396, doi:10.3189/002214311796905631.

Howat, I. M., I. Joughin, S. Tulaczyk, and S. Gogineni (2005), Rapid retreat and acceleration of Helheim Glacier, east Greenland, *Geophys. Res. Lett.*, **32**(22), L22502, doi:10.1029/2005GL024737.

Howat, I. M., I. Joughin, and T. A. Scambos (2007), Rapid changes in ice discharge from Greenland outlet glaciers, *Science*, **315**(5818), 1559–1561, doi:10.1126/science.1138478.

Howat, I. M., I. Joughin, M. Fahnestock, B. E. Smith, and T. Scambos (2008),

Synchronous retreat and acceleration of southeast Greenland outlet glaciers 2000–2006: ice dynamics and coupling to climate, *J. Glaciol.*, **54**(187), 646–660, doi:10.3189/ 002214308786570908.

Howat, I. M., J. E. Box, Y. Ahn, A. Herrington, and E. M. McFadden (2010), Seasonal variability in the dynamics of marine-terminating outlet glaciers in Greenland, *J. Glaciol*., **56**(198), 601–613, doi:10.3189/002214310793146232.

Howat, I. M., Y. Ahn, I. Joughin, M. R. van den Broeke, J. T. M. Lenaerts, and B. Smith (2011), Mass balance of Greenland's three largest outlet glaciers, 2000–2010, *Geophys*. *Res*. *Lett*., **38**, L12501, doi:10.1029/2011GL047565.

Howat, I. M., A. Negrete, and B. E. Smith (2014), The Greenland Ice Mapping Project (GIMP) land classification and surface elevation data sets, *Cryosphere*, **8**(4), 1509–1518, doi:10.5194/tc-8-1509-2014.

Ibarzabal y Donangelo, T., J. Hoffmann, and R. Naruse (1996), Recent climate changes in Southern Patagonia, *Bull. Glacier Res.*, **14**, 29–36.

Joughin, I., E. Rignot, C. E. Rosanova, B. K. Lucchitta, and J. Bohlander (2003), Timing of Recent Accelerations of Pine Island Glacier, Antarctica, *Geophys*. *Res*. *Lett*., **30**, 1706, doi:10.1029/2003GL017609.

Joughin, I., W. Abdalati, and M. Fahnestock (2004), Large fluctuations in speed on Greenland's Jakobshavn Isbræ glacier, *Nature*, **432**(7017), 608–610, doi:10.1038/nature03130.

Joughin, I., I. M. Howat, R. B. Alley, G. Ekstrom, M. Fahnestock, T. Moon, M. Nettles, M. Truffer, and V. C. Tsai (2008a), Ice-front variation and tidewater behavior on Helheim and Kangerdlugssuaq Glaciers, Greenland, *J. Geophys*. *Res*., **113**, F01004, doi:10.1029/2007JF000837.

Joughin, I., I. M. Howat, M. Fahnestock, B. Smith, W. Krabill, R. B. Alley, H. Stern, and M. Truffer (2008b), Continued evolution of Jakobshavn Isbrae following its rapid speedup, *J. Geophys*. *Res*., **113**, F04006, doi:10.1029/2008JF001023.

Joughin, I., B. E. Smith, I. M. Howat, T. Scambos, and T. Moon (2010), Greenland flow variability from ice-sheet-wide velocity mapping, *J. Glaciol*., **56**(197), 415–430, doi:10.3189/002214310792447734.

Joughin, I., B. E. Smith, I. M. Howat, D. Floricioiu, R. B. Alley, M. Truffer, and M. Fahnestock (2012), Seasonal to decadal scale variations in the surface velocity of Jakobshavn Isbrae, Greenland: Observation and model-based analysis, *J. Geophys*. *Res*., **117**, F02030, doi:10.1029/2011JF002110.

Kääb, A. (2005), Combination of SRTM3 and repeat ASTER data for deriving alpine

glacier flow velocities in the Bhutan Himalaya, *Remote Sens*. *Environ*., **94**(4), 463–474, doi:10.1016/j.rse.2004.11.003.

Kääb, A., B. Lefauconnier, and K. Melvold (2005), Flow field of Krönebreen, Svalbard, using repeated Landsat 7 and ASTER data, *Ann. Glaciol*., **42**, 7–13.

Kargel, J. S., et al. (2005), Multispectral imaging contributions to global land ice measurements from space, *Remote Sens. Environ*., **99**, 187–219, doi:10.1016/j.rse.2005.07.004.

Khan, S. A., J. Wahr, M. Bevis, I. Velicogna, and E. Kendrick (2010), Spread of ice mass loss into northwest Greenland observed by GRACE and GPS, *Geophys*. *Res*. *Lett*., **37**, L06501, doi:10.1029/2010GL042460.

Kjær, K. H., S. A. Khan, N. J. Korsgaard, J. Wahr, J. L. Bamber, R. Hurkmans, M.van den Broeke, L. H. Timm, K. K. Kjeldsen, A. A. Bjørk, N. K. Larsen, L. T. Jørgensen, A. Færch-Jensen, and E. Willerslev (2012), Aerial photographs reveal late-20th-century dynamic ice loss in northwestern Greenland, *Science*, **337**, 569, doi:10.1126/science.1220614.

Lopez, P., P. Chevallier, V. Favier, B. Pouyaud, F. Ordenes, and J. Oerlemans (2010), A regional view of fluctuations in glacier length in southern South America, *Global Planet. Change*, **71**, 85–108.

Luckman, A., T. Murray, R. de Lange, and E. Hanna (2006), Rapid and synchronous ice-dynamic changes in East Greenland, *Geophys*. *Res*. *Lett*., **33**, L03503, doi:10.1029/2005GL025428.

Masiokas, M. H., A. Rivera, L. E. Espizua, R. Villalba, S. Delgado, and J. C. Aravena (2009), Glacier fluctuations in extratropical South America during the past 1000 years, *Palaeogeogr. Palaeoclimatol. Palaeoecol.*, **281**, 242–268.

McClellan, J. H., R. W. Schafer, and M. A. Yoder (2003), Signal Processing First, Pearson Education, Inc., Pearson Prentice Hall, ISBN:0-13-120265-0.

McFadden, E. M., I. M. Howat, I. Joughin, B. E. Smith, and Y. Ahn (2011), Changes in the dynamics of marine terminating outlet glaciers in west Greenland (2000–2009), *J. Geophys*. *Res*., **116**, F02022, doi:10.1029/2010JF001757.

McNabb, R. W., and R. Hock (2014), Alaska tidewater glacier terminus positions, 1948–2012, *J. Geophys*. *Res*. *Earth Surf*., **119**, 153–167, doi:10.1002/2013JF002915.

McNabb, R. W., R. Hock, and M. Huss (2015), Variations in Alaska tidewater glacier frontal ablation, 1985–2013, *J. Geophys*. *Res*. *Earth Surf*., **120**, 120–136, doi:10.1002/2014JF003276.

Meier, M. F., and A. Post (1987), Fast tidewater glaciers, *J. Geophys. Res.*, **92**(B9), 9051–9058, doi:10.1029/JB092iB09p09051.

Meier, M. F., M. B. Dyurgerov, U. K. Rick, S. O'Neel, W. T. Pfeffer, R. S. Anderson, S. P. Anderson, and A. F. Glazovsky (2007), Glaciers Dominate Eustatic Sea-Level Rise in the 21st Century, *Science*, **317**(5841), 1064–1067, doi:10.1126/science.1143906.

Michel, R., and E. Rignot (1999), Flow of Glaciar Moreno, Argentina, from repeat-pass Shuttle Imaging Radar images: comparison of the phase correlation method with radar interferometry, *J. Glaciol.*, **45**(149), 93–100.

Moffat, C. (2014), Wind-driven modulation of warm water supply to a proglacial fjord, Jorge Montt Glacier, Patagonia, *Geophys. Res. Lett.*, **41**, 3943–3950, doi:10.1002/2014GL060071.

Moon, T., and I. Joughin (2008), Changes in ice front position on Greenland's outlet glaciers from 1992 to 2007, *J. Geophys. Res.,* **113**(F2), F02022, doi:10.1029/2007JF000927.

Moon, T., I. Joughin, B. Smith, and I. M. Howat (2012), 21st-century evolution of Greenland outlet glacier velocities, *Science*, **336**(6081), 576–578, doi:10.1126/science.1219985.

Murray, T., K. Scharrer, T. D. James,S. R. Dye, E. Hanna, A. D. Booth, N. Selmes, A. Luckman, A. L. C. Hughes, S. Cook, and P. Huybrechts (2010), Ocean regulation hypothesis for glacier dynamics in southeast Greenland and implications for ice sheet mass changes, *J. Geophys. Res.*, **115**, F03026, doi:10.1029/2009JF001522.

Muto, M., and M. Furuya (2013), Surface velocities and ice-front positions of eight major glaciers in the Southern Patagonian Ice Field, South America, from 2002 to 2011, *Remote Sens. Environ.*, **139**, 50–59, doi:10.1016/j.rse.2013.07.034.

Naruse, R., and P. Skvarca (2000), Dynamic features of thinning and retreating Glaciar Upsala, a lacustrine calving glacier in southern Patagonia, *Arct. Antarct. Alp. Res.*, **32**(4), 485–491.

Naruse, R., M. Aniya, P. Skvarca, and G. Casassa (1995), Recent variations of calving glaciers in Patagonia, South America, revealed by ground surveys, satellite-data analyses and numerical experiments, *Ann. Glaciol.*, **21**, 297–303.

Nick, F. M., A. Vieli, I. M. Howat, and I. Joughin (2009), Large scale changes in Greenland outlet glacier dynamics triggered at the terminus, *Nature Geosci.*, **2**(2), 110–114, doi:10.1038/ngeo394.

Nick, F. M., C. J. Van der Veen, A. Vieli, and D. I. Benn (2010), A physically based calving model applied to marine outlet glaciers and implications for the glacier dynamics, *J. Glaciol*., **56**, 781–794, doi:10.3189/002214310794457344.

Nick, F. M., A. Vieli, M. L. Andersen, I. Joughin, A. J. Payne, T. L. Edwards, F. Pattyn, and R. S. W. van de Wal (2013), Future sea-level rise from Greenland's main outlet glaciers in a warming climate, *Nature*, **497**(7448), 235–238, doi:10.1038/nature12068.

O'Neel, S., W. T. Pfeffer, R. Krimmel, and M. Meier (2005), Evolving force balance at Columbia Glacier, Alaska, during its rapid retreat, *J. Geophys. Res*., **110**, F03012, doi:10.1029/2005JF000292.

Payne, A. J., A. Vieli, A. P. Shepherd, D. J. Wingham, and E. Rignot (2004), Recent dramatic thinning of largest West Antarctic ice stream triggered by oceans, *Geophys. Res. Lett*., **31**, L23401, doi:10.1029/2004GL021284.

Pelto, M. S., and C. R. Warren (1991), Relationship between tidewater glacier calving velocity and water depth at the calving front, *Ann. Glaciol*., **15**, 115–118.

Pfeffer, W. T. (2007), A simple mechanism for irreversible tidewater glacier retreat, *J. Geophys. Res*., **112**, F03S25, doi:10.1029/2006JF000590.

Pfeffer, W. T., J. T. Harper, and S. O'Neel (2008), Kinematic Constraints on Glacier Contributions to 21st-Century Sea-Level Rise, *Science* **321**(5894), 1340–1343, doi:10.1126/science.1159099.

Pritchard, H. D., R. J. Arthern, D. G. Vaughan, and L. A. Edwards (2009), Extensive dynamic thinning on the margins of the Greenland and Antarctic ice sheets, *Nature*, **461**(7266), 971–975, doi:10.1038/nature08471.

Rasmussen, L. A., H. Conway, and C. F. Raymond (2007), Influence of upper air conditions on the Patagonia icefields, *Global Planet. Change,* **59**(1–4), 203–216.

Raup, B., A. Racoviteanu, S. Jodha, S. Khalsa, C. Helm, R. Armstrong, and Y. Arnaud (2007), Remote sensing and GIS technology in the Global Land Ice Measurements from Space (GLIMS) project, *Comput. Geosci*., **33**, 104 – 125.

Rignot, E., and P. Kanagaratnam (2006), Changes in the velocity structure of the Greenland Ice Sheet, *Science*, **311**(5673), 986–990, doi:10.1126/science.1121381.

Rignot, E., A. Rivera, and G. Casassa (2003), Contribution of the Patagonia Icefields of South America to sea level rise, *Science*, **302**(6544), 434–437, doi:10.1126/science.1087393.

Rignot, E., I. Velicogna, M. R. Van den Broeke, A. Monaghan, and J. Lenaerts (2011),

Acceleration of the contribution of the Greenland and Antarctic ice sheets to sea level rise, *Geophys. Res. Lett.*, **38**(5), L05503, doi:10.1029/2011GL046583.

Rivera, A., H. Lange, J. C. Aravena, and G. Casassa (1997), The 20th century advance of Glaciar Pío XI, Chilean Patagonia, *Ann. Glaciol.,* **24**, 66–71.

Rivera, A., T. Benham, G. Casassa, J. Bamber, and J. Dowdeswell (2007), Ice elevation and areal changes of glaciers from the Northern Patagonia Icefield, Chile, *Global and Planetary Change*, **59**, 126–137.

Rivera, A., J. Corripio, C. Bravo, and S. Cisternas (2012a), Glaciar Jorge Montt (Chilean Patagonia) dynamics derived from photos obtained by fixed cameras and satellite image feature tracking, *Ann. Glaciol.*, **53**(60), 147–155.

Rivera, A., M. Koppes, C. Bravo, and J. Aravena (2012b), Little ice age advance and retreat of Glaciar Jorge Montt, Chilean Patagonia, *Clim. Past*, **8**, 403–414.

Rosenblüth, B., G. Casassa, and H. Fuenzalida (1995), Recent climatic changes in western Patagonia, *Bull. Glacier Res.*, **13**, 127–132.

Rott, H., M. Stuefer, A. Siegel, P. Skvarca, and A. Eckstaller (1998), Mass fluxes and dynamics of Moreno Glacier, Southern Patagonia Icefield. *Geophys. Res. Lett.,* **25**(9), 1407–1410.

Sakakibara, D., and S. Sugiyama (2014), Ice-front variations and speed changes of calving glaciers in the Southern Patagonia Icefield from 1984 to 2011, *J. Geophys. Res. Earth Surf.*, **119**, 2541–2554, doi:10.1002/2014JF003148.

Sakakibara, D., S. Sugiyama, T. Sawagaki, S. Marinsek, and P. Skvarca (2013), Rapid retreat, acceleration, and thinning of Glaciar Upsala in the Southern Patagonia Icefield, initiated in 2008, *Ann. Glaciol.*, **54**(63), 131–138.

San, B. T., and M. L. Suzen (2005), Digital elevation model (DEM) generation and accuracy assessment from ASTER stereo data, *Int. J. Remote Sens.*, **26**(22), 5013–5027, doi:10.1080/01431160500177620.

Scambos, T. A., M. J. Dutkiewicz, J. C. Wilson, and R. A. Bindschadler (1992), Application of image cross-correlation to the measurement of glacier ice speed using satellite image data, *Remote Sens. Environ.*, **42**, 177–186.

Schaefer, M., H. Machguth, M. Falvey, and G. Casassa (2013), Modeling past and future surface mass balance of the Northern Patagonia Icefield, *J. Geophys. Res. Earth Surf.*, **118**, doi:10.1002/jgrf.20038.

Schoof, C. (2007), Ice sheet grounding line dynamics: Steady states, stability, and hysteresis, *J. Geophys. Res.*, **112**, F03S28, doi:10.1029/2006JF000664.

Schwikowski, M., M. Schläppi, P. Santibañez, A. Rivera, and G. Casassa (2013), Net accumulation rates derived from ice core stable isotope records of Pío XI glacier, Southern Patagonia Icefield, *Cryosphere*, **7**, 1635–1644.

Shiraiwa, T., S. Kohshima, R. Uemura, N. Yoshida, S. Matoba, J. Uetake, and M. A. Godoi (2002), High net accumulation rates at Campo de Hielo Patagonico Sur, South America, revealed by analysis of a 45.97 m long ice core, *Ann. Glaciol*., **35**(35), 84–90, doi:10.3189/172756402781816942.

Skvarca, P., H. de Angelis, R. Naruse, C. R. Warren, and M. Aniya (2002), Calving rates in fresh water: new data from southern Patagonia, *Ann. Glaciol*., **34**, 379–384.

Skvarca, P., B. Raup, and H. de Angelis (2003), Recent behaviour of Glaciar Upsala, a fast-flowing calving glacier in Lago Argentino, southern Patagonia, *Ann. Glaciol*., **36**, 184–188.

Skvarca, P., S. Marinsek, and M. Aniya. (2010), Documenting 23 years of areal loss of Hielo Patagónico Sur, recent climate data and potential impact on Río Santa Cruz water discharge: *Abstract Book of International Glaciological Conference Ice and Climate Change: A View from the South*, Valdivia, Chile, Centro de Estudios Cientificos, 82.

Sohn, H. G., K. C. Jezek, and C. J. van der Veen (1998), Jakobshavn Glacier, West Greenland: 30 years of Spaceborne observations, *Geophys*. *Res*. *Lett*., **25**(14), 2699–2702.

Sole, A. J., D. W. F. Mair, P. W. Nienow, I. D. Bartholomew, M. A. King, M. J. Burke, and I. Joughin (2011), Seasonal speedup of a Greenland marine-terminating outlet glacier forced by surface melt–induced changes in subglacial hydrology, *J. Geophys*. *Res*., **116**, F03014, doi:10.1029/2010JF001948.

Stuefer, M., H. Rott, and P. Skvarca (2007), Glaciar Perito Moreno, Patagonia: climate sensitivities and glacier characteristics preceding the 2003/04 and 2005/06 damming events, *J. Glaciol*., **53**(180), 3–16.

Sugiyama, S., P. Skvarca, N. Naito, H. Enomoto, S. Tsutaki, K. Tone, S. Marinsek, and M. Aniya (2011), Ice speed of a calving glacier modulated by small fluctuations in basal water pressure, *Nature Geosci*., **4**(9), 597–600, doi:10.1038/ngeo1218.

Sugiyama, S., D. Sakakibara, S. Tsutaki, M. Maruyama, and T. Sawagaki (2015), Glacier dynamics near the calving front of Bowdoin Glacier, northwestern Greenland, *J. Glaciol*., **61**(226), 223–232, doi:10.3189/2015JoG14J127.

Sundal, A. V., A. Shepherd, P. Nienow, E. Hanna, S. Palmer, and P. Huybrechts (2011), Melt-induced speed-up of Greenland ice sheet offset by efficient subglacial drainage, *Nature*, **469**, 521–524, doi:10.1038/nature09740.

Thomas, R. H. (2004), Force-perturbation analysis of recent thinning and acceleration of Jakobshavn Isbræ, Greenland, *J. Glaciol*., **50**(168), 57–66, doi:10.3189/172756504781830321.

Thomas, R. H., W. Abdalati, E. Frederick, W. B. Krabill, S. Manizade, and K. Steffen (2003), Investigation of surface melting and dynamic thinning on Jakobshavn Isbrae, Greenland, *J. Glaciol*., **49**(165), 231–239, doi:10.3189/172756503781830764.

van den Broeke, M., J. Bamber, J. Ettema, E. Rignot, E. Schrama, W. J. van de Berg, E. Van Meijgaard, I. Velicogna, and B. Wouters (2009), Partitioning recent Greenland mass loss, *Science*, **326**, 984–986, doi:10.1126/science.1178176.

van der Veen, C. J. (1996), Tidewater calving, *J. Glaciol*, **42**, 375–385.

van der Veen, C. J. (1998), Fracture mechanics approach to penetration of bottom crevasses on glaciers, *Cold Reg. Sci. Technol*., **27**, 213–223, doi:10.1016/S0165-232X(98)00006-8.

van der Veen, C. J. (2002), Calving glaciers, *Prog. Phys. Geogr*., **26**(1), 96–122, doi:10.1191/0309133302pp327ra.

van de Wal, R. S. W., W. Boot, M. R. van den Broeke, C. J. P. P. Smeets, C. H. Reijmer, J. J. A. Donker, and J. Oerlemans (2008), Large and rapid melt-induced velocity changes in the ablation zone of the Greenland ice sheet, *Science*, **321**, 111–113, doi:10.1126/science.1158540.

Vaughan, D. G., J. C. Comiso, I. Allison, J. Carrasco, G. Kaser, R. Kwok, P. Mote, T. Murray, F. Paul, J. Ren, E. Rignot, O. Solomina, K. Steffen and T. Zhang (2013), Observations: Cryosphere, in *Climate Change 2013: The Physical Science Basis. Contribution of Working Group I to the Fifth Assessment Report of the Intergovernmental Panel on Climate Change*, edited by Stocker, T.F., D. Qin, G.-K. Plattner, M. Tignor, S.K. Allen, J. Boschung, A. Nauels, Y. Xia, V. Bex and P.M. Midgley, Cambridge University Press, Cambridge, United Kingdom, and New York, NY, USA.

Vieli, A., M. Funk, and H. Blatter (2001), Flow dynamics of tidewater glaciers: Numerical modelling approach, *J. Glaciol*., **47**, 595–606.

Vieli, A., J. Jania, and L. Kolondra (2002), The retreat of a tidewater glacier: Observations and model calculations on Hansbreen, Spitsbergen, *J. Glaciol*., **48**(163), 592– 600.

Warren, C. R., and D. E. Sugden (1993), The Patagonian Icefields: A glaciological review, *Arct. Alp. Res*., **25**(4), 316–331.

Willis, M. J., A. K. Melkonian, M. E. Pritchard, and J. M. Ramage (2012a), Ice loss rates at the Northern Patagonian Ice Field derived using a decade of satellite remote sensing, *Remote Sens*. *Environ*., **117**, 184–198, doi:10.1016/j.rse.2011.09.017.

Willis, M. J., A. K., Melkonian, M. E., Pritchard, and A. Rivera (2012b), Ice loss from the Southern Patagonian Ice Field, South America, between 2000 and 2012, *Geophys. Res. Lett.,* **39**(16), L17501, doi:10.1029/2012GL053136.

Zwally, H. J., W. Abdalati, T. Herring, K. Larson, J. Saba, and K. Steffen (2002), Surface melt-induced acceleration of Greenland ice-sheet flow, *Science*, **297**, 218–222, doi: 10.1126/science.1072708.

Acknowledgements

First and foremost, I would like to express my gratitude to Dr. Shin Sugiyama, Chair of the doctoral degree supervisory committee, and who supervised the graduate study for the last 5 years since the beginning of the master program. He provided many opportunities, and supported this study with frequent discussions. Professor Ralf Greve, Professor Tsutomu Watanabe, Dr. Yasushi Fukamachi, and Professor Masato Furuya, members of the doctoral degree supervisory committee, encouraged the study, and made important comments on the thesis.

Dr. Takanobu Sawagaki, Faculty of Social Sciences, Hosei University, Professor Nozomu Naito, Department of Global Environmental Studies, Hiroshima Institute of Technology, and Ing. Pedro Skvarca, Museo del Hielo Patagónico, supported field campaigns in the Southern Patagonia Icefield, and made valuable comments on the study. Masahiro Minowa, a member of the Glacier and Ice Sheet Research Group in the Institute of Low Temperature Science, Hokkaido University, helped all activities in the Southern Patagonia Icefield. Professor Masamu Aniya, Professor Emeritus, University of Tsukuba, and Dr. Renji Naruse, Glacier and Cryospheric Environment Research Laboratory, encouraged the study, and made valuable comments. Thanks are also due to Hielo y Aventura, Viva Patagonia, and Prefectura Naval Argentina based at Punta Bandera for their help to the campaigns.

I would like to thank Dr. Shun Tsutaki, Arctic Environmental Research Center, National Institute of Polar Research. He gave me many ideas through the discussions in the laboratory and the field. Professor Hiroyuki Enomoto, Arctic Environmental Research Center, National Institute of Polar Research, supported the research as a Principal Investigator of Green Network of Excellence (GRENE) Arctic Climate Research Project. Thanks are also due to all members of the field campaigns in northwestern Greenland from 2012 to 2014. Special thanks also go to all the members of the Glacier and Ice Sheet Research Group in the Institute of Low Temperature Science, Hokkaido University for their kind supports and pleasant atmosphere during my graduate study.

Finally, I wish to dedicate this thesis to my most enthusiastic supports: my parents, sister and brother. They always believe my success in the study.

This research was funded by the Japan Society for the Promotion of Science through a Grant-in-Aid for Scientific Research (B) 23403006 (2011–2014) and a Grant-in-aid for JSPS Fellows 14J02632 (2014–2016) and by the Japanese Ministry of Education, Culture, Sports, Science and Technology through the Green Network of Excellence (GRENE) Arctic Climate Change Research Project. Financial support was also provided by the Global COE Program (Establishment of Center for Integrated Field Environmental Science).